Mon. Not. R. Astron. Soc. **340,** 1095–1135 (2003)

Quasars, their host galaxies and their central black holes

J. S. Dunlop,[1⋆] R. J. McLure,[2] M. J. Kukula,[1] S. A. Baum, [3] C. P. O'Dea[3] and D. H. Hughes[4]

[1]*Institute for Astronomy, University of Edinburgh, Royal Observatory, Blackford Hill, Edinburgh EH9 3HJ*
[2]*Department of Physics, University of Oxford, Nuclear & Astrophysics Laboratory, Keble Road, Oxford OX1 3RH*
[3]*Space Telescope Science Institute, 3700 San Martin Drive, Baltimore, MD 21218, USA*
[4]*Instituto Nacional de Astrofísica, Óptical y Electrónica (INAOE), Apartado Postal 51 y216, 72000 Puebla, Puebla, Mexico*

Accepted 2002 November 29. Received 2002 November 29; in original form 2001 August 31

ABSTRACT

We present the final results from our deep *Hubble Space Telescope* (*HST*) imaging study of the host galaxies of radio-quiet quasars (RQQs), radio-loud quasars (RLQs) and radio galaxies (RGs). We describe and analyse new Wide Field & Planetary Camera 2 (WFPC2) *R*-band observations for 14 objects, which when combined with the first tranche of *HST* imaging reported in McLure et al., provide a complete and consistent set of deep, red, line-free images for statistically matched samples of 13 RQQs, 10 RLQs and 10 RGs in the redshift band $0.1 < z < 0.25$. We also report the results of new deep VLA imaging that has yielded a 5-GHz detection of all but one of the 33 active galactic nuclei (AGN) in our sample.

Careful modelling of our images, aided by a high dynamic-range point spread function, has allowed us to determine accurately the morphology, luminosity, scalelength and axial ratio of *every* host galaxy in our sample. Armed with this information we have undertaken a detailed comparison of the properties of the hosts of these three types of powerful AGN, both internally and with the galaxy population in general.

We find that spheroidal hosts become more prevalent with increasing nuclear luminosity such that, for nuclear luminosities $M_V < -23.5$, the hosts of both radio-loud *and* radio-quiet AGN are virtually all massive ellipticals. Moreover, we demonstrate that the basic properties of these hosts are indistinguishable from those of quiescent, evolved, low-redshift ellipticals of comparable mass. This result rules out the possibility that radio-loudness is determined by host-galaxy morphology, and also sets severe constraints on evolutionary schemes that attempt to link low-z ultraluminous infrared galaxies with RQQs.

Instead, we show that our results are as expected given the relationship between black hole and spheroid mass established for nearby galaxies, and apply this relation to estimate the mass of the black hole in each object. The results agree remarkably well with completely independent estimates based on nuclear emission-line widths; all the quasars in our sample have $M_{\rm bh} > 5 \times 10^8$ M$_\odot$, while the radio-loud objects are confined to $M_{\rm bh} > 10^9$ M$_\odot$. This apparent mass-threshold difference, which provides a natural explanation for why RQQs outnumber RLQs by a factor of 10, appears to reflect the existence of a minimum and a maximum level of black hole radio output, which is a strong function of black hole mass ($\propto M_{\rm bh}^{2-2.5}$). Finally, we use our results to estimate the fraction of massive spheroids/black holes that produce quasar-level activity. This fraction is $\simeq$0.1 per cent at the present day, rising to $>$10 per cent at $z \simeq 2$–3.

Key words: black hole physics – galaxies: active – galaxies: photometry – quasars: general – infrared: galaxies.

⋆E-mail: jsd@roe.ac.uk

© 2003 RAS

1 INTRODUCTION

Studies of the host galaxies of low-redshift quasars can enable us to define the subset of the present-day galaxy population, which is capable of producing quasar-level nuclear activity. This is of obvious importance for constraining physical models of quasar evolution (Small & Blandford 1992; Haehnelt & Rees 1993; Kauffmann & Haehnelt 2000), and for exploring the connection between black hole and galaxy formation (Silk & Rees 1998; Fabian 1999; Franceschini et al. 1999; Granato et al. 2001; Kormendy & Gebhardt 2001). Such observations are also of value for testing unified models of radio-loud active galactic nuclei (AGN) (e.g. Peacock 1987; Barthel 1989; Urry & Padovani 1995), constraining possible evolutionary links between ultraluminous infrared galaxies (ULIRGs) and quasars (Sanders & Mirabel 1996), exploring the origin of radio loudness (Blandford 2000), and as a means to estimate the masses of the central black holes that power the active nuclei (McLure et al. 1999).

Our view of low-redshift quasar hosts has been clarified enormously over the last 5 years, primarily as a result of the angular resolution and dynamic range offered by the *Hubble Space Telescope* (*HST*). After some initial confusion, recent *HST*-based studies have now reached agreement that the hosts of all luminous quasars ($M_V < -23.5$) are bright galaxies with $L > L^{\star}$ (Bahcall et al. 1997; McLure et al. 1999; McLeod & McLeod 2001). However, it can be argued, (with considerable justification) that this much had already been established from earlier ground-based studies (e.g. Smith et al. 1986; Véron-Cetty & Woltjer 1990; Taylor et al. 1996).

In fact, as first convincingly demonstrated by Disney et al. (1995), the major advance offered by the *HST* for the study of quasar hosts is that it allows host galaxies to be mapped out over a sufficient angular and dynamic range for a de Vaucouleurs $r^{1/4}$-law spheroidal component to be clearly distinguished from an exponential disc, at least for redshifts $z < 0.5$. This is not to suggest that AGN host-galaxy morphological discrimination has proved impossible from the ground. Indeed, for lower-luminosity AGN at $z < 0.1$, such as Seyfert galaxies, ground-based imaging has proved perfectly adequate for this task (e.g. Hunt et al. 1999) and, in fact, some early ground-based attempts to determine the morphology of low-redshift quasar hosts have also proved to be robust (e.g. Smith et al. 1986). However, to ensure an unbiased comparison of radio-quiet quasar (RQQ) and radio-loud quasar (RLQ) hosts it is necessary to study host galaxies at $z > 0.15$ and to be able to determine host-galaxy morphologies for quasars with luminosities up to $M_V < -26$. Even by moving to the infrared to minimize the nuclear–host ratio, Taylor et al. (1996) found that this could not be reliably achieved with typical ground-based seeing.

Nevertheless, great care needs to be taken to extract the full benefit of *HST* imaging of quasar hosts. In particular, deep observations are required to detect the extended low-surface-brightness emission of even a massive host galaxy at $z \simeq 0.2$ to a radius of several arcsec from the nucleus. Unfortunately, however, this inevitably leads to saturation of the nucleus, making accurate characterization of the luminosity of the central source impossible. This is crucial because, at the depths of interest for reliable host-galaxy characterization, scattered light in the Wide Field & Planetary Camera 2 (WFPC2) point spread function (PSF) still makes a significant contribution to surface brightness out to an angular radius $\simeq$10 arcsec (McLure, Dunlop & Kukula 2000). As demonstrated by McLeod & Rieke (1995), these problems of surface-brightness bias, saturation and inadequate knowledge of the large-angle properties of the true WFPC2 PSF, can explain much of the confusion produced by the first studies of quasar hosts undertaken after the correction of the *HST* optics with COSTAR (e.g. Bahcall, Kirhakos & Schneider 1994).

In this paper we present the final results from our 34-orbit cycle-6 imaging study of quasar hosts, which was carefully designed to avoid these problems. Specifically, we acquired images of each quasar spanning a wide range of integration times (to allow an unsaturated, high dynamic-range image of each object to be constructed) and devoted an entire orbit to the construction of the necessary high dynamic-range PSF (via observations of a star of similar colour to the quasar nuclei, imaged at the same location on the same WF chip). Results from the first half of this programme were reported in McLure et al. (1999), where images for 19 objects from our 33-source sample were presented, modelled and analysed. Here we present and model the images for the 14 targets that were observed in the latter half of 1998 and in 1999, and then summarize and discuss the results derived from the analysis of the completed sample. The results presented in this paper thus complete, extend and in several cases supercede those presented in McLure et al. (1999) (e.g. estimated black hole masses for all objects are now calculated using more recent estimates of the black hole–spheroid mass relation, yielding significantly lower values than were calculated by McLure et al. based on the relation presented by Magorrian et al. 1998).

Several other substantial studies of low-redshift quasar hosts have now been undertaken with the *HST* (e.g. Bahcall et al. 1997; Hooper, Impey & Foltz 1997; Boyce et al. 1998; McLeod & McLeod 2001). However, one unique feature of the present study is the deliberate focus on a comparison of the hosts of the three main classes of powerful AGN, namely radio-quiet quasars, radio-loud quasars and radio galaxies (RGs). Moreover, we have ensured that this comparison can be performed in an unbiased manner by confining our sample to a narrow range in redshift ($0.1 < z < 0.25$) and requiring that the individual subsamples are matched in terms of their luminosity distributions (optical luminosity in the case of the RQQ and RLQ subsamples, and radio luminosity in the case of the RLQ and RG subsamples – see Dunlop et al. 1993, McLure et al. 1999 and Section 2 for further details). Another strength of this study is the wealth of pre-existing data at other wavelengths, as detailed in Section 2. This has allowed us to maximize the impact of the *HST* imaging (through, for example, the determination of $R - K$ colours for all the host galaxies). Finally, it is worth emphasizing that in this study we have sought to extract the properties of the stellar population that dominates the mass of the host galaxy. Thus, while we do include a statistical analysis of the prevalence of peculiar features such as tidal tails, we have endeavoured to minimize the distorting effect of the more transient activity by insisting on line-free imaging longward of the 4000-Å break, and masking out obvious asymmetries prior to modelling the host morphology. This approach, coupled with the careful design of our observations, is the most probable explanation for why the results presented in this paper are generally cleaner and more homogenous than the results of many other recent studies.

The layout of this paper is as follows. In Section 2 we review the main properties of the matched RG, RLQ and RQQ samples, and summarize the wealth of supporting ground-based multifrequency data that now exists for these objects. In Section 3 we give details of the *HST* observations and briefly review the process of data reduction and PSF determination (McLure et al. 1999, 2000). Then, in Section 4 we give a brief description of the new VLA observations of the RQQs in our sample that escaped previous radio detection by Kukula et al. (1998), and present new 5-GHz flux densities and positions. In Section 5 we present the new *HST* data and briefly

summarize the approach taken to modelling the WFPC2 images; the images and two-dimensional (2D) model fits for the 14 new objects are provided in Appendix A (along with brief notes on each source), with observed and fitted luminosity profiles presented in Appendix B. Next, in Section 6 we analyse the results of modelling the *HST* images of the complete sample, and assess the implications of our results for unified models of AGN. In Section 7 we explore how quasar hosts relate to the general population of massive galaxies, and demonstrate via the Kormendy relation that the quasar hosts are drawn from the population of massive 'boxy' ellipticals that are found predominantly in cluster environments. We also include a comparison of the environments and interaction statistics for quasar hosts and brightest cluster galaxies. In Section 8 we exploit our results to investigate the properties of the central engines that power these luminous AGN, deriving estimates of the black hole mass and the Eddington ratio, and exploring possible clues to the origin of radio loudness. Finally, in Section 9 we briefly discuss the implications of our results for the cosmological evolution of quasars and massive galaxies. Our conclusions are summarized in Section 10.

For ease of comparison with previous work we adopt an Einstein–de Sitter universe with $H_0 = 50$ km s^{-1} Mpc^{-1} for the calculation of physical quantities throughout this paper.

2 SAMPLE AND ASSOCIATED OBSERVATIONS

The *HST* imaging observations reported here complete the imaging of the full sample of 33 objects (10 RLQs, 13 RQQs and 10 RGs) defined for this study. This sample was selected from the slightly larger (40-source) sample imaged in the infrared by Dunlop et al. (1993) and Taylor et al. (1996) through the imposition of the slightly more restrictive redshift limits $0.1 < z < 0.25$. As described in McLure et al. (1999), this restriction in redshift range ensures that our *R*-band imaging through the F675W filter is not contaminated by the presence of strong emission lines such as [O III] or Hα. The main effect of this additional redshift restriction is to exclude a small number of objects from the original sample of Dunlop et al. (1993) that have $0.25 < z < 0.35$. However, this has not significantly compromised the original statistical merits of this sample, namely that the RLQ and RQQ subsamples are matched in terms of optical luminosity, and that the RLQ and RG samples are matched in terms of radio luminosity and radio spectral index (Dunlop et al. 1993).

Of the 33 sources in this sample, 19 were observed during the first year of our cycle-6 allocation. The observations and analysis of these objects were presented by McLure et al. (1999). The remaining 14 objects for which the observations are presented and analysed in this paper are listed in Table 1, along with the dates on which they were observed with the *HST*.

Also included in this paper are new, deep VLA observations of a subset of our RQQ sample. These 4.8-GHz observations, the results of which are presented in Section 4, go a factor of 3 deeper than the observations of Kukula et al. (1998), which were utilized by McLure et al. (1999). The important outcome of these observations is that we have now detected all but one of the RQQs in this sample at radio wavelengths. These new radio detections, coupled with completion of the *HST* observations, have allowed us to re-investigate and clarify a number of the relations between optical and radio properties that could only be tentatively explored by McLure et al. (1999).

We have also obtained improved infrared (UKIRT *K*-band) images for a small number of the more luminous quasars in our sample since the publication of McLure et al. (1999). These have been published in McLure et al. (2000), but the results of modelling these images are utilized in this paper to assist in the improved analysis of galaxy colours, which is presented in Section 6.6.

Finally, we note that Hβ emission-line spectroscopy of the RLQ and RQQ samples discussed here has recently been completed by McLure & Dunlop (2001). The results of this spectroscopic study are referred to in the discussion of black hole mass estimation presented in Section 8.

Table 1. Observing dates for the objects presented in this paper. Note that, despite its archive designation as 3C 59, 0204+292 is in fact now classified as an RQQ (see Taylor et al. 1996, and the radio luminosity quoted in Table 3).

Object	*HST* archive designation	Type	Observing date
0307+169	3C 79	RG	1998 Jul 10
0230−027	PKS 0230−027	RG	1998 Sep 25
1342−016	1342−016	RG	1998 Dec 10
1215+013	1215+013	RG	1999 Jan 2
1215−033	1215−033	RG	1999 Jan 6
1330+022	1330+022	RG	1999 Apr 13
1217+023	PKS 1217+02	RLQ	1998 Jul 7
1020−103	PKS 1020−103	RLQ	1998 Jul 12
2135−147	PKS 2135−14	RLQ	1998 Oct 19
2355−082	PKS 2355−082	RLQ	1998 Oct 19
0204+292	3C 59	RQQ	1998 Jul 9
1549+203	1E 15498+203	RQQ	1998 Sep 3
2215−037	EX 2215−037	RQQ	1998 Sep 26
0052+251	PG 0052+251	RQQ	1998 Nov 6

3 *HST* OBSERVATIONS

The observations were made using the Wide Field & Planetary Camera 2 (WFPC2, Trauger et al. 1994) on the *Hubble Space Telescope* through the F675W filter. The filter spans a wavelength range of 877 Å from 6275.5 to 7152.5 Å, roughly equivalent to the standard *R* band. This filter was selected in preference to a wider filter because it allowed both [O III] and Hα emission lines to be excluded from the bandpass for source redshifts in the range $0.1 < z < 0.25$, and thus ensured that a clean measure could be made of the level of continuum light emitted by the quasar host galaxy at wavelengths longwards of the 4000-Å break. As in McLure et al. (1999) target sources were centred on the WF2 chip, which was chosen in preference to WF1 or WF3 because of its marginally superior performance over the period immediately prior to our observations.

Deep sensitive images of the host galaxies are obviously desirable, but the necessary long, background-limited exposures inevitably mean that, in the case of the quasars, the central source becomes saturated. From such saturated images it is extremely difficult to reliably disentangle host-galaxy emission from the contribution of the PSF-convolved nuclear source.

Slightly different strategies were therefore adopted for the quasar and radio-galaxy samples. For the quasars, exposures of 5, 26 and 3×600 s were taken. The short exposures ensured that at least one unsaturated image of each quasar would be obtained, thus enabling an accurate measurement of the central flux density. The three 600-s exposures each yielded a 3σ surface-brightness sensitivity of $\mu_R = 23.8$ mag arcsec^{-2} pixel^{-1}, and their comparison facilitated reliable cosmic ray removal using standard IRAF tasks. With azimuthal averaging, the combined 1800-s image of each quasar allows extended emission to be traced reliably down to a surface-brightness level of $\mu_R > 26$ mag arcsec^{-2}.

For the radio galaxies there was little danger of saturation and so short exposures were not required. Three 700-s exposures were therefore obtained for each radio galaxy. Any remaining time in the orbit was filled with a shorter exposure of flexible length (usually 40–100 s). Calibration was carried out using the standard pipeline.

As described in McLure et al. (1999) we devoted one orbit of our allotted *HST* time to constructing a deep, unsaturated stellar PSF using the F657W filter, with the star centred on exactly the same part of the WF2 chip as the target objects. Full details (magnitude, colour, etc.) of the chosen star can be found in McLure et al. (1999), along with a detailed description of how we constructed a properly sampled PSF of the required large dynamic range using dithered observations of a series of exposures ranging from 0.23 to 160 s.

Here we simply re-emphasize that the resulting high dynamic range PSF, tailored as closely as possible to match our quasar observations, has proved to be absolutely crucial in allowing the reliable extraction of host-galaxy parameters from the WFPC2 images.

4 NEW RADIO OBSERVATIONS OF RQQS

Kukula et al. (1998) reported radio continuum observations of a sample of 27 low-redshift radio-quiet quasars, including all of the RQQs in the current sample, made with the Very Large Array (VLA) at 1.4, 4.8 and 8.4 GHz. Although flux densities were obtained for the majority of the sample, six objects remained undetected at all three frequencies (the flux-density limit of the survey was $\simeq$0.2 mJy at 4.8 GHz).

To remedy this situation additional high-sensitivity observations were made of these six RQQs on 1999 August 5 at 4.8 GHz, again using the VLA in its high-resolution 'A' configuration. Data reduction was carried out using the standard procedure within AIPS. The angular resolution of the maps is $\sim$0.4 arcsec (FWHM) at this frequency, corresponding to a physical size of $\sim$1.5 kpc at the redshift of the quasars – thus neatly encompassing the nuclear region of the quasar host.

The results of these observations are listed in Table 2. Radio sources are detected within $\sim$1 arcsec of all bar one of the RQQs (positional accuracies are estimated to be within $\sim$100 mas). Owing to scheduling problems 1549+203 could only be allocated half the time given to the other five RQQs and the map of this object suffers from a correspondingly higher noise level.

5 NEW *HST* RESULTS

The WFPC2 F675W images, two-dimensional model fits, and the model-subtracted residual images of the 14 *new* objects are presented in Appendix A in Figs A1–A14, along with brief notes on each individual source. Comparable images and notes for the other 19 objects in the sample can be found in McLure et al. (1999). The observed luminosity profiles for the 14 *new* objects are presented in Appendix B in Figs B1–B14, along with the best-fitting model profiles extracted from the two-dimensional model fits.

Full details of the two-dimensional model procedure that we have used to determine the properties of the host galaxies can be found in McLure et al. (2000), along with the results of extensive tests of its ability to reclaim host-galaxy parameters from simulated data based on a wide range of host-galaxy–nucleus combinations at different redshifts. As emphasized in McLure et al. (2000), the success of this modelling depends on an accurate high dynamic range PSF and the construction of an accurate error frame for each quasar image.

In brief, the modelling of the *HST* images was carried out in three separate stages. The first stage involves assessing how well the data can be reproduced, *assuming* that the host galaxy is *either* an elliptical galaxy (with a surface-brightness distribution described by a de Vaucouleurs $r^{1/4}$-law) or a pure exponential disc. The remaining five parameters (host-galaxy position angle, host-galaxy axial ratio, host-galaxy scalelength, host-galaxy luminosity and nuclear luminosity) are then adjusted until, when convolved with the PSF, the model best fits the data as determined by χ-squared minimization (note that it is not assumed a priori that the radio galaxies have a negligible nuclear component). Then, if one assumed galaxy morphology yields a significantly better fit than the other, we can say that the galaxy is *better* described by a de Vaucouleurs law or by an exponential disc. As with all the modelling performed on the *HST* sample, once the minimum χ^2 solution had been found, the modelling code was repeatedly restarted from close to the minimum χ^2 solution, in order to ensure that the solution was stable.

The results of applying this procedure to the new *HST* images are given in Table 3, alongside the results already determined by McLure et al. (1999). The striking feature of these results, now confirmed with the complete sample, is that with the exception of three RQQs (0052+251 and the two lowest-luminosity RQQs 0257+024 and 2344+184) every single host galaxy is better described by a de Vaucouleurs law.

In our second approach we have removed the requirement of assuming that the host galaxy can be described as either a pure $r^{1/4}$-law or an exponential disc, and allow a sixth parameter β [where the luminosity profile of the galaxy is given by $I(r) \propto \exp(-r^{\beta})$] to vary continuously. Thus $\beta = 1$ should result if the galaxy is best described by a pure exponential disc and $\beta = 0.25$ should result if the galaxy really does follow a pure de Vaucouleurs law, but *all* values of β are available to the program if this results in an improved quality of fit. The results of applying this procedure to the

Table 2. High-sensitivity VLA observations of the six previously undetected RQQs in our sample. Optical positions were measured from Digitized Sky Survey plates using the STSDAS package in IRAF. All radio observations were made in *C* band (4.8 GHz) with the VLA in A-configuration (angular resolution $\simeq$0.4 arcsec) on 1999 August 5. The uncertainties in the measured flux densities are given as three times the rms noise in the image. Radio positions are accurate to within 100 mas.

Quasar	z	M_V	Optical position (J2000)		Radio Position (J2000)		4.8-GHz flux	$\log(P_{4.8\,\mathrm{GHz}}/$
			RA (h m s)	Dec. (deg arcmin arcsec)	RA (h m s)	Dec. (deg arcmin arcsec)	density mJy^{-1}/W	Hz^{-1} sr^{-1})
0244+194	0.176	−23.55	02 47 40.85	+19 40 57.8	02 47 40.84	+19 40 57.8	0.18 ± 0.06	21.3
PG 0923+201	0.190	−24.56	09 25 54.71	+19 54 04.4	09 25 54.74	+19 54 05.0	0.14 ± 0.06	21.3
PG 0953+414	0.239	−25.36	09 56 52.35	+41 15 22.5	09 56 52.39	+41 15 22.2	0.25 ± 0.07	21.7
1549+203	0.250	−24.51	15 52 02.36	+20 14 00.5	–	–	<0.12	<21.4
2215−037	0.241	−23.73	22 17 47.77	−03 32 38.8	22 17 47.72	−03 32 38.5	0.13 ± 0.08	21.4
2344+184	0.138	−23.76	23 47 25.71	+18 44 50.8	23 47 25.77	+18 44 50.7	0.19 ± 0.08	21.1

Table 3. The outcome of attempting to model the AGN host galaxies as either an exponential disc or a de Vaucouleurs spheroid. Source name and redshift are given in the first two columns, with the logarithm of radio luminosity given in column 3. The preferred host-galaxy morphology is given in column 4, with the $\Delta\chi^2$ between the chosen and alternative model listed in column 5. In column 6 $r_{1/2}$ is given irrespective of the chosen host morphology. Column 7 lists $\mu_{1/2}$ in units of R mag arcsec^{-2}. Columns 8 and 9 list the integrated apparent magnitudes of the host galaxy and fitted nuclear component converted from F675W to Cousins R band, while column 10 gives the ratio of integrated galaxy and nuclear luminosities. Columns 11 and 12 give the axial ratio and position angle (east of north) of the best-fitting host-galaxy model.

Source	z	$\log(P_{4.8\,\mathrm{GHz}}/\mathrm{W\,Hz^{-1}\,sr^{-1}})$	Host morphology	$\Delta\chi^2$	$r_{1/2}$ (kpc^{-1})	$\mu_{1/2}$	R_{host}	R_{nuc}	$L_{\mathrm{nuc}}/L_{\mathrm{host}}$	b/a	PA (deg)
RG											
0230−027	0.239	24.8	Elliptical	5900	7.7	21.8	17.5		0.00	0.95	113
0307+169	0.256	25.5	Elliptical	3500	9.4	21.4	17.2	20.9	0.03	1.00	13
0345+337	0.244	25.5	Elliptical	2400	13.1	23.3	18.0	21.1	0.06	0.70	99
0917+459	0.174	25.7	Elliptical	33 000	21.9	23.0	16.1	19.4	0.05	0.76	36
0958+291	0.185	25.3	Elliptical	7800	8.5	22.0	17.1	18.5	0.27	0.95	45
1215−033	0.184	24.1	Elliptical	9300	8.5	22.0	17.1	22.3	0.008	0.87	60
1215+013	0.118	24.0	Elliptical	14 000	4.7	21.0	16.5	19.9	0.05	0.94	142
1330+022	0.215	25.4	Elliptical	7400	15.7	22.9	17.1	19.5	0.11	0.79	79
1342−016	0.167	24.4	Elliptical	29 000	23.3	22.9	15.6	21.8	0.003	0.93	96
2141+279	0.215	25.2	Elliptical	8500	24.8	23.5	16.7	25.6	0.0003	0.74	148
RLQ											
0137+012	0.258	25.2	Elliptical	5100	14.2	22.6	17.2	17.3	0.8	0.85	35
0736+017	0.191	25.4	Elliptical	8900	13.3	22.9	16.9	16.2	1.9	0.97	13
1004+130	0.240	24.9	Elliptical	500	8.2	21.5	16.9	15.0	5.8	0.94	29
1020−103	0.197	24.7	Elliptical	4200	7.1	20.8	17.2	16.8	1.4	0.73	46
1217+023	0.240	25.9	Elliptical	2400	11.1	21.7	17.3	16.3	2.5	0.8	16
2135−147	0.200	25.3	Elliptical	2700	11.6	22.7	17.2	16.2	2.5	0.95	72
2141+175	0.213	24.8	Elliptical	570	8.2	21.2	17.3	15.9	3.7	0.47	118
2247+140	0.237	25.3	Elliptical	8100	13.5	22.4	17.2	16.9	1.3	0.63	118
2349−014	0.173	24.9	Elliptical	13 000	19.2	22.7	15.9	16.0	0.9	0.89	45
2355−082	0.210	24.5	Elliptical	3000	10.4	22.0	17.1	17.4	0.77	0.73	177
RQQ											
0052+251	0.154	21.6	Bulge/disc	2500	3.2	20.8	16.7	15.4	3.2	0.61	117
0054+144	0.171	21.9	Elliptical	6100	10.4	21.7	16.6	15.5	2.7	0.61	108
0157+001	0.164	22.8	Bulge/disc	3900	15.5	22.0	15.6	16.2	0.57	0.88	116
0204+292	0.109	22.7	Elliptical	33 000	8.8	20.9	15.9	16.0	0.89	0.73	71
0244+194	0.176	21.3	Elliptical	2700	9.3	22.7	17.5	16.8	1.9	0.92	77
0257+024	0.115	22.2	Disc/bulge	10 000	11.7	21.7	15.9	21.0	0.009	0.88	134
0923+201	0.190	21.3	Elliptical	1700	8.2	22.1	17.2	15.7	4.2	0.98	141
0953+415	0.239	21.7	Elliptical	90	7.6	22.4	18.2	15.2	15.4	0.86	115
1012+008	0.185	22.0	Elliptical	1100	28.7	23.8	16.6	16.2	1.5	0.64	109
1549+203	0.250	< 21.4	Elliptical	510	5.0	22.2	18.9	16.8	6.5	0.88	34
1635+119	0.146	23.0	Elliptical	35 000	7.6	21.6	16.8	18.1	0.3	0.69	179
2215−037	0.241	21.4	Elliptical	1500	6.7	21.4	17.5	18.2	0.56	0.84	88
2344+184	0.138	21.1	Disc/bulge	8900	17.5	23.8	16.8	20.3	0.04	0.67	103

HST images are given in Table 4 (again for the complete sample) and illustrated in Fig. 1. These results are discussed in more detail in Section 6.1.

Finally, an examination of Table 4 and Fig. 1 reveals that, whereas a very clean preference for $\beta = 0.25$ is displayed by the RGs and RLQ hosts, a few of the RQQ hosts (in particular, as mentioned above, 0052+251 and the two lowest-luminosity RQQs 0257+024 and 2344+184) have best-fitting β values that are intermediate between the values of 0.25 or 1.0 expected for pure elliptical or disc hosts. For this reason it was decided that the RQQ hosts should all be remodelled with a nine free-parameter fit, which allowed for the combination of both disc and bulge contributions to the surface-brightness distribution of the host. For nine out of the 13 RQQs this extra freedom still resulted in no significant disc component. However, for four objects (the above-mentioned three RQQs plus 0157+001) this procedure produced a significantly improved model fit, and it is the L_{host} and L_{nuc} values from these combined fits that are used in all of the subsequent analyses. These four bulge–disc combinations are also noted in Table 3, and in that table (and in subsequent analysis) it is the scalelength, axial ratio and position angle of the dominant component, which are adopted for these combined-fit objects.

The luminosity profiles, extracted from the two-dimensional model fits are presented for the 14 new objects in Appendix B. The profiles are followed out to a radius of 10 arcsec, which is representative of the typical outer radii used in the modelling ($\langle r \rangle = 11$ arcsec).

6 ANALYSIS OF THE FULL SAMPLE

6.1 Host-galaxy morphologies

Examination of the results presented in Tables 3 and 4 confirms that the somewhat complex observing strategy outlined in Section 3 has

Table 4. The outcome of the variable-β modelling. Column 2 lists the host morphology of the best-fitting 'fixed β' model (results of which are given in Table 3). The best-fitting values for the β profile parameter are given in column 3. Column 4 gives $\Delta\chi^2$, which quantifies the improvement in fit offered by the variable-β model over that already achieved with the best-fitting pure disc or elliptical model. Simulations indicate that β can be reclaimed to within a typical uncertainty of 0.01–0.02.

Source	Host	β	$\Delta\chi^2$
RG			
0230−027	Elliptical	0.25	0
0307+169	Elliptical	0.21	52
0345+337	Elliptical	0.25	2
0917+459	Elliptical	0.23	264
0958+291	Elliptical	0.25	16
1215−033	Elliptical	0.24	0
1215+013	Elliptical	0.25	3
1330+022	Elliptical	0.24	16
1342−016	Elliptical	0.23	90
2141+279	Elliptical	0.25	2.2
RLQ			
0137+012	Elliptical	0.19	126
0736+017	Elliptical	0.19	239
1004+130	Elliptical	0.25	5
1020−103	Elliptical	0.19	132
1217+023	Elliptical	0.26	2
2135−147	Elliptical	0.25	0
2141+175	Elliptical	0.28	23
2247+140	Elliptical	0.25	17
2349−014	Elliptical	0.26	10
2355−082	Elliptical	0.26	383
RQQ			
0052+251	Bulge/disc	1.09	267
0054+144	Elliptical	0.25	3
0157+001	Bulge/disc	0.24	133
0204+292	Elliptical	0.24	216
0244+194	Elliptical	0.22	47
0257+024	Disc/bulge	0.75	2792
0923+201	Elliptical	0.30	44
0953+415	Elliptical	0.27	9
1012+008	Elliptical	0.38	102
1549+203	Elliptical	0.25	0
1635+119	Elliptical	0.18	550
2215−037	Elliptical	0.25	0
2344+184	Disc/bulge	0.43	1044

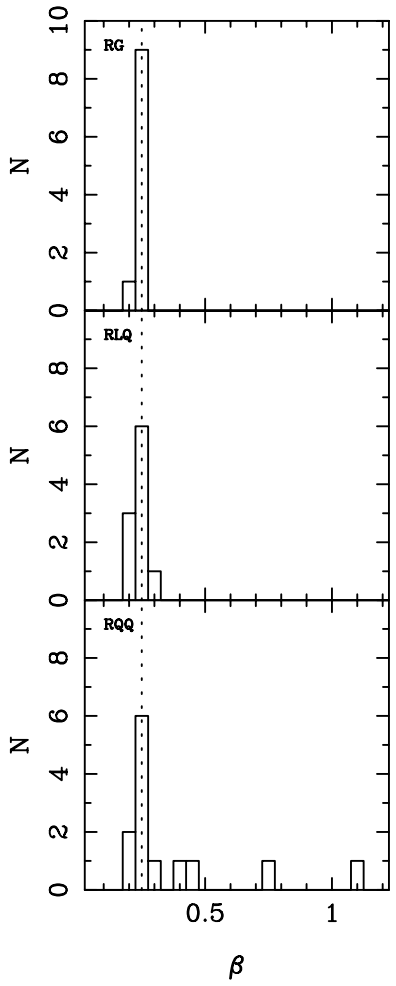

Figure 1. Subsample histograms of the best-fitting β values from the variable-β modelling. The dotted line lies at $\beta = 0.25$, corresponding to a perfect de Vaucouleurs law.

successfully allowed the determination of host-galaxy morphology for all 33 objects in the sample. Also immediately apparent from Table 3 is that the huge amount of information available to the modelling code has not only allowed a clear morphological preference to be made, but can formally exclude the alternative host in all cases ($\Delta\chi^2 = 25.7$ corresponds to a 99.99 per cent confidence level for a five-parameter fit).

The results from the modelling of the RG and RLQ subsamples are in good agreement with orientation-based unification, with all 20 objects found to have elliptical host galaxies. A perhaps more striking feature of these results is the extent to which the classic $r^{1/4}$ de Vaucouleurs law provides a near-perfect description of the host galaxies of the radio-loud objects (see Fig. 1). As can be seen from Table 4 the best-fitting β values for the combined RG and RLQ subsamples all lie in the narrow range $0.19 < \beta < 0.26$, with the RG sample alone displaying an even narrower spread, $0.21 < \beta < 0.25$. This conclusion is further strengthened by a comparison of the beta histogram for the three subsamples with that from the β-modelling tests performed by McLure et al. (2000). The application of the Kolmogorov–Smirnov test to the β distribution of the 29 objects that were found to have single-component elliptical host galaxies, and those resulting from the β-model testing, returns a probability of $p = 0.23$. This confirms that, as far as the modelling code is concerned, any differences between these hosts and pure elliptical galaxies are not statistically significant. The best match between the test results and the actual data is for the RG subsample ($p = 0.39$), perhaps as would be expected considering the lack of a dominant point-source contribution.

Considering the long-standing belief that RQQs are often located in disc galaxies, the results from modelling of the RQQ subsample are quite unambiguous, with nine of the 13 host galaxies showing no evidence for any disc component. Of the four objects that are best matched by a combined disc/bulge model, the luminosities of 0157+001 and 0052+251 are dominated by their bulge components, which, respectively, account for 83 and 71 per cent of the total host luminosity. This means that the number of bulge-dominated RQQ hosts is 11 out of the 13 objects.

It is interesting to note that the two most disc-dominated galaxies, 0257+024 and 2344+184, are the hosts of by far the lowest-luminosity AGN in the entire 33-object sample. In fact, converting

their total luminosity (host+nucleus) from the model fits for these two objects to the equivalent absolute V-magnitudes gives $M_V = -22.6$ and $M_V = -21.9$, respectively (assuming $V - R = 0.8$ at $z = 0$, Fukugita, Shimasaku & Ichikawa 1995). Given that for this study the adopted quasar/Seyfert borderline is $M_V = -23.0$, it is clear that these two objects are not actually bona fide RQQs. The clear implication from this result is that all *true* quasars, with $M_V < -23.0$, reside in luminous bulge-dominated hosts, irrespective of their radio power.

The morphological determinations for the RQQ host galaxies have placed on a firm footing the suggestion made previously by Taylor et al. (1996) and McLeod & Rieke (1995) that the probability of a RQQ having an early-type host was an increasing function of the quasar luminosity. Unlike the previous ground-based studies, the high-resolution and temporally stable PSF offered by *HST* has permitted the confirmation of what were hitherto necessarily tentative conclusions, owing to the uncertainties introduced by ground-based seeing conditions. Therefore, a strong conclusion from the morphological analysis of the new *HST* images is that the radio luminosity of an AGN is not directly related to host-galaxy morphology. The relationship between host morphology and AGN luminosity is explored further in Section 7.

6.2 Host-galaxy and AGN luminosities

The host and nuclear luminosities are presented in the form of integrated absolute Cousins R-band magnitudes in Table 5, and in Figs 2 and 3. These have been derived from the apparent magnitudes listed in Table 3, which have been calculated by integrating the best-fitting model components to infinite radius, and adopting the F675W flight-system zero-point given by Holtzman et al. (1995). The similarity between the F675W filter and the standard Cousins R band is such that, with the use of this zero-point, the difference is of the order of ± 0.05 mag. The conversion from apparent to absolute magnitudes has been performed using k-corrections assuming spectral indices of $\alpha = 1.5$ and 0.2 for the host and nucleus, respectively ($f_\nu \propto \nu^{-\alpha}$).

For all but four of the sources, the values of M_R(host) listed in Table 5 can be regarded as equivalent to the value of M_R(bulge). For the four objects that benefited from a combined disc+bulge model, the best-fitting values of M_R(bulge) are as follows: 0052+251:M_R(bulge) $= -22.95$, 0157+001:M_R(bulge) $= -24.32$, 0257+024:M_R(bulge) $= -21.48$, 2344+184:M_R(bulge) $= -22.44$.

6.2.1 *Host-galaxy luminosities*

The mean and median integrated absolute magnitudes of the best-fitting host galaxies in each subsample are:

$\langle M_R \rangle = -23.53 \pm 0.09$ median $= -23.52$ (all)
$\langle M_R \rangle = -23.66 \pm 0.16$ median $= -23.63$ (RG)
$\langle M_R \rangle = -23.73 \pm 0.10$ median $= -23.67$ (RLQ)
$\langle M_R \rangle = -23.28 \pm 0.15$ median $= -23.30$ (RQQ).

Two features of these results merit comment. First, the agreement between the absolute magnitudes of the host galaxies of the RG and RLQ subsamples can be seen to be extremely good, with the median figures differing by only 0.04 mag. This can be interpreted as strong evidence in favour of orientation-based radio-loud unification (see also Section 6.7). The second obvious feature of these results is that these new *HST* images appear to confirm the traditional finding that the hosts of RQQs are less luminous than those of RLQs, although the median difference of 0.37 mag is a factor of 2 smaller than the difference typically claimed (e.g. Kirhakos et al. 1999). This does not seem to be an artefact of the inclusion of RQQ hosts with a substantial disc component, since if attention is confined to the nine RQQs with solid elliptical model fits the values remain virtually unchanged, i.e.

$\langle M_R \rangle = -23.30 \pm 0.17$ median $= -23.30$ (RQQ).

A large variation in the luminosity difference between RQQ and RLQ host galaxies has been reported in the literature. Differences have ranged from RQQ hosts being fainter than their RLQ counterparts by 0.7–1.0 mag in optical studies (e.g. Smith et al. 1986; Véron-Cetty & Woltjer 1990; Bahcall et al. 1997), to no formal luminosity difference being detected from the near-infrared

Table 5. Absolute magnitudes (M_R), and optical–infrared ($R - K$) colours of the best-fitting host galaxy and nuclear component for each AGN. Column 2 gives the R-band absolute magnitudes (M_R) of the total host galaxy derived from the current modelling of the *HST* data, assuming a spectral index of $\alpha = 1.5$ (where $f_\nu \propto \nu^{-\alpha}$). Column 3 gives the R-band absolute magnitudes (M_R) of the nuclear component as derived from the current modelling of the *HST* data assuming a spectral index of $\alpha = 0.2$. Columns 4 and 5 list the observed $R - K$ colours of the host galaxy and nuclear component, respectively. These colours were derived by combining 12-arcsec aperture R-band photometry from our *HST*-based models with the 12-arcsec aperture K-band photometry derived by Taylor et al. (1996) and McLure et al. (2000), to minimize the uncertainty introduced by errors in constraining the galaxy scalelengths at K (see the text for further details).

Source	M_R(host)	M_R(nucl)	$(R-K)_{\rm host}$	$(R-K)_{\rm nucl}$
RG				
0230−027	−23.55	–	2.1	–
0307+169	−23.96	−19.94	2.1	6.7
0345+337	−23.05	−19.63	3.6	5.8
0917+459	−24.20	−20.65	3.4	5.0
0958+291	−23.36	−21.70	1.9	4.5
1215+013	−22.85	−19.35	2.5	6.9
1215−033	−23.29	−17.87	2.6	5.1
1330+022	−23.70	−21.00	2.8	5.0
1342−016	−24.58	−18.35	2.6	6.0
2141+279	−24.09	−14.94	3.3	10.4
RLQ				
0137+012	−24.04	−23.53	2.8	3.1
0736+017	−23.58	−24.01	3.2	3.2
1004+130	−24.10	−25.70	3.0	2.0
1020−103	−23.36	−23.47	2.3	3.6
1217+023	−23.71	−24.40	3.2	3.2
2135−147	−23.37	−24.09	2.5	4.0
2141+175	−23.43	−24.52	2.7	1.9
2247+140	−23.80	−23.80	2.8	2.6
2349−014	−24.32	−24.00	2.9	3.6
2355−082	−23.62	−23.06	2.7	3.0
RQQ				
0052+251	−23.33	−24.39	2.5	2.0
0054+144	−23.61	−24.49	3.1	1.8
0157+001	−24.52	−23.70	2.8	2.8
0204+292	−23.30	−23.03	2.5	3.2
0244+194	−22.77	−23.24	2.3	3.2
0257+024	−23.46	−19.69	2.6	6.7
0923+201	−23.25	−24.57	3.2	3.2
0953+415	−22.86	−25.52	3.0	2.5
1012+008	−23.78	−23.95	3.2	2.2
1549+203	−22.26	−23.98	3.4	3.1
1635+119	−23.05	−21.54	3.3	3.7
2215−037	−23.52	−22.58	2.7	4.4
2344+184	−22.97	−20.30	2.6	5.7

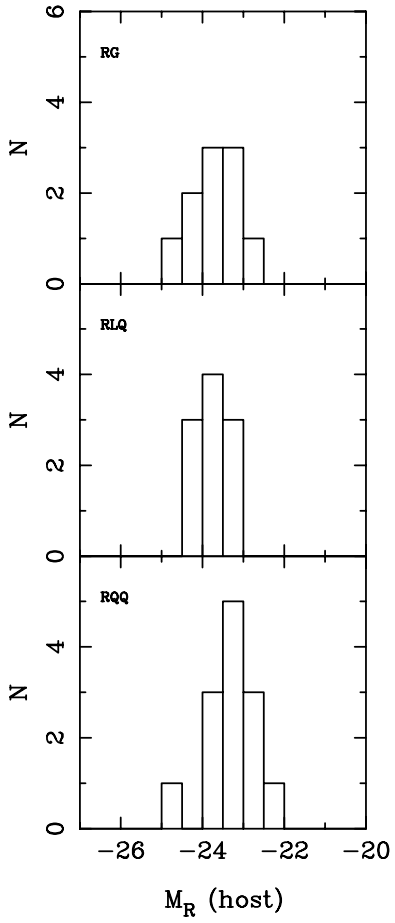

Figure 2. Subsample histograms of the host-galaxy, absolute, integrated *R*-Cousins magnitudes.

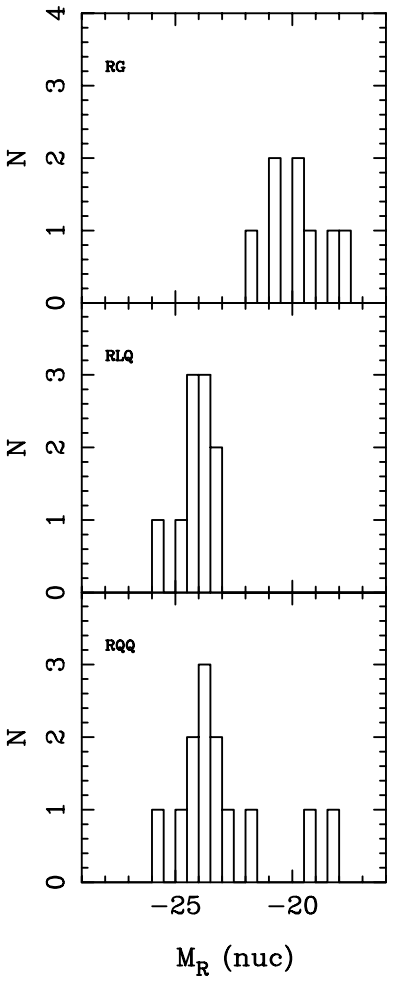

Figure 3. Subsample histograms of the nuclear, absolute, integrated *R*-Cousins magnitudes.

imaging of this *HST* sample (Taylor et al. 1996). It is therefore interesting to compare the difference in luminosity detected here with the results of the other two recent *HST R*-band imaging studies of Hooper et al. (1997) and Boyce et al. (1998), both of which also used two-dimensional modelling to analyse the host galaxies. Below we list the mean differences detected in the three studies ($\langle M_{\rm RQQ}\rangle - \langle M_{\rm RLQ}\rangle$) with the associated standard error. In calculating the figures for the Hooper et al. programme, where no attempt was made to distinguish the host galaxy morphologies, the luminosities of the best-fitting $r^{1/4}$ model have been used:

$\Delta M_R = 0.43 \pm 0.20$ this work
$\Delta M_R = 0.53 \pm 0.23$ Hooper et al.
$\Delta M_R = 0.67 \pm 0.29$ Boyce et al.

The clear implication from these results is that the host galaxies of RQQs are consistently fainter than those of RLQs by ∼0.5 mag in the *R* band. Unlike in earlier studies, this difference can no longer be attributed to the model fitting of RQQs producing disc fits, since only two of the 26 RQQ host magnitudes included in the above figures are derived from an exponential host model. The common bias of the RLQ redshifts being consistently higher than those of the RQQs can also be firmly rejected as a possible cause of the difference, with the two quasar types having well-matched redshift distributions in all three studies. At least for the results presented here, and those of Hooper et al., the selection of the RLQ and RQQ quasar samples to have matched optical magnitudes, also excludes the possibility that the host magnitude difference is as a result of the RLQs being intrinsically more luminous. However, it is possible that the host-galaxy results of Boyce et al. may have been influenced by this effect, considering that the RLQs in that study are intrinsically 0.6 ± 0.8 mag brighter than the RQQs, although, as can be seen from the large error associated with this difference, the overlap of the total quasar luminosities is significantly larger than that of the hosts. It is worth noting at this point that although the results of Taylor et al. certainly do not formally support a difference in host magnitudes (with $\Delta M_K = 0.4 \pm 0.3$), they are in fact perfectly consistent with the three sets of *R*-band *HST* results. The question of whether there is any detectable correlation between the host-galaxy and nuclear luminosities is explored below in Section 6.2.3.

A general result that can be taken from the luminosities of the best-fitting host galaxies is that, with the exception of the two Seyfert objects, all of them lie at the extreme end of the elliptical galaxy luminosity function. Adopting $M_R^\star = -22.2$ (Lin et al. 1996), after having converted the published value of $M_R^\star = -21.8$ to an integrated magnitude, it can be seen that *all* of the hosts have luminosities of $L \geqslant L^\star$, with 25 of the 33 having luminosities $L \geqslant 2L^\star$. These results are in good agreement with those of the previous *K*-band imaging study that also found all the hosts to be brighter than $L_K^\star$. Independent support for this result comes from the findings of Hooper et al. (1997) and Boyce et al. (1998), both of which used the F702W (wide *R*) filter on WFPC2. Using the Lin et al. value for

$M_R^\star$, Hooper et al. found 15 of their 16 ($z \simeq 0.4$) quasars to have $L \geqslant L^\star$, while Boyce et al. found all 11 of their 14 objects for which a host model was fitted, to have $L \geqslant L^\star$ (both sets of results having been converted to our adopted cosmology).

6.2.2 *Nuclear luminosities*

The luminosities of the best-fitting nuclear components are listed in Table 5 and illustrated in Fig. 3, with subsample averages summarized below. The radio galaxy 0230−027 has been excluded from these summary statistics as the modelling code detected no unresolved component in this object.

$\langle M_R \rangle = -22.27 \pm 0.45$ median $= -23.36$ (all)
$\langle M_R \rangle = -19.27 \pm 0.64$ median $= -19.64$ (RG)
$\langle M_R \rangle = -24.07 \pm 0.22$ median $= -24.01$ (RLQ)
$\langle M_R \rangle = -22.95 \pm 0.57$ median $= -23.70$ (RQQ).

As expected, the unresolved nuclear components displayed by the RGs are nearly two orders of magnitude weaker than those of the RLQs, in good agreement with the orientation-based radio-loud unification scheme first described by Peacock (1987) and Barthel (1989) (see Section 6.7). It would appear from the mean figures given above that there is a substantial difference in the nuclear components of the RQQ and RLQ quasar samples. However, the noticeable offset in the difference between the mean and median figures, combined with examination of the histogram shown in Fig. 3, reveals that the RQQ mean is being biased by the three objects, which have total luminosities fainter than $M_V = -23.0$. If these three objects are excluded from the RQQ sample, the mean and median values of nuclear luminosity become

$\langle M_R \rangle = -23.95 \pm 0.26$ median $= -23.97$ (RQQ)

completely consistent with the equivalent RLQ figures. The similarity between the nuclear components of the RQQ and RLQ subsamples is reassuring considering that the sample-selection process was indeed originally designed to produce two quasar samples well matched in luminosity. This result also re-affirms that the measured difference in the respective host magnitudes of the RQQs and RLQs *cannot* be attributed to some bias arising from the RLQs in our sample having, on average, more powerful nuclei.

6.2.3 *Quasar host–nuclear luminosity correlation*

Because the measured difference between the RQQ and RLQ host-galaxy magnitudes is substantially greater than the average difference between their respective nuclear components (excluding the three subluminous objects) it is not expected that there should be a strong host–nuclear luminosity correlation. This is indeed the case, and application of the Spearman rank correlation test confirms that there is no evidence for any correlation, returning a probability $p = 0.95$ that the null hypothesis of no correlation is acceptable.

The null result found here contrasts with the positive correlations found previously by many authors (e.g. Smith et al. 1986; Bahcall et al. 1997; Hooper et al. 1997). The suspicion often cast upon the reality of a positive host-galaxy–nuclear correlation is that there are two obvious selection effects at work. The first of these is that it is obviously much more difficult to detect faint galaxies, which host brighter quasars. It seems clear that given the difficulties associated with ground-based seeing, and the perils of PSF subtraction on *HST* data (e.g. Bahcall et al. 1997), that this could well be a contributing factor. In the present study there are several RQQs with bright nuclear components, and relatively faint host galaxies (e.g. 0953+415), providing confidence that the techniques employed here have been successful in overcoming this possible source of false correlation. The other selection effect that could contribute to a false positive result is that weak AGN in bright host galaxies will not be classified as quasars.

Although the results presented here for powerful low-z quasars show no evidence for a correlation, it does appear to exist for lower-luminosity Seyfert galaxies. In the case of Seyferts, the reduction in both redshift and contrast between the host and nuclear components means that it can be confidently assumed that all of the host galaxies are being detected, removing one of the sources of bias mentioned above. Indeed, the work of McLeod & Rieke (1994) on two samples of low- and high-power AGN at low z has led them to suggest that the relation between host and nuclear luminosity is of the form that there is a minimum host luminosity required to produce a particular quasar luminosity. This would be consistent with both the positive correlation found at lower AGN power, and the flat relation found here for higher-powered quasars. The host galaxies for the quasars studied here have already been shown to be among the brightest known, and therefore demand that the galaxy–quasar relation tails-off at high quasar luminosity. The question of how the nuclear and host-galaxy luminosities relate to central black hole mass and quasar fuelling rate is pursued in Section 8.

6.3 Scalelengths

The best-fitting values of the host-galaxy scalelengths listed in Table 3 are displayed as histograms for the separate subsamples in Fig. 4. The average figures for the three subsamples are:

$\langle r_{1/2} \rangle = 12.23 \pm 1.00$ median $= 10.45$ (all)
$\langle r_{1/2} \rangle = 13.76 \pm 2.18$ median $= 11.27$ (RG)
$\langle r_{1/2} \rangle = 11.73 \pm 1.07$ median $= 11.28$ (RLQ)
$\langle r_{1/2} \rangle = 11.45 \pm 1.66$ median $= 9.30$ (RQQ).

Taking the median figures, the RG and RLQ subsamples can again be seen to be in remarkable agreement, while the RQQ hosts are $\sim$20 per cent smaller.

Galaxy half-light radii of $\simeq$10 kpc mark out these radio galaxies and quasar hosts as being giant elliptical galaxies. In a study of the galaxies in the Virgo cluster, Capaccioli, Caon & D'Onofrio (1992) found that beyond a scalelength of $\sim$3 kpc the only galaxies to be found were extremely luminous ellipticals, or cD-type brightest cluster galaxies (BCG). The question of how the properties of the host galaxies studied here relate to those of BCGs is explored further in Section 7. In further support of the radio-loud unification scheme the scalelength figures obtained here for the RG and RLQ subsamples can be compared with the B- and V-band study of Smith & Heckman (1990), who determined the scalelengths of 41 powerful radio galaxies in the redshift range $0 < z < 0.26$. The median scalelength figure determined is equivalent to $\sim$17 kpc in the cosmology adopted here, somewhat larger than the results presented above. However, if the comparison is restricted to the 22 objects studied by Smith & Heckman that have strong optical emission lines, more likely to have the same FR II morphology as the majority of radio-loud objects studied here, then the median scalelength falls to 13 kpc, in excellent agreement with the figures presented above.

If the host scalelengths are plotted against the integrated model luminosities, as in Fig. 5, a tight correlation is found, and a least-squares fit to these data produces a relation of the form $L \propto r^{0.75}$. This is in impressively close agreement with the corresponding result

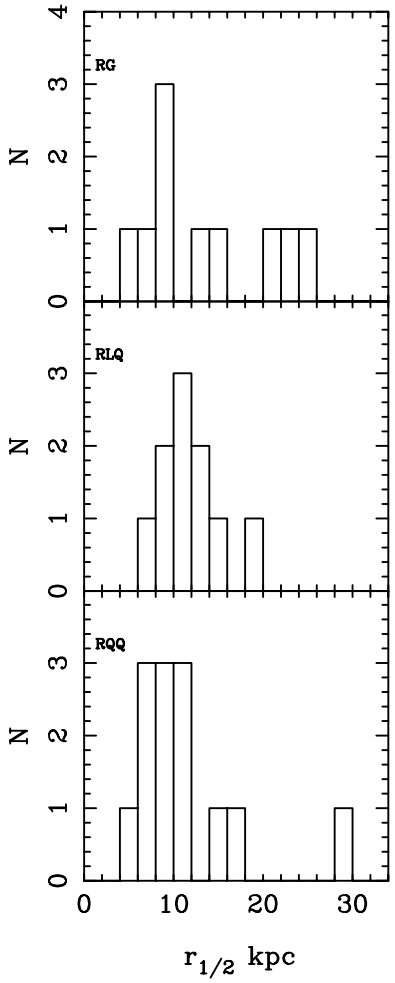

Figure 4. Histograms of the best-fitting host-galaxy scalelengths for the three AGN subsamples.

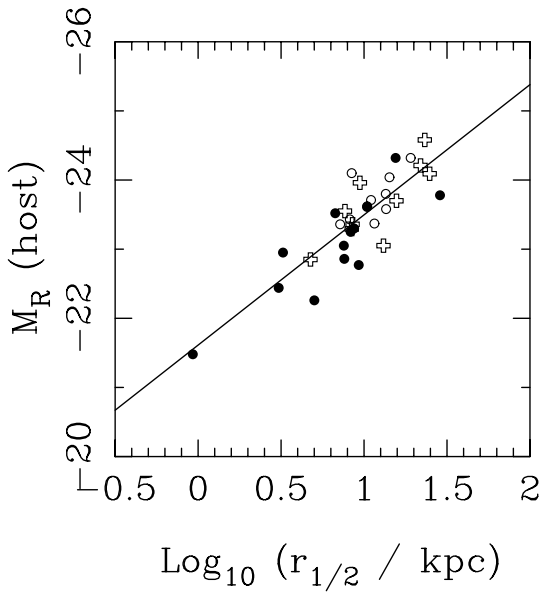

Figure 5. Plot of absolute host magnitude against the best-fitting host scalelength for the RGs (crosses), RLQs (open circles) and RQQs (filled circles) in the *HST* sample. The solid line is the least-squares fit to the data, which has the form $L \propto r^{0.75}$. For the four RQQs that required a combined disc/bulge fit, the best-fitting bulge parameters have been plotted.

$L \propto r^{0.70}$ found for low-z inactive ellipticals by Kormendy (1977). Given this result, it is obviously of interest to ask whether the best-fitting model parameters for $\mu_{1/2}$ and $r_{1/2}$ given in Table 3 do in fact yield a Kormendy relation of slope $\sim$3.

6.4 The Kormendy relation

The $\mu_{1/2}$–$r_{1/2}$ relation for the host galaxies of all 33 objects is shown in Fig. 6. For the four RQQ sources that have combined disc/bulge fits it is the parameters for the bulge component that have been plotted. The least-squares fit to the data (solid line) has the form

$$\mu_{1/2} = 2.90_{\pm 0.22} \log_{10} r_{1/2} + 18.35_{\pm 0.22} \quad \text{(all)}$$

(errors are $\pm 1\sigma$) showing for the first time from optical imaging, that the host galaxies of quasars lie on this photometric projection of the fundamental plane. The individual fits to the $\mu_{1/2}$–$r_{1/2}$ relations for the individual subsamples are:

$$\mu_{1/2} = 2.86_{\pm 0.32} \log r_{1/2} + 18.44_{\pm 0.36} \quad \text{(RG)}$$
$$\mu_{1/2} = 3.98_{\pm 0.71} \log r_{1/2} + 17.02_{\pm 0.75} \quad \text{(RLQ)}$$
$$\mu_{1/2} = 2.99_{\pm 0.34} \log r_{1/2} + 18.39_{\pm 0.30} \quad \text{(RQQ).}$$

It is readily apparent from the individual Kormendy relations that the RG and RQQ subsamples follow very similar relations, consistent with each other in terms of slope and normalization. One encouraging aspect of this is that the best-fitting bulge components for the RQQ objects that have combined disc/bulge model fits lie naturally on the Kormendy relation defined by the other nine, single-component RQQ hosts. With no restrictions placed on the range of parameter values available to the modelling code, the fact that the fitted bulge components have physically sensible values gives further confidence that the introduction of the combined disc/bulge fits was justified, and does not involve overfitting of the data.

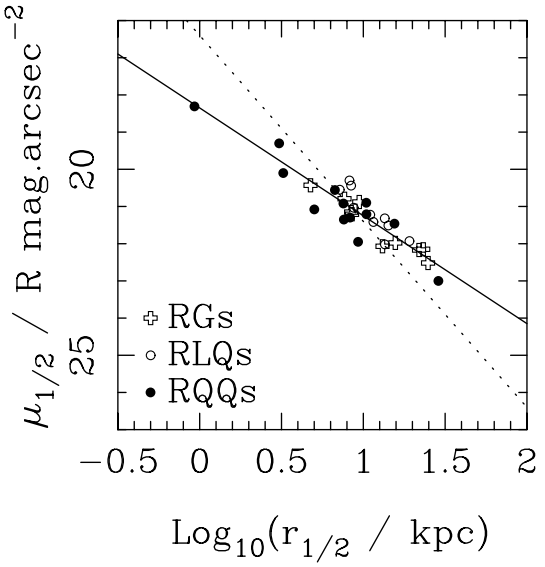

Figure 6. The Kormendy relation followed by the hosts of all 33 objects in the *HST* sample. For the four RQQs that have a significant disc component the best-fitting bulge component has been plotted. The solid line is the least-squares fit to the data, which has a slope of 2.90, in excellent agreement with the slope of 2.95 found by Kormendy (1977) for inactive ellipticals in the *B* band. The dotted line has a slope of 5, indicative of what would be expected if the scalelengths of the host galaxies had not been properly constrained (see the text).

It would appear from the individual fits given above that the RLQ subsample follows a steeper slope, compared with the best-fitting relation for the other two subsamples. It is also noticeable that the 1σ error returned by the least-squares fitting procedure is more than twice that returned from the fitting to the RG subsample (which also has 10 objects), suggesting that there may well be outliers within the RLQ subsample that are biasing the fit.

This is indeed the case, with two outlying RLQ hosts (1004+130, 2141+175), one of which (1004+130) is the most nuclear-dominated RLQ in the sample, apparently distorting the fit owing to the probable underestimation of their host-galaxy scalelengths. If these two objects are removed the best-fitting relation for the RLQ hosts becomes

$$\mu_{1/2} = 3.19_{\pm 0.67} \log_{10} r_{1/2} + 17.95_{\pm 0.72}. \quad (1)$$

Thus, with the exclusion of the two outlying RLQ hosts, the three Kormendy relations followed by the subsamples are internally consistent with each other and, perhaps more importantly, formally inconsistent with a slope of 5 which, as highlighted by Abraham, Crawford & McHardy (1992), would be a clear indication that the data and/or the modelling procedure employed to analyse the images is unable to break the $\mu_{1/2}$–$r_{1/2}$ degeneracy.

We stress this point here because some authors have claimed to have demonstrated that AGN hosts follow a Kormendy relation, when in fact the derived relation simply reflects a failure to constrain galaxy scalelengths. Indeed, some authors (e.g. de Vries et al. 2000) have even mistakenly interpreted a slope of 5 as evidence that AGN hosts do not follow the same Kormendy relation as normal giant ellipticals.

The reason that a 'pseudo-Kormendy relation' with a slope of 5 can be produced with inadequate data and/or modelling follows simply from the fact that the integrated luminosity of a galaxy model follows the relation

$$L_{\rm int} \propto I_{1/2} r_{1/2}^2, \quad (2)$$

where $I_{1/2}$ is the surface brightness at $r_{1/2}$. Given that $\mu_{1/2} \propto -2.5 \log I_{1/2}$, it follows that if the modelling procedure can successfully constrain the host luminosity, but not the scalelength, then the apparent best-fitting values of $\mu_{1/2}$ and $r_{1/2}$ will be randomly distributed along a relation obeying

$$\mu_{1/2} \propto 5 \log r_{1/2} \quad (3)$$

with appropriate normalization to fit the integrated luminosity. Owing to the fact that the host galaxies display a relatively small spread in luminosity (mean $M_R = -23.44$, $\sigma = 0.64$) it might be expected that, *if* our analysis were unable to accurately determine the individual host scalelengths, the resulting $\mu_{1/2} - r_{1/2}$ relation would be well fitted with a slope of 5 (as found by de Vries et al. 2000) and a normalization to match $M_R = -23.44$. Such a relation has the form

$$\mu_{1/2} = 5.0 \log_{10} r_{1/2} + 16.40 \quad (4)$$

and is plotted as the dotted line in Fig. 6. It is obvious from Fig. 6 that this relation is not consistent with the data, giving confidence that the methods of analysis employed here have allowed the accurate determination of the host-galaxy scalelengths.

The diagnostic power of Fig. 6 is discussed in the context of recent studies of the fundamental plane in Section 7.2.

6.5 Axial ratios

If the AGN host galaxies are indeed indistinguishable from massive inactive ellipticals then they should display an axial ratio distribution that is also identical. The axial ratio distribution of normal ellipticals is well studied and known to peak at values of $b/a \geqslant 0.8$ (Sandage, Freeman & Stokes 1970; Ryden 1992). The best-fitting axial ratios from the two-dimensional modelling are listed in Table 3 and displayed in the form of separate subsample histograms in Fig. 7. The corresponding mean and median values are:

$\langle b/a \rangle = 0.81 \pm 0.02$ median $= 0.85$ (all)
$\langle b/a \rangle = 0.86 \pm 0.03$ median $= 0.90$ (RG)
$\langle b/a \rangle = 0.80 \pm 0.05$ median $= 0.82$ (RLQ)
$\langle b/a \rangle = 0.78 \pm 0.03$ median $= 0.84$ (RQQ).

It can be seen from these figures that the axial ratio distributions of all three subsamples are perfectly consistent with that expected from a sample of elliptical galaxies. There is a slight suggestion that the RGs have higher axial ratios than average, but this is not formally significant.

The axial ratio results from the two-dimensional modelling agree well with the recently published findings of Boyce et al. (1998), who found that all 11 of the quasars from their 14-object ($z \simeq 0.3$) sample for which a model fit was possible, displayed axial ratios with $b/a > 0.65$. In contrast, Hooper et al. (1997) found only two of their 16 ($z \sim 0.45$) quasars to have axial ratios with $b/a > 0.6$. The reasons for this apparently contradictory result probably lie in a combination of the higher redshifts of the Hooper et al. objects, and their use of the PC instead of the WF detectors. As has been explained, these two factors will undoubtedly result in a reduced sensitivity to

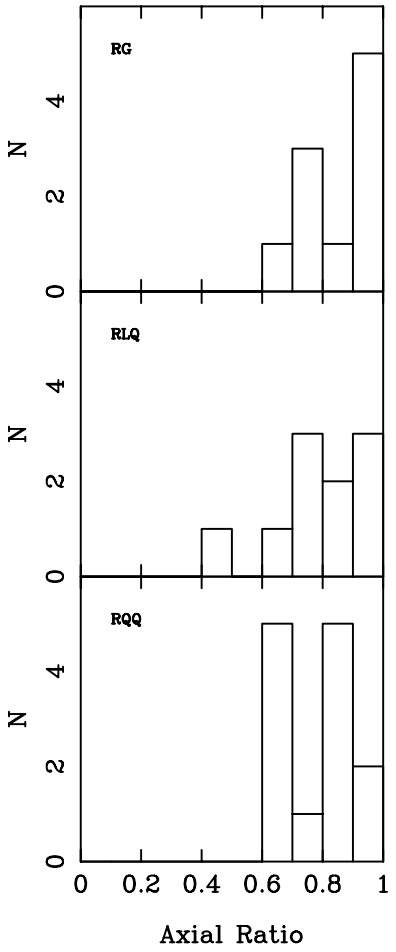

Figure 7. The axial ratio distributions for the three host-galaxy subsamples as determined by the two-dimensional modelling.

low-surface-brightness features, given that the exposure times used were the same as adopted in this study. In fact, Hooper et al. noted their concern that their modelling technique of two-dimensional cross-correlation could have been influenced by high-surface-brightness features such as bars or tidal tails. Given the clear result presented here, and the support of the Boyce et al. results at similar redshifts, this seems the most probable explanation of the Hooper et al. result.

6.6 Host-galaxy colours

The results presented in the latter five subsections strongly suggest that in terms of morphology, luminosity, scalelength, Kormendy relation and axial-ratio distribution, the hosts of powerful AGN are identical to normal, massive, inactive ellipticals. The one final parameter that can be readily recovered from the modelling is host-galaxy colour. The desire to obtain reliable optical–infrared colours for the host galaxies was one of the original motivations for this *HST* imaging study. Given that the results presented thus far suggest the host galaxies are otherwise normal massive ellipticals, it is now even more interesting to investigate whether the hosts also display the red colours associated with old stellar populations, or whether they have significantly bluer colours, indicative of either a generally young stellar population, or of substantial secondary star formation induced by interactions, the central AGN or both.

The simplest and most obvious way to calculate $R-K$ colours for the host galaxies is to combine the integrated optical magnitudes presented in Table 5 with the integrated absolute K-band magnitudes derived for the sample by Taylor et al. (1996). However, there are two potentially serious problems with this strategy. First, Taylor et al. did not always decide on the same host morphology as has now been revealed by the *HST* imaging, and so in some cases their quoted absolute K magnitude is derived from, for example, a disc fit that originally appeared marginally preferable to a de Vaucouleurs law. This obviously matters because the disc fits to the K-band data were 0.5–1.0 mag fainter than the equivalent elliptical fits. Secondly, in the light of the new, better-constrained models derived from the *HST* data, and the results of more recent tip-tilt infrared imaging reported by McLure et al. (2000), it is now clear that the half-light radii derived by Taylor et al. were systematically overestimated [most probably caused by the $\sim$1 arcsec seeing and coarse spatial resolution (0.62 arcsec pixel^{-1}) of the original K-band observations – see also Simpson, Ward & Wall 2000]. Given that the integrated luminosity of the standard de Vaucouleurs $r^{1/4}$-law is proportional to $I_{1/2}r_{\rm e}^2$, it is clear that scalelength errors of the order of 1.5–2 could seriously bias the integrated K-band luminosity.

Therefore, to obtain a robust value for the $R-K$ colour of each host from the existing data we proceeded as follows. First, the K-band luminosities were based on the best-fitting model with the same morphology as the equivalent *HST* result. Secondly, the $R-K$ colours were based on 12-arcsec diameter aperture photometry performed on both the *HST* and K-band model fits, to minimize the impact of scalelength errors on the derived colour, while at the same time including the vast majority (>75 per cent) of host-galaxy light.

The results of these host-galaxy $R-K$ calculations are listed in Table 5, with absolute $R-K$ histograms for the separate subsamples shown in Fig. 8. The absolute colours have been calculated assuming spectral indices of $\alpha = 1.5$ and 0.0 for the R and K bands, respectively.

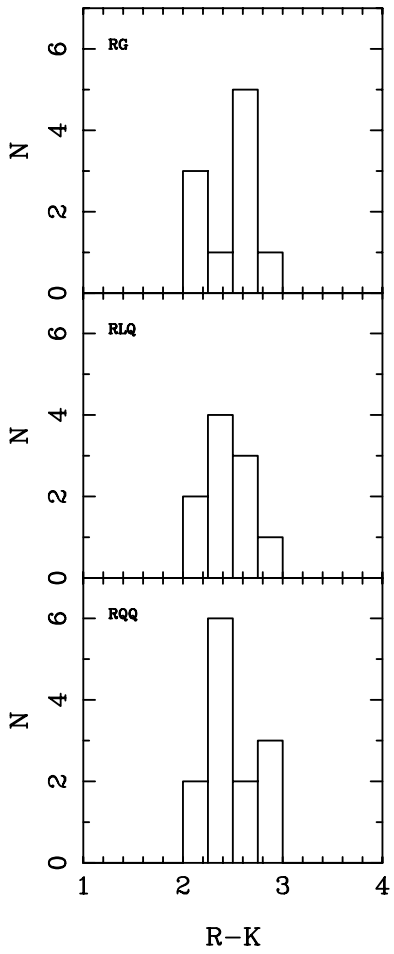

Figure 8. The rest-frame $R-K$ colours for the three host-galaxy subsamples. The three subsamples can be seen to be consistent with each other, tightly distributed around a value of $R-K \simeq 2.5$.

It is readily apparent from Fig. 8 that the colour distributions of the three subsamples are consistent with each other, with mean and median absolute colours:

$\langle M_R - M_K \rangle = 2.48 \pm 0.05$ median $= 2.44$ (all)
$\langle M_R - M_K \rangle = 2.47 \pm 0.09$ median $= 2.56$ (RG)
$\langle M_R - M_K \rangle = 2.48 \pm 0.07$ median $= 2.46$ (RLQ)
$\langle M_R - M_K \rangle = 2.48 \pm 0.08$ median $= 2.41$ (RQQ).

As demonstrated by Nolan et al. (2001) such colours are consistent with those expected of an evolved stellar population of age 10–13 Gyr. The homogeneity of these colours provides a further strong indication that the hosts of all three classes of AGN are derived from the same parent population of massive, well-evolved elliptical galaxies. The inevitable conclusion from this is that these galaxies, or at least the bulk of their stellar populations, must have formed at high redshift, a theme that is revisited in Section 9. The fact that the $R-K$ colours are so similar to passive ellipticals forces the further conclusion that any star formation associated with AGN activity must either be dust enshrouded, confined to tidal features masked from the modelling, or possibly restricted to the central $\sim$1 kpc of the host (in which case the additional emission would almost certainly be attributed to the unresolved nuclear component). Large-scale star formation involving a substantial fraction of the mass of the host galaxy, is effectively ruled out by these results.

6.7 Nuclear colours: implications for unified models of radio-loud AGN

The $R - K$ colours of the fitted nuclei for all 33 objects (except RG 0230−027, see above) are plotted against absolute nuclear R magnitude in Fig. 9. It is clear from this plot that there is no significant difference between the colours of the nuclei of the RQQs or RLQs. More importantly, however, this plot allows us to explore the relationship between the relatively weak nuclear components found in the RGs, and the (naturally) brighter components found in the RLQs.

This is of value because it allows us to perform another test of the proposed unification of RLQs and RGs by orientation (Peacock 1987; Barthel 1989). As discussed above, our host-galaxy results can already be viewed as providing strong support for such a picture, owing to the fact that the basic properties (i.e. luminosity, size, axial ratio, age, etc.) of the RGs and RLQ hosts in our matched samples are indistinguishable. However, it must also be realized that identical RG and RLQ host galaxy properties would also be expected in a scenario where the two classes of radio-loud AGN are in fact linked by evolution in time, rather than by orientation.

Fig. 9 offers the possibility of differentiating between these two alternative explanations, by allowing us to test whether the $R - K$ colours of the RG nuclear components are consistent with dust-obscured quasar nuclei. If it is assumed that the reddening of the RG nuclei obeys a $\kappa_\lambda \propto \lambda^{-1}$-law, then the reddening vector, which should connect the RGs and RLQs in Fig. 9 would be expected to be given by $E(R - K) = 0.70A_R$.

In fact, the slope of the least-squares fit in Fig. 9 (solid line) is 0.68 ± 0.05, which corresponds to a dust reddening law $\kappa_\lambda \lambda^{-0.95\pm0.15}$. Furthermore, if the fitted R-band nuclear components of the RGs are dereddened using a slope of 0.68, until each object has the mean colour of the RLQ nuclei ($R - K = 3.0$), then the mean luminosity of the dereddened RG nuclei is $M_R = -23.90 \pm 0.46$. It can be seen that this is perfectly consistent with the previously determined mean nuclear luminosity of the RLQ sample, $M_R = -23.73 \pm 0.10$. Given the clean nature of this result, there seems little room for argument that the RG and RLQ subsamples are most consistent with being drawn from the same population of objects, viewed from different orientations, with every RG displaying evidence of a buried quasar nucleus.

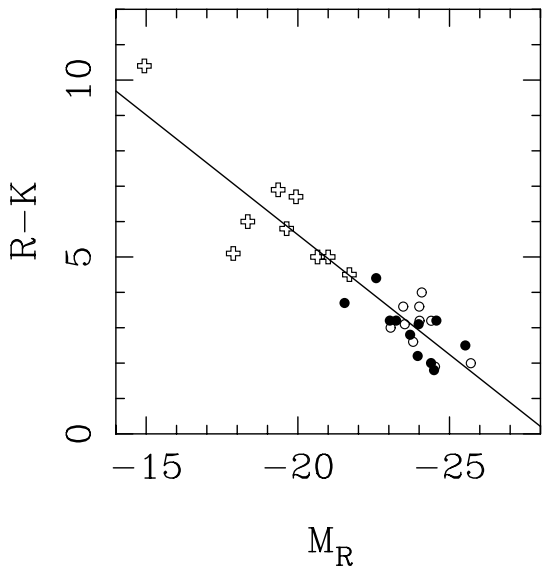

Figure 9. A plot of apparent $R - K$ colour versus absolute R-band luminosity of the fitted nuclear components of the objects in the *HST* sample. Shown in the plot are the RG nuclei (crosses), RLQ nuclei (open circles) and RQQ nuclei (filled circles). Also shown is the least-squares fit to the data that has a slope of 0.68 ± 0.05.

7 THE RELATION OF QUASAR HOSTS TO 'NORMAL' GALAXIES

7.1 Dependence of host morphology on nuclear luminosity

In the preceding section we presented a series of results that together lead to the inescapable conclusion that the hosts of virtually all powerful AGN are essentially normal, massive ellipticals. This result is particularly clean for the radio-loud objects in our sample. However, exceptions to any rule are often of great significance, and one should not ignore the fact that we have found two disc-dominated hosts in our RQQ sample, along with two bulge-dominated RQQ hosts that do, however, possess significant disc components.

What might such exceptions to the general 'perfect elliptical' rule be telling us? An important clue comes from the fact that, as discussed above, the two disc-dominated hosts in our sample transpire to contain the two least-luminous nuclei. Indeed, in much of the preceding analysis, these two objects have had to be deliberately excluded from sample comparisons owing to the fact that they are not actually luminous enough to be classed as quasars. However, the fact that these two radio-quiet low-luminosity interlopers are the only RQQs in our sample with disc-dominated hosts strongly suggests that host morphology is a function of nuclear *optical* luminosity.

Our own samples do not span a sufficient range in optical luminosity to allow a statistical test of this hypothesis. However, we can explore this possibility, and place our results in a wider context, by combining them with those of Schade, Boyle & Letawsky (2000) who have studied the morphologies of the host galaxies of a large sample of X-ray-selected AGN spanning a wider but lower range of optical luminosities. This we have done in Fig. 10, which shows the ratio of bulge-to-total host luminosity plotted as a function of nuclear optical power.

This instructive diagram illustrates a number of important points. First, it shows that while pure spheroidal galaxies can host AGN with optical luminosities ranging over two orders of magnitude, very disc-dominated hosts start to die out for $M_V(\mathrm{nucl}) < -21$ and no disc-dominated galaxies appear capable of hosting nuclear emission more luminous than $M_V \simeq -23$ (close to the traditional, albeit rather ad hoc, quasar–Seyfert classification boundary). Secondly, this plot confirms that the two most 'discy' hosts uncovered in the present study do indeed lie in a region of the parameter space where disc-dominated host galaxies are quite common. Thirdly, in the context of this diagram, the persistence of significant discs around two of the more luminous RQQs in our sample (0052+251 and 0157+001) seems perfectly natural, and certainly not inconsistent with the clear trend towards more spheroid-dominated hosts with increasing nuclear output.

Fig. 10 clarifies the origin of much of the confusion that has surrounded the nature of RQQ hosts. In particular, it is clear that studies of RQQ samples that extend to include significant numbers of objects with nuclei less luminous than $M_V \simeq -23$ are likely to uncover significant numbers of hosts with substantial discs, in contrast to the results of the present study. This does indeed appear to be the case. For example, Bahcall et al. (1997) and Hamilton, Casertano & Turnshek (2002) have reported that approximately one-third to

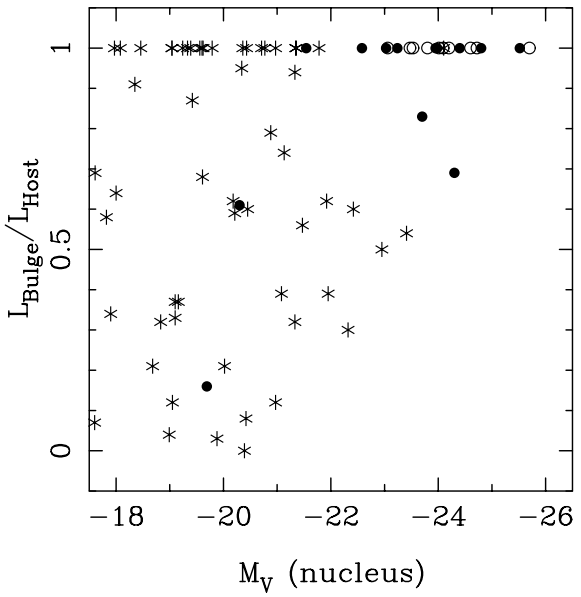

Figure 10. A plot of relative contribution of the bulge/spheroidal component to the total luminosity of the host galaxy versus absolute V-band luminosity of the fitted nuclear components. The plot shows the results for our own *HST* sample (RLQs as open circles, RQQs as filled circles) along with the results from Schade et al. (2000) for a larger sample of X-ray-selected AGN (stars). This plot illustrates very clearly how disc-dominated host galaxies become increasingly rare with increasing nuclear power, as is expected if more luminous AGN are powered by more massive black holes that in turn are housed in more massive spheroids.

one-half of radio-quiet quasars lie in disc-dominated hosts. However, if one restricts their results to quasars with nuclear magnitudes $M_V < -23.5$ (for which we find 10 out of 11 RQQs lie in ellipticals), it transpires that six out of the seven remaining objects in the Bahcall et al. study lie in ellipticals, while 17 out of the remaining 20 objects in the archival study of Hamilton et al. also have elliptical host galaxies.

Fig. 10 is also at least qualitatively as expected if AGN are, in fact, drawn at random from the general galaxy population, subject to the constraint that the host galaxy contains a black hole of sufficient mass to produce the observed nuclear output (see also Wisotzki, Kuhlbrodt & Jahnke 2001). As discussed further in Section 8, a black hole mass $m_{bh} > 5 \times 10^8$ M$_\odot$ appears to be required to produce a quasar with $M_V < -23.5$. When this constraint is combined with the now apparently inescapable result that black hole mass is proportional to spheroid mass $M_{bh} \simeq 0.001$–$0.003 M_{sph}$, then Fig. 10 can be viewed as a simple manifestation of the fact that spheroids in the present-day Universe with baryonic masses $>3 \times 10^{11}$ M$_\odot$ are rarely accompanied by significant discs (and are thus classed as massive ellipticals).

This conclusion leads naturally to the question of why most massive black holes in the present-day Universe should be inactive, while a subset are receiving sufficient fuel to shine as quasars. Below we present the results of a series of statistical comparisons designed to decide whether there are, in fact, *any* significant observable differences between the hosts (and host environments) of quasars and comparably massive, but inactive, elliptical galaxies.

7.2 Comparison with ULIRG merger remnants

Before proceeding to compare quasar hosts with old passively evolving massive ellipticals, it is worth pausing to consider whether host galaxies with the properties we observe could plausibly be produced as the outcome of a (relatively recent) violent merger of two disc galaxies. This might already seem fairly implausible given the series of results presented in Section 6, in particular the red host-galaxy colours consistent with old evolved populations. Nevertheless, it is well known from both simulations (Barnes & Hernquist 1992) and observations that the red→infrared light from ULIRGs often follows an $r^{1/4}$-law (Wright et al. 1990; Scoville et al. 2000) and it is possible that dust extinction in such objects could also produce red colours (albeit such colours would be unlikely to mimic the properties of an evolved population so well, as discussed by Nolan et al. 2001. Moreover, several authors have proposed an evolutionary scheme in which ULIRGs might evolve into radio-quiet quasars on a time-scale <1 Gyr (Sanders & Mirabel 1996).

Fortunately, the data on quasar hosts presented here are of sufficiently high quality to completely exclude the possibility that they are the recent outcome of the violent disc–disc mergers that appear to be the origin of most ULIRGs in the low-redshift universe. While it is true that ULIRGs such as Arp220 have surface-brightness profiles well described by an $r^{1/4}$-law, recent observations (Genzel et al. 2001) have shown that such remnants lie in a completely different region of the fundamental plane than that which we have shown is occupied by quasar hosts. Specifically, the effective radii of ULIRGs is typically $\simeq$1 kpc, an order of magnitude smaller than the typical effective radii of the quasar hosts as illustrated in Figs 4–6.

Indeed, one can go further and conclude that, whereas ULIRGs can be the progenitors of the population of intermediate-mass ellipticals that display compact cores and cusps (Faber et al. 1997), the quasar hosts lie in a region of the μ_e–r_e plane that is occupied by boxy, giant ellipticals with large cores, a large fraction of which lie in the centres of clusters (Faber et al. 1997). This is demonstrated in Fig. 11 where we have constructed a composite R-band Kormendy

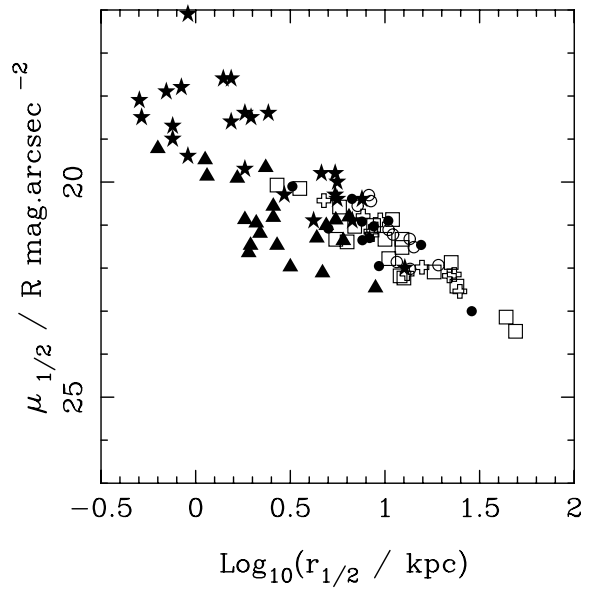

Figure 11. A comparison of the properties of the AGN hosts with those displayed by various other types of spheroid on the photometric projection of the fundamental plane. Symbols for the quasar hosts and radio galaxies are as in Figs 5 and 6. The stars are the data for ULIRGs and LIRGs from Genzel et al. (2001) transformed from the infrared to the R band assuming $R - K = 2.5$. Triangles and squares indicate the positions of 'discy' and 'boxy' ellipticals from Faber et al. (1997) after conversion to $H_0 = 50$ km s^{-1} Mpc^{-1}.

Table 6. The model results for the four brightest galaxies in each of five clusters obtained from the *HST* archive, spanning a range in richness from Abell Class 0 to Abell Class 4. The redshifts of the clusters are 0.11, 0.19, 0.23, 0.175 and 0.171, respectively. The images of A0018, A0103 and A2390 were taken through the F702W (wide *R*) filter. The images of A2390 and A1689 were taken through the F814 (*I*-band) filter. The conversion between *I*- and *R*-magnitudes has been performed assuming $R - I = 0.8$ (Fukugita et al.). The final reduced images had a signal-to-noise ratio comparable to the *HST* host-galaxy data.

Galaxy	Class	0	Class	0	Class	1	Class	4	Class	4
	Abell	0018	Abell	0103	Abell	2390	Abell	1689	Abell	2218
	r_e (kpc^{-1})	M_R	r_e (kpc^{-1})	M_R	r_e (kpc^{-1})	M_R	r_e (kpc^{-1})	M_R	r_e (kpc^{-1})	M_R
1	30.5	−22.65	24.9	−23.62	27.8	−24.52	75.8	−25.33	100.5	−25.51
2	25.4	−22.50	3.4	−22.74	21.2	−23.14	59.0	−24.70	51.9	−24.54
3	16.6	−21.47	7.6	−22.69	12.1	−22.99	18.7	−23.62	35.7	−23.68
4	5.2	−21.14	7.6	−22.69	4.1	−22.21	7.6	−23.50	28.8	−23.29

diagram, combining our own results on the 31 bulge-dominated AGN hosts with the data from Genzel et al. (2001) on LIRGs and ULIRGs, and the data from Faber et al. (1997) on 'discy' and 'boxy' ellipticals.

This plot provides strong evidence that the quasar hosts belong to the class of large 'boxy' ellipticals, which various authors have suggested form at earlier times than their lower-mass 'discy' counterparts (Kormendy & Bender 1996; Faber et al. 1997).

In summary, all the available evidence indicates that luminous low-redshift quasars are the result of the retriggering of a massive black hole at the centre of an old evolved elliptical, and do not generally occur in the remnants of the recent disc–disc mergers that power ULIRGs. While there is one RQQ in our sample that is also a ULIRG (0157+001), in this case it is clear that at least one of the merging galaxies already has a massive spheroid capable of containing a pre-existing massive black hole. Thus, while there is clearly some overlap between the ULIRG and quasar phenomenon, present evidence suggests that, at least at low redshift, the ULIRG $\rightarrow$ quasar evolutionary route can only apply to a fairly small subset of objects.

7.3 Comparison with brightest cluster galaxies

Having established that the hosts of quasars are massive ellipticals, it is then of interest to explore how their properties compare with those of inactive comparably massive ellipticals at similar redshift. In this subsection we compare the properties of the quasar hosts, and in particular their scalelengths, with those of bright galaxies found in rich clusters. This comparison is motivated, in part, by the location of the host galaxies on the μ_e–r_e projection of the fundamental plane as discussed in the previous subsection. However, this motivation is further strengthened by the results of a study of the environments of the quasars and radio galaxies undertaken by McLure & Dunlop (2000). McLure & Dunlop (2000) used the full WFPC2 images of our AGN sample to measure the spatial clustering amplitude (B_{gq}). This quantity is inevitably rather poorly constrained for each individual object, but, on average, they found that all three classes of AGN typically inhabit environments as rich as Abell Class $\simeq$ 0. Moreover, several objects appeared to lie in noticeably richer environments (Abell Class 1).

Given these clustering results, and the fact that the quasar hosts are clearly comparable to many BCGs in terms of optical luminosity, it is interesting to explore whether the sizes of the quasar hosts are as expected in the light of their apparent cluster environment. Strong circumstantial evidence that the quasar host galaxies are directly comparable to first-ranked cluster galaxies comes from a comparison of the host-galaxy Kormendy relation with that found for cD galaxies by Hamabe & Kormendy (1987) in the *B* band:

$$\mu_{1/2} = 2.94 \log_{10} r_{1/2} + 20.75. \quad (5)$$

If a typical elliptical galaxy colour at $z = 0.2$ of $B - R = 2.4$ is assumed (Fukugita et al. 1995), then the inferred *B*-band Kormendy relation for all 33 objects in the *HST* sample presented in Section 6.4 becomes

$$\mu_{1/2} = 2.90 \log_{10} r_{1/2} + 20.75, \quad (6)$$

which can be seen to be in excellent agreement with the Hamabe & Kormendy result.

To explore further the connection between host cluster environment and galaxy size, a sample of 51 first-ranked cluster galaxies (confined to the same redshift range as the *HST* sample but spanning a range of Abell classes) was constructed from the study of Hoessel & Schneider (1985). Application of the Kolmogorov–Smirnov (KS) test to the scalelength distributions of the AGN host galaxies, and the 14 first-ranked cluster galaxies in this sample from Abell clusters of Classes 0 and 1, shows that the two are not significantly different ($p = 0.22$). However, the extension of the comparison sample to include the first-ranked galaxies of Abell Class 2 clusters (15 objects), shows these two distributions to be different at the 2σ level ($p = 0.011$).

This is a very interesting result because it provides independent support for the results of the cluster analysis of McLure & Dunlop (2000), which also favour an environment more consistent with Abell Class 0, or at most (in only a few cases) Abell Class 1.

Finally, to check that the ground-based results discussed above can be confirmed by modelling of more recent *HST* data, and to minimize possible systematic errors, we decided to model a series of *HST* images of bright cluster galaxies (at comparable redshift to our quasars) using the same 2D modelling code used to model the AGN hosts. *HST* WFPC2 images of five Abell clusters with similar redshifts to the objects in the *HST* sample were therefore retrieved from the *HST* archive facility.[1] Following the production of reduced images of comparable signal-to-noise ratio to the host galaxy images, the four brightest galaxies in each cluster were identified and modelled in identical fashion to the AGN hosts. The results of the elliptical model fits to these 20 galaxies are presented in Table 6.

The scalelengths and absolute magnitudes listed for the BCGs in Table 6 can be instructively compared with the corresponding quantities for the AGN hosts listed in Tables 3 and 5. First, it is clear that none of our AGN hosts is comparable in size to either the

[1] http://archive.stsci.edu

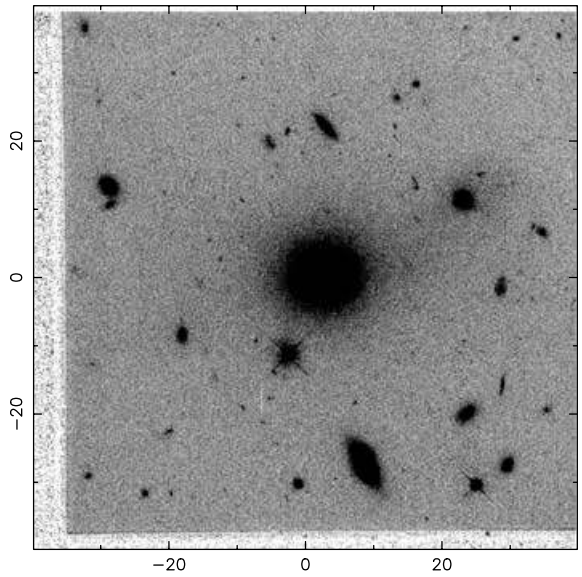

Figure 12. The full WF2 image of the radio galaxy 1342−016 covering an area of 80 × 80 arcsec^2. A large number of companion objects can be seen which, if at the redshift of the quasar, would appear consistent with a moderately rich cluster environment.

first- or second-ranked cluster galaxies in very rich, Abell Class 4 clusters. However, the *largest* of the AGN hosts are comparable in size to the first- or second-ranked galaxies in the Abell Class 0 and Class 1 clusters. This more detailed galaxy-by-galaxy comparison thus provides further support for the basic conclusions of McLure & Dunlop (2000) already mentioned above. Indeed, at least within the radio-loud subsamples, there is a suggestion of a rather clean link between the biggest galaxies and the richest cluster environments. Specifically, the two radio galaxies found by McLure & Dunlop (2000) to have the richest environments [1342−016 (see Fig. 12) and 0917+459] transpire (see Table 3) to be two out of the three RGs with $r_e > 20$ kpc. Moreover, both the values of B_{gq} for these objects ($\simeq$1500 and $\simeq$1000) and their half-light radii both point towards the same conclusion (given Table 6), namely that these most massive hosts are the first- or second-ranked BCGs in clusters of richness Abell Class 0–1. A similar remarkably clean correspondence can be found within the RLQ sample. The two RLQs found by McLure & Dunlop (2000) to have the richest environments (2349−014 and 0137+012) transpire (see Table 3) to be the only two RLQs with hosts for which $r_e > 14$ kpc. However, no such clean correspondence is evident within the RQQ sample. This may mean that RQQs, even when found in cluster environments, are less likely to be central cluster galaxies than their radio-loud counterparts. However, given the large errors on B_{gq} such a conclusion may perhaps be premature.

In summary, this comparison of the properties of the hosts of powerful AGN and bright cluster galaxies supports the basic conclusion reached by McLure & Dunlop (2000) via the completely independent measure of clustering amplitude. The larger AGN hosts have properties comparable to first- or second-ranked BCGs in Abell Class 0–1 clusters. Both radio-loud and radio-quiet quasars thus appear to occur in a range of environments, which is certainly consistent with the range of environments occupied by inactive ellipticals of comparable size and luminosity. While none of our host galaxies are comparable to the largest known BCGs, we must caution that this does not mean AGN avoid such environments (as has sometimes been inferred for FRII radio sources from the results of, for example, Prestage & Peacock 1988). In fact, because Abell Class 3 and 4 clusters are very rare, with a number density less than $<1.6 \times 10^{-6}\ h^3$ Mpc^{-3} (Croft et al. 1997), even an all-sky survey covering the redshift band of this study ($0.1 < z < 0.25$) would be expected to contain $<$1500 such rich clusters. Consequently, given that only one in $\simeq$1000–10 000 massive black holes appears to be active in the present-day Universe (see Section 9 and Wisotzki et al. 2001), we should not be surprised by the fact that no low-redshift quasar has yet been found to lie within such a rich environment or hosted by an ultramassive BCG.

7.4 Interactions

It is often stated in the literature (e.g. Smith et al. 1986; Hutchings & Neff 1992; Bahcall et al. 1997) that morphological disturbance is a common feature of the host galaxies of powerful AGN. In fact, at first sight, the *R*-band images presented in Appendix A and in McLure et al. (1999) show a relatively low occurrence of morphological disturbance, with only three objects (1012+008, 2349−014 and 0157+001) undergoing obvious, large-scale, interactions. However, as can be seen from the model-subtracted images, the removal of the best-fitting axisymmetric model for each host galaxy does reveal the presence of peculiarities such as excess flux, tidal tails and close companions, at lower surface-brightness levels. It is tempting to conclude from this that many of these AGN may have been triggered into action by recent interaction with companion objects. However, the true significance of the levels of interaction seen in the AGN host galaxies can only be judged by comparison with an equally detailed investigation of the morphologies of a control sample of comparable, inactive galaxies. Here we attempt to quantify the significance of such peculiarities by constructing a control sample based on the 20 bright cluster galaxies taken from the *HST* archive discussed in the previous subsection.

With the range of redshifts covered by the five Abell clusters it was possible to construct 19 object pairs, each consisting of one of our AGN sample paired with a suitable control, drawn from the 20 cluster galaxies. Model-subtracted images of each of the galaxy pairs were then assessed in a blind test for the occurrence of four possible indicators of disturbance or interaction, i.e.

(i) residual tidal/spiral arm features;
(ii) residual asymmetric flux;
(iii) residual symmetric flux;
(iv) companion object inside a 10− arcsec radius,

where neither the identity of the AGN, nor which object in each pair was active, was known to the decision maker. The results of this process are shown in Table 7.

The one clear result of this test is that, taken as a group, the active galaxies display a greater occurrence of tidal/spiral arm features in their model-subtracted images than the control sample. There is no significant difference in the other three indicators. It is noteworthy, however, that of the six occurrences of tidal/spiral arms, only one of these (2349−014) is a radio-loud object. To test whether or not this indicates an inherent difference between the radio-loud and

Table 7. The results of the blind test to determine any difference in the prevalence of features indicative of interaction or disturbance in the AGN sample (active) compared with inactive galaxies, using 20 BCG as an inactive control sample (see the text for details).

Object type	Tidal/spiral	Asymmetric flux	Symmetric flux	Companion
Active	5	8	5	7
Inactive	0	10	7	9

Table 8. The results of the blind test to determine whether any differences exist in the occurrence of features indicative of interaction or disturbance between the AGN subsamples (see the text for details).

Object type	Tidal/spiral	Asymmetric flux	Symmetric flux	Companion
RQQ	6	5	1	2
RLQ	1	6	2	4
RG	0	4	2	3

radio-quiet AGN, the blind test was repeated for all 33 *HST* objects, without control galaxies, but still keeping the identity of each AGN secret, in order to prevent any subconscious bias. The results of this test are presented in Table 8.

Several features of the results presented in Table 8 merit comment. First, it can be seen that there is no significant difference between the RG and RLQ subsamples, consistent with all the other results presented in this paper. Secondly, it would initially appear that there is a significant difference between the radio-loud objects and the RQQ subsample in terms of the occurrence of tidal/spiral arm features. However, an examination of which of the RQQs are contributing to this result shows that four of them are the objects that have combined disc/bulge model fits. Therefore, if the comparison is restricted to include only those RQQs with single-component elliptical host galaxies, this apparent difference disappears.

The results of these blind comparison tests thus support two separate conclusions. First, the finding that there are no detectable differences between the elliptical AGN host galaxies and the BCG control sample provides further evidence that these two classes of object are directly comparable. Secondly, the apparently more frequent occurrence of tidal/spiral arm features in the RQQ subsample is only a manifestation of the previously determined fact that a minority of RQQ host galaxies, two of which are not actually true quasars, have substantial disc components, and thus does not provide evidence for an inherent difference in interaction rates between radio-quiet and radio-loud objects.

Perhaps one should not be surprised by the lack of evidence for spectacular large-scale ULIRG-like interactions in our quasar sample, given that as described below, the activation of a quasar requires the delivery of only $\simeq$1 $M_\odot$ yr^{-1} to the central black hole.

8 THE AGN–HOST CONNECTION

As discussed by McLure et al. (1999), our finding that the hosts of quasars are almost all spheroidal galaxies allows exploitation of the now well-established correlation between black hole mass and spheroid mass to estimate the masses of the central black holes in these objects, completely independent of any of their observed *nuclear* properties. We can then use this information to explore which, if any, of the observed properties of the AGN are linked to black hole mass.

In this section we revisit this issue for a number of reasons. First, of course, our matched subsamples are now complete. Secondly, in the intervening 2 years the application of three-integral models has resulted in a revising down of the constant of proportionality between $M_{\rm bh}$ and $M_{\rm sph}$ from 0.006 (Magorrian et al. 1998) to $\simeq$ 0.003–0.001 (Kormendy & Gebhardt 2001). Thirdly, independent estimates of the black hole mass in a substantial number of our AGN have now been made on the basis of nuclear Hβ linewidth by McLure & Dunlop (2001). Fourthly, the new VLA data presented in Section 4 mean that we can now explore the relationship between black hole mass and radio luminosity without being hampered by a large number of upper limits within the 'radio-quiet' subsample.

8.1 The black hole spheroid connection

As summarized by Kormendy & Gebhardt (2001), 'reliable' black hole mass estimates are now available for at least 37 nearby galaxies. As a result of this now substantial sample, clear correlations have been uncovered between the black hole mass and the host-spheroid luminosity, and between the black hole mass and the host stellar velocity dispersion. It has been claimed that the latter is the tighter correlation, indicating that the basic physical link is with spheroid mass. Since in the present study we do not possess measurements of host stellar velocity dispersions, we obviously have to estimate the host spheroid mass on the basis of the spheroid luminosity returned by our 2D modelling. However, a recent re-analysis of the bulge luminosities of low-redshift galaxies indicates that the relationship between bulge luminosity and black hole mass is in fact just as tight as that between black hole mass and central galaxy velocity dispersion (McLure & Dunlop 2002).

To estimate black hole masses on the basis of host spheroid luminosities we have therefore adopted the following relations, while acknowledging the significant scatter present in both:

$$M_{\rm sph} = 0.00123L^{1.31} \quad (7)$$

$$M_{\rm bh} = 0.0025M_{\rm sph} \quad (8)$$

consistent with the mass-to-light ratio relation for ellipticals determined by Jørgensen, Franx & Kjaergaard (1996) and the results of Gebhardt et al. (2000). We note that while these conversion factors are certainly also consistent with those quoted in the recent review by Kormendy & Gebhardt (2001), there is now a growing body of evidence that the true conversion factor between $M_{\rm sph}$ and $M_{\rm bh}$ may be a factor of $\simeq$ 2 lower than that adopted here (Merritt & Ferrarese 2001; McLure & Dunlop 2002). If one wishes to adopt this lower factor (i.e. $M_{\rm bh} = 0.0013\ M_{\rm sph}$) then the estimates of black hole mass utilized in the analyses that follow in the remainder of this paper can simply be divided by a factor of 2. Obviously, none of the arguments concerning relative masses is affected by this uncertainty, and indeed none of the physical arguments is significantly altered by such a further modest reduction in the black hole mass estimates.

The results of applying these relations to calculate inferred bulge and black hole masses are presented in Table 9. Also given in Table 9 (column 4) are black hole masses derived for the majority of the quasars in these samples by McLure & Dunlop (2001) on the basis of assuming that the Hβ-producing broad-line clouds are in Keplerian orbits.

The new spheroid-based black hole estimates are compared with the Hβ-derived values in Fig. 13. This diagram shows that, with few exceptions, there is very good agreement ($\simeq$0.2 dex) between the two completely independent estimates of black hole mass. Indeed, given the well-known uncertainties in both approaches, the level of agreement demonstrated by Fig. 13 can be viewed as adding considerable credence to the estimated values of black hole mass, and indeed also provide support for the basic premise of a gravitationally bound broad-line region as assumed by McLure & Dunlop (2001, 2002). The fact that four objects (three visible on the diagram) have Hβ-based black hole masses that lie well below the corresponding host-spheroid-derived values is not really surprising since the Hβ linewidth analysis is clearly capable of yielding a severe underestimate of black hole mass for any object the

Table 9. The results of estimating black hole mass from the *R*-band luminosity of the host spheroid. Columns two and three list the predicted galaxy spheroid mass and central black hole mass, respectively. For comparison with the results given in column 3, column 4 gives the black hole mass estimates as derived from the Hβ linewidth by McLure & Dunlop (2001). Column 5 lists the predicted absolute *R*-band Eddington luminosity of the black hole, calculated according to the prescription given in Section 8.1. Column 6 gives the ratio of the predicted Eddington luminosity to the best-fitting nuclear model component.

Source	$m_{\rm sph}/10^{11}$ M$_\odot$	$m_{\rm bh}/10^9$ M$_\odot$	$m_{\rm bh-H\beta}/10^9$ M$_\odot$	M_R (Eddington)	$L_{\rm nuc}/L_{\rm edd}$
RG					
0230−027	4.8	1.2			
0307+169	7.9	2.0			
0345+337	2.6	0.7			
0917+459	10.6	2.6			
0958+291	3.8	0.9			
1215+013	2.1	0.5			
1215−033	3.8	0.9			
1330+022	5.8	1.4			
1342−016	16.7	4.2			
2141+279	9.3	2.3			
RLQ					
0137+012	8.7	2.2	1.1	−28.2	0.013
0736+017	5.0	1.3	0.3	−27.6	0.035
1004+130	9.4	2.3	3.7	−28.3	0.089
1020−103	3.8	1.0	0.7	−27.4	0.028
1217+023	5.9	1.5	0.8	−27.8	0.043
2135−147	3.9	1.0	2.6	−27.4	0.049
2141+175	4.2	1.1	1.7	−27.5	0.061
2247+140	6.5	1.6	0.1	−27.9	0.022
2349−014	12.2	3.1	1.8	−28.6	0.014
2355−082	5.3	1.3	0.7	−27.7	0.014
RLQ					
0052+251	2.3	0.6	0.6	−26.8	0.107
0054+144	5.2	1.3	2.5	−27.7	0.052
0157+001	12.2	3.1	0.2	−28.6	0.011
0204+292	3.6	0.9	0.6	−27.3	0.020
0244+194	1.9	0.5	0.3	−26.6	0.046
0257+024	0.4	0.1		−24.9	0.008
0923+201	3.4	0.8	2.6	−27.2	0.088
0953+414	2.1	0.5	0.7	−26.6	0.355
1012+008	6.4	1.6	0.02	−27.9	0.026
1549+203	1.0	0.3		−25.9	0.169
1635+119	3.2	0.7	0.4	−26.9	0.007
2215−037	4.7	1.2		−27.6	0.010
2344+184	1.3	0.3		−26.8	0.002

broad-line region of which is orbiting close to the plane of the sky (but should be incapable of yielding a comparably serious overestimate of black hole mass). Thus for 2247+140, 0736+017, 0157+001 and 1012+008 there is a good reason for trusting the black hole mass estimates of $\simeq 10^9$ M$_\odot$ given in column 3 of Table 9, more than the lower values yielded by the Hβ analysis in column 4.

Accepting this, and excluding the two low-luminosity RQQs, the third column of Table 9 shows that a black hole of minimum mass $M_{\rm bh} > 5 \times 10^8$ M$_\odot$ appears to be required to produce a nuclear luminosity corresponding to $M_R < -23$.

Beyond confirming the basic plausibility of the black hole mass estimates, the most interesting result contained in Fig. 13 is that, as suggested by the initial results of McLure et al. (1999), the black hole masses in the radio-loud quasars are systematically larger than in their radio-quiet counterparts. In terms of summary statistics of central tendency, this difference, although clear, might not appear very dramatic – specifically, excluding the two low-luminosity RQQs:

$$\langle M_{\rm bh}/10^9 {\rm M}_\odot \rangle = 1.67 \pm 0.36 \quad {\rm median} = 1.3 \quad ({\rm RG})$$
$$\langle M_{\rm bh}/10^9 {\rm M}_\odot \rangle = 1.64 \pm 0.22 \quad {\rm median} = 1.4 \quad ({\rm RLQ})$$
$$\langle M_{\rm bh}/10^9 {\rm M}_\odot \rangle = 1.05 \pm 0.24 \quad {\rm median} = 0.8 \quad ({\rm RQQ}).$$

However, the difference becomes more striking when one notices that there is an apparent threshold mass of $\simeq 10^9$ M$_\odot$ *above* which lie eight out of ten RGs and all RLQs, but *below* which lie nine out of 13 of the RQQs. In other words, using the black hole mass estimation procedure outlined above, at least within this particular sample it appears that a black hole mass $> 10^9$ M$_\odot$ is a necessary (albeit perhaps not sufficient) condition for the production of a powerful radio source. As measured via the KS test, this difference between the black hole mass distributions of the radio-loud and radio-quiet subsamples is significant at the 3σ level, a significance that must be taken seriously given the almost perfect matching of the distributions of nuclear optical output demonstrated in Fig. 4. Further support for

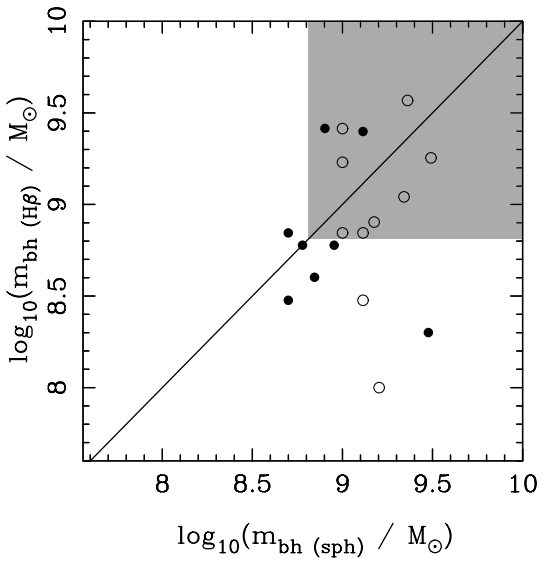

Figure 13. A comparison between the black hole masses predicted from host-galaxy spheroid luminosity and those determined from the Hβ linewidth by McLure & Dunlop (2001). The shaded area illustrates that there is a region in which both approaches agree that $M_{\rm bh} > 10^{8.8}$ M$_\odot$, and that this region contains all except two of the RLQs (open circles), but excludes all except two of the RQQs (filled circles).

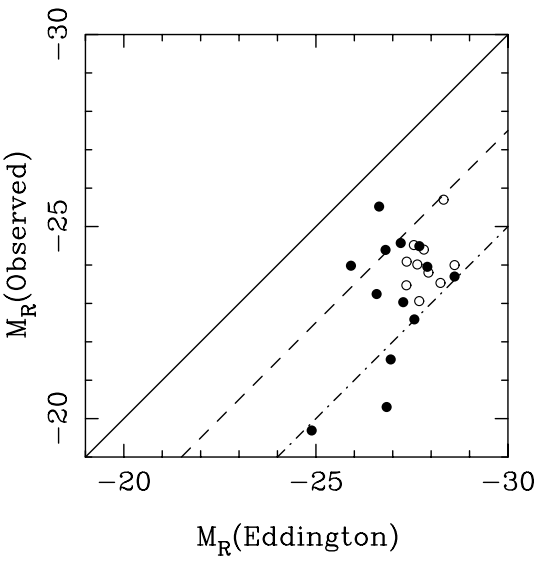

Figure 14. The observed absolute magnitude M_R of the nuclear component in each quasar plotted against the absolute magnitude that is predicted by assuming that each quasar contains a black hole of mass $m_{\rm bh} = 0.0025\, m_{\rm spheroid}$, and that the black hole is emitting at the Eddington luminosity (RLQs, open circles; RQQs, filled circles). The solid line shows where the quasars should lie if they were all radiating at their respective Eddington luminosities, while the dashed line indicates 10 per cent of predicted Eddington luminosity, and the dot-dashed line indicates 1 per cent of predicted Eddington luminosity. The nuclear components of the radio galaxies are not plotted because all the evidence suggests they are substantially obscured by dust – see Section 6.7.

its reality comes from the Hβ study by McLure & Dunlop (2001) already referred to above, in which it was found that 11 out of 13 RLQs had $M_{\rm bh} > 10^{8.8}$ M$_\odot$, while only four out of 18 RQQs had black hole masses above this threshold. A similar conclusion was also reached by Laor (2000) from a study of the virial masses of PG quasars.

An inevitable consequence of the matching of nuclear optical luminosities demonstrated in Fig. 4, and the systematic offset in black hole mass described above is that, on average, the black holes at the heart of the RQQs in our sample must, on average, be emitting more efficiently than their radio-loud counterparts. This is quantified in the final two columns of Table 9 which give an estimated Eddington luminosity (converted to R-band absolute magnitude) and then an emitting efficiency $L/L_{\rm Edd}$. The potential R-band Eddington luminosity of each quasar was derived in the following manner. Initially, the host-galaxy bulge luminosities provided by the two-dimensional modelling were converted into a spheroidal mass estimate using the Jørgensen et al. mass-to-light ratio (equation 7). The linear relation between black hole mass and spheroidal mass (equation 8) was then used to estimate the central black hole mass and the resulting bolometric Eddington luminosity of each quasar. To calculate the corresponding R-band magnitudes it was assumed that, on average, the bolometric luminosity of a quasar can be estimated via $L_{\rm bol} \simeq 10\lambda L_{5100}$ (Laor et al. 1997), where L_{5100} is the absolute monochromatic luminosity at 5100 Å. The resulting estimate of the absolute luminosity at 5100 Å was then transformed to the central wavelength of the R filter (6500 Å) assuming a power-law quasar spectrum ($\alpha = 0.2$). Using this prescription, a quasar with a central black hole mass of 10^9 M$_\odot$ will have an Eddington-limit absolute R-band magnitude of $M_R({\rm Edd}) = -27.5$.

The observed nuclear M_R is plotted against the potential Eddington-limited M_R in Fig. 14. As can be seen from this figure, the maximum luminosity produced by any quasar is within a factor of 2 of the predicted Eddington limit, while the majority appear to be radiating at ∼1–10 per cent of the Eddington luminosity. Taken as a group there is a suggestion that the RQQs are radiating at a higher percentage of the Eddington limit, but the difference is not formally significant (KS, $p = 0.29$).

8.2 The black hole–radio connection

When the matched samples of RLQs and RQQs were first defined, all that was known concerning the radio properties of the RQQs was that their 5-GHz luminosities were lower than $P_{5\,\rm GHz} \simeq 10^{24}$ W Hz^{-1} sr^{-1} (Dunlop et al. 1993). However, with the completion of the VLA detection programme described in Section 4 we can now explore how the radio properties of *all* the AGN in our combined sample relate to their estimated black hole masses.

In Fig. 15 the total radio luminosity, $P_{5\,\rm GHz}$, is plotted against the estimated black hole mass for all the objects in our combined sample (with the single exception of 1549+203, which was not observed with the VLA to the same depth as the other objects). Also included in this diagram are the appropriate points for eight nearby galaxies taken from Franceschini, Vercellone & Fabian (1998), with the Milky Way and M87 highlighted.

Several significant trends are evident in this diagram. First, it can be seen that, within the RQQ sample, radio luminosity correlates, albeit weakly, with black hole mass, although our sample does not span a wide dynamic range and the correlation is not formally significant. Secondly, and perhaps more interestingly, the RQQs are consistent with the locus described by the nearby galaxies (for which, of course, the black hole masses are based directly on stellar dynamics). This simultaneously reinforces the plausibility of our black hole mass estimates, and suggests a common physical origin for the radio emission from RQQs and nearby optically more-quiescent bulges. Whatever this physical mechanism is, it must explain the

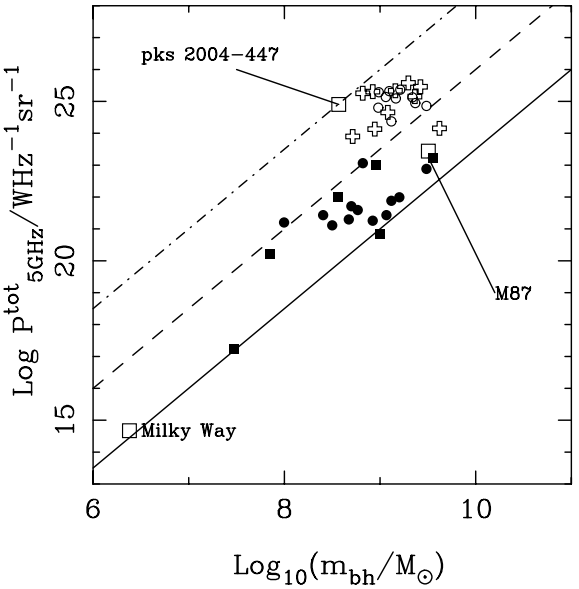

Figure 15. Total radio luminosity $P_{5\,\mathrm{GHz}}^{\mathrm{total}}$ versus black hole mass showing the data on low-redshift 'normal' galaxies from Franceschini et al. (1998) (as squares, with the Milky Way and M87 highlighted), and the AGN from the *HST* sample (RGs, crosses; RLQs, open circles; RQQs, filled circles). The lines that bracket the data are relations of the form $P_{5\,\mathrm{GHz}} \propto m_{\mathrm{bh}}^{5/2}$ offset by 2.5 orders of magnitude from each other. The solid line therefore indicates the apparent existence of a *lower* limit to the radio output of a black hole that scales as $m_{\mathrm{bh}}^{5/2}$ while the dot-dash line indicates the apparent *upper* limit required by our data. While our own data are insufficient to constrain the slope of such an upper envelope, adoption of the same slope as the lower envelope (as done here) is consistent with the data of Lacy et al. (2001) and is further reinforced by the results of McLure & Dunlop (in preparation). PKS 2004−447 has been included in this plot because it has recently been claimed that this object contradicts the existence of any such mass-dependent upper envelope (Oshlack et al. 2001). The position of this compact and variable source on this diagram has been here recalculated on the assumption that its radio axis lies with $\simeq 5^{\circ}$ of the line of sight, but without making any corrections for relativistic beaming of its radio output (see the text for details). As can be seen, the resulting increase in estimated black hole mass from $m_{\mathrm{bh}} \simeq 5 \times 10^6$ to 4×10^8 $\mathrm{M}_{\odot}$ is sufficient to bring it into consistency with the upper envelope suggested by the other data.

observed strong dependence of minimum radio output on black hole mass, in which the power-law index γ is at least 2 (adopting $P_{\mathrm{radio}} \propto M_{\mathrm{bh}}^{\gamma}$). As noted by Franceschini et al. (1998), $\gamma = 2.2$ is the prediction of advection-dominated accretion flow models, while $\gamma \simeq 2$ is a generic prediction of any mechanism in which radio output is proportional to the area of the accretion disc.

Our results therefore provide further support for previous claims that there is a minimum radio output from black holes and that this is a strong function of mass. However, while this obviously implies that the most massive black holes can never be *very* radio-quiet, Fig. 15 graphically demonstrates that the genuine radio-loud objects lie on a quite distinct relation. Interestingly, our radio-loud sample also displays an (albeit weak) internal correlation between $P_{5\,\mathrm{GHz}}$ and the estimated black hole mass. Either this relationship must be much steeper ($P \propto M_{\mathrm{bh}}^4$) than the minimum radio-output relation, or, as illustrated in Fig. 15, the black hole mass dependence of the upper envelope may be consistent with that of the lower envelope but offset by several orders of magnitude.

In fact, the findings of Lacy et al. (2001) strongly favour the latter option. They report a relationship between the logarithm of radio power and black hole mass that has a slope of 1.4 ± 0.2. However, inspection of their fig. 2 shows that their data are also consistent with an upper and lower envelope with slope $\simeq 2.5$ as illustrated here in Fig. 15.

We note here that it has recently been claimed by Oshlack, Wenster & Whiting (2001) that the radio-loud Seyfert galaxy PKS 2004−447 contradicts the existence of such an envelope, and shows that relatively low-mass black holes can produce a powerful radio source. However, this claim is based on their black hole mass estimate for this object of $\simeq 5 \times 10^6$ $\mathrm{M}_{\odot}$ and it seems almost certain that this value, derived from the relatively narrow emission lines displayed by PKS 2004−447, is a serious underestimate of the true mass. The reason for this is that since this object displays optical variability and has a compact radio source, it seems very probable that its orbiting broad-line region lies close to the plane of the sky. In this situation (as found in our own sample for, e.g. 1012+008 – see Table 9) the black hole mass derived from the Hβ emission-line width can underestimate the true value by a factor >100. In Fig. 15 we have plotted the position of PKS 2004−447 after recalculating its black hole mass on the assumption that the orbital plane of its broad-line region is oriented within $\simeq 5^{\circ}$ of the plane of the sky (see McLure & Dunlop 2001). This increases the estimated black hole mass to $\simeq 4 \times 10^8$ $\mathrm{M}_{\odot}$, and moves PKS 2004−447 into complete consistency with the upper envelope delineated by the other available data. We have not corrected the observed radio emission for Doppler boosting – if we did then this object would simply move downwards in Fig. 15.

Thus both our own results and other currently available data support the existence of both a lower and an upper envelope to the radio luminosity that can be produced by a black hole of given mass. Indeed, Fig. 15 serves to provide an elegant explanation not only of our own findings, but also of several other well-known results in the literature.

First, because we selected our radio-loud objects on the basis that their radio luminosities were greater than $\log_{10}(P/\mathrm{W\,Hz^{-1}\,sr^{-1}}) = 24$, the form of the upper envelope in these figures can be seen to be perfectly consistent with our finding that virtually all our radio-loud objects have $M_{\mathrm{bh}} > 10^9$ $\mathrm{M}_{\odot}$. In the context of this diagram this finding can be seen to be a result of our radio-selection criterion rather than the existence of some critical black hole mass for the production of relativistic jets within a galaxy mass halo.

Secondly, the steep dependence of this apparent upper envelope on black hole mass means that radio sources up to $\log_{10}(P/\mathrm{W\,Hz^{-1}\,sr^{-1}}) = 27$–$28$, consistent with the most luminous 3CR galaxies even at $z = 1$ *can* be produced by black holes (and hence hosts) only a factor of 2–3 more massive, and most probably *will* be because of the steep high-mass slope of the black hole mass function. This provides a natural explanation of why radio galaxies spanning the top two orders of magnitude in radio power all appear to be giant ellipticals with stellar masses that agree to within a factor of $\simeq 2$ (Jarvis et al. 2001).

Thirdly, from Fig. 15 it can be seen that the properties of AGN hosts will inevitably become more mixed if the radio-luminosity threshold is moved down to, say, $P_{5\,\mathrm{GHz}} \simeq 10^{22}$ $\mathrm{W\,Hz^{-1}\,sr^{-1}}$. Given the lower boundary in Fig. 15, radio sources in this power range can still be produced by black holes as massive as 10^9 $\mathrm{M}_{\odot}$ living in giant ellipticals, but it is also clear that black holes with masses as low as $10^{7.5}$ $\mathrm{M}_{\odot}$ are capable of producing detectable radio sources at this level. As demonstrated by the properties of the lower-luminosity objects in our own sample, and by the studies of 'normal' galaxies at low redshift, such black holes can be housed in disc-dominated galaxies and discless lower-mass spheroids.

8.3 The origin of radio loudness

While the broad dependence of radio luminosity on black hole mass may explain the relative numbers of radio-quiet and radio-loud objects, it is also clear from Fig. 15 that the black hole mass cannot be invoked to explain the *range* of radio luminosities displayed by quasars of very similar optical luminosity. Specifically, it is clear from this figure that objects powered by equally massive black holes can differ in radio luminosity by $\simeq$4 orders of magnitude.

Interestingly, Fig. 15 also allows us to rule out the possibility that the radio output of a black hole of given mass is driven simply by fuel supply. This is because, while it has long been known that RQQs are not radio silent, it can be seen from Fig. 15 that several of the RQQs in our sample are in fact as radio-silent as they could possibly be, given their estimated black hole masses. In other words, at least some of the black holes in RQQs produce as little radio output as their counterparts in completely quiescent nearby galaxies, despite the fact that black holes in quasars are clearly in receipt of sufficient fuel to produce powerful *optical* emission.

Thus, while the results of this study cannot by themselves provide a definitive answer to the long standing question of the origin of radio loudness, they can be used to focus the argument by excluding several possible explanations. In summary, our results can be used to exclude host galaxy morphology, black hole mass or black hole fuelling rate as the primary physical causes of radio loudness.

We are thus forced to the conclusion that the production of powerful relativistic radio jets is driven by some other property of the black hole itself, the most probable candidate being black hole spin (e.g. Blandford 2000; Wilson & Colbert 1995). Indeed, following the suggestion by Blandford (2000), we speculate that the evolutionary track followed by an activated black hole may manifest itself as a near vertical descent in Fig. 15, with an active rapidly spinning hole appearing first as a powerful radio source close to the upper envelope in this diagram, and then descending towards the lower envelope as the spin energy of the hole is exhausted.

9 COSMOLOGICAL IMPLICATIONS

9.1 Relative numbers of radio-loud and radio-quiet quasars

One interesting aspect of the different black hole mass thresholds for RQQs and RLQs uncovered by this study is that this difference of a factor of 2 in minimum black hole mass provides a natural explanation of why radio-quiet quasars outnumber their radio-loud counterparts by a factor of $\simeq$10 (and why this factor may reduce with increasing optical luminosity; Hooper et al. 1995; Goldschmidt et al. 1999).

This is because if our black hole mass thresholds of $M_{\rm bh} > 5 \times 10^8$ M$_\odot$ for RQQs, and $M_{\rm bh} > 1 \times 10^9$ M$_\odot$ for radio-loud objects are converted back into absolute spheroid magnitudes in the K band (using the absolute R-band magnitudes given in Table 4, and then converting into K adopting $R - K = 2.5$ as justified by the results in Section 6.6), we find that RQQs can be hosted by spheroids with $M_K < -25.3$, while radio-loud objects require a host spheroid with $M_K < -26$. With reference to the K-band luminosity function these absolute magnitude limits correspond to $L > 1.5L^\star$ and $L > 3L^\star$, respectively (Gardner et al. 1997; Szokoly et al. 1998; Kochanek et al. 2001), which leads to the prediction that, in the present-day Universe there are 1×10^{-4} galaxies Mpc^{-3} capable of hosting an RQQ brighter than $M_V = -23$, but only 1×10^{-5} galaxies Mpc^{-3} are capable of hosting an RLQ. This means that, assuming low-redshift quasars arise from a randomly triggered subset of massive black holes in spheroids, the factor of 2 difference in black hole mass threshold translates into a factor of 10 difference in the number density of RQQs and RLQs owing simply to the steepness of the bright end of the spheroid luminosity function.

9.2 Black hole activation fraction at $z \simeq 0$

We can go further and use the above numbers to estimate the activation fraction for massive black holes in the local universe. First, we note that the radio-loud objects in our sample have $P_{2.7\,\rm GHz} > 1 \times 10^{25}$ W Hz^{-1} sr^{-1} (assuming a spectral index of $\alpha \simeq 0.8$). Reference to the local radio luminosity function in Dunlop & Peacock (1990), or to the more recent determination at 1.4 GHz from the 2dF by Sadler et al. (2002), indicates that the present-day number density of radio sources above this threshold is $\simeq 1 \times 10^{-8}$ Mpc^{-3}. Thus, in the present-day Universe we find that one in every 1000 black holes more massive than 1×10^9 M$_\odot$ (or equivalently spheroids more luminous than $3L^\star$) is radio active in the present-day Universe.

Turning to the RQQ population, the present-day number density of quasars with $M_V < -23$ can be estimated by extrapolating the quasi-stellar object (QSO) optical luminosity function (OLF) deduced at $z \simeq 0.4$ by Boyle et al. (2000) back to $z = 0$ assuming luminosity evolution $\propto (1 + z)^3$. This produces an estimated number density of $\simeq 5 \times 10^{-8}$ Mpc^{-3}, which is at least consistent with the direct determination of the low-z OLF attempted by Londish, Boyle & Schade (2000). Boosting this number by a factor of 2 to allow for obscured quasars (i.e. adopting an opening angle of $\simeq 45^\circ$ for consistency with the correction factor, which appears to apply to the radio-loud population) then leads to the conclusion that one in every 1000 black holes more massive than 5×10^8 M$_\odot$ (or equivalently spheroids more luminous than $1.5L^\star$) is producing quasar-level optical activity.

Thus both of these comparisons yield the same result, namely that in the present-day ($z < 0.1$) Universe one in every 1000 massive black holes is active, and that the reason RQQs outnumber RLQs by a factor of 10 is a direct result of the fact that their respective minimum black hole masses differ by a factor of 2.

We note here that Wisotzki et al. (2001) have recently concluded that the present-day black hole activation fraction is one in 10 000, or one in 5000 if the quasar LF is boosted by a factor of 2 as assumed above. However, reference to their fig. 2 shows that this factor results from adopting the spheroid luminosity function of Lin et al. (1999). If instead Wisotzki et al. were to adopt the Kochanek et al. (2001) luminosity function then it is clear that (at least for the mass range probed by the present study) Wisotzki et al.'s analysis would also yield an activation fraction of 0.1 per cent.

9.3 Black hole activation fraction at $z \simeq$ 2–3

At the peak epoch of quasar activity between $z \simeq 2$ and 3, the comoving number density of powerful radio sources with $P_{2.7\,\rm GHz} > 1 \times 10^{25}$ W Hz^{-1} sr^{-1} has risen to $\simeq 1 \times 10^{-6}$ Mpc^{-3} (Dunlop & Peacock 1990), while that of optically selected quasars brighter than $M_V = -23$ is $\simeq 5 \times 10^{-6}$ Mpc^{-3} (Warren, Hewett & Osmer 1995; Boyle et al. 2000). Doubling the latter figure to make the same correction for obscured RQQs as applied in the previous subsection at low redshift, leads to the conclusion that, as at $z \simeq 0$, RQQs at $z \simeq 2.5$ outnumber their radio-loud counterparts by a factor of $\simeq$10. However, at $z \simeq 2.5$ the comoving number density of both classes of object is enhanced by a factor of 100, giving an activation fraction of massive black holes of $\simeq$10 per cent, assuming that the entire massive black hole population is in place by that epoch.

9.4 The cosmological evolution of AGN

A renewed attempt to model the cosmological evolution of AGN in the light of our host-galaxy results is obviously beyond the scope of this paper. However, if one assumes that the same mass thresholds uncovered in our low-redshift study apply at high redshift, then one simple interpretation of the dramatic (and very similar) evolution of radio-loud and radio-quiet AGN between $z \simeq 2.5$ and the present day is that it is primarily caused by density evolution, with the active fraction of massive black holes dropping from 10 to 0.1 per cent over this period. There must of course also be an element of luminosity evolution because pure density evolution was excluded long ago as an acceptable representation of the evolving radio luminosity function (RLF) or OLF. However, as suggested by Miller, Percival & Lambert (in preparation) if individual quasars produce declining light curves it is inevitable that a larger fraction will be observed closer to the peak luminosity as the activation rate rises, and Fig. 14 indicates that at least some of the host galaxies uncovered in the present study should be capable of producing quasars with $M_V \simeq -28$ if observed while accreting at the Eddington limit.

One prediction of this scenario is that, as a larger fraction of massive black holes become more efficiently fuelled, the apparent mass difference between RLQ and RQQ hosts should grow with increasing redshift. The reason for this is that, if fuelling rates are, on average, somewhat higher at high redshift we can expect optically selected QSOs of a given luminosity to be produced by black holes with, on average, lower masses than at low redshift. However, if the $m_{\rm bh} > 10^9$ M$_\odot$ mass threshold for powerful radio activity found in this study continues to apply at high redshift, then radio selection will continue to yield only the most massive black holes residing (presumably) in the most massive spheroids.

In fact, studies of the hosts of RLQs and RQQs out to $z \simeq 2$ are already uncovering evidence of just such a trend. Specifically, Kukula et al. (2001) have used NICMOS on the *HST* to measure the rest-frame *R*-band luminosities of the hosts of matched samples of RLQs and RQQs at $z \simeq 1$ and 2. Kukula et al. find that the hosts of RLQs are essentially unchanged in mass over this redshift range, suggesting that the minimum mass threshold for powerful radio emission indicated by the upper locus in Fig. 15 applies at all redshifts and is therefore of physical significance. However, they also find that the average ratio of RLQ:RQQ host luminosity rises from the value of 1.5 found here at $z \simeq 0.2$, to $\simeq$2 at $z \simeq 1$, and $\simeq$3 at $z \simeq 2$, suggesting a progressive drop in the average mass of RQQ hosts with increasing redshift, a finding supported by the results of other recent studies (Ridgway et al. 2001; Rix et al. 2001).

10 CONCLUSIONS

In this paper we have reported the extensive results that follow from completion of our *HST* imaging programme of the host galaxies of low-redshift radio-quiet quasars, radio-loud quasars and radio galaxies. This paper represents the completion of a programme that has spanned most of the previous decade, commencing with the deep infrared imaging of the same sample of objects by Dunlop et al. (1993). The depth and quality of our *HST* data have now allowed us to determine accurately all the basic structural parameters of the hosts of these three classes of powerful AGN. Because of this, and because of the wealth of data now available for this sample at other wavelengths (including the new deep VLA observations also reported here), we have been able to address a wide range of issues that are hopefully of interest to workers in several different areas of extragalactic research. Consequently, we conclude with a detailed summary of the main conclusions of this study, structured to assist the interested reader in moving directly to the sections that may be of most relevance to their own work.

10.1 Results from analysis of the *HST* images

From the detailed two-dimensional modelling of the new *HST* images presented here in combination with the data reported by McLure et al. (1999) we find the following (as detailed in Sections 5 and 6).

(i) All except the two least luminous RQQs in the sample have bulge-dominated hosts, and in only two of the remaining 31 objects (the RQQs 0052+251 and 0157+001) can we find any evidence for a significant disc component. Thus both radio-loud and radio-quiet quasars live, almost universally, in elliptical galaxies.

(ii) The hosts of all three classes of powerful AGN are luminous galaxies with $L > L^\star$, and almost always $L > 2L^\star$. The average luminosities of the RG and RLQ hosts are essentially identical (consistent with radio-loud unification), and equivalent to $4L^\star$. The average luminosity of the RQQ hosts is somewhat smaller, equivalent to $\simeq 3L^\star$.

(iii) The hosts of all three classes of powerful AGN are large galaxies with typical half-light radii $r_{1/2} \simeq 10$ kpc. As with the luminosities, the average values of host-galaxy scalelength for the radio-loud subsamples are indistinguishable, while the hosts of the RQQs are typically smaller by a modest factor ($\simeq$1.5).

(iv) The hosts of all three classes of powerful AGN display a surface-brightness scalelength (Kormendy) relation identical (in both slope and normalization) to that displayed by inactive massive ellipticals predominantly found in clusters.

(v) The hosts of all three classes of powerful AGN display a distribution of axial ratio, which is indistinguishable from that which has been long established for normal elliptical galaxies.

10.2 Results incorporating infrared images

From a joint analysis of the *HST* optical images with existing *K*-band images of the same sample (Dunlop et al. 1993; Taylor et al. 1996; McLure et al. 2000) we find the following (as detailed in Subsections 6.6 and 6.7).

(i) The hosts of all three classes of powerful AGN are red galaxies, with typical rest-frame optical–infrared colours $R - K \simeq 2.5$. Consistent with the results of Nolan et al. (2001), these colours are as expected from an evolved stellar population of age 10–13 Gyr, indicating that, as for quiescent massive ellipticals, the stellar mass of an AGN host galaxy is dominated by a well-evolved stellar population formed at high redshift ($z > 2$).

(ii) The optical–infrared colours of the RQQ and RLQ nuclei are statistically indistinguishable, and lie in the range $R - K \simeq 2$–4. For the RG nuclei, the relation between $R - K$ colour and *R*-band luminosity is as expected under the assumption that they all contain obscured nuclei with intrinsic optical luminosities comparable to the quasars, reddened by dust with $\kappa_\lambda \propto \lambda^{-0.95}$. This result strongly favours unification of RGs and RLQs via orientation rather than time.

10.3 Relation of quasar hosts to normal galaxies

From a comparison of our results with those derived from recent studies of the 'normal' massive galaxy population, and of low-redshift ULIRGs and Seyferts, we find the following (as detailed in Section 7).

(i) The bulge–disc ratio of AGN hosts is a function of AGN luminosity, with disc-dominated hosts dying out above the traditional quasar–Seyfert boundary at $M_V(\mathrm{nucl}) \simeq -23$.

(ii) In contrast to ULIRGs, quasar hosts lie in a region of the fundamental plane (as judged from the photometric projection of the FP offered by the Kormendy relation) that has been shown to be occupied by the most massive and apparently old population of ellipticals that display 'boxy' isophotes and distinct kinematic cores. This provides a strong argument against the possibility that the $r^{1/4}$-law luminosity profiles displayed by the vast majority of the quasar hosts in our sample are the result of recent mergers between massive disc galaxies. This result also offers little support for a strong evolutionary connection between ULIRGS and quasars in the low-redshift universe.

(iii) The basic structural properties of AGN hosts are indistinguishable from those of inactive brightest cluster galaxies. Consistent with the environmental study of McLure & Dunlop (2000), the largest host galaxies in our sample are of comparable mass to the BCGs found at the heart of Abell Class 1 or Class 2 clusters. However, the lack of any host galaxies as massive as an Abell Class 4 cluster BCG is as expected given the relative rarity of such rich environments. All the evidence considered is consistent with the AGN hosts being drawn, essentially at random, from the present-day massive-elliptical galaxy population.

(iv) There is no statistically significant evidence that AGN hosts display more signs of large- (kpc) scale disturbance, or multiple nuclei than normal comparably massive quiescent ellipticals.

10.4 The black hole spheroid connection

Combining our *HST* data with our new VLA data, and utilizing recent results on the black hole–spheroid mass relation in both quiescent and active galaxies, we find the following (as detailed in Section 8).

(i) Estimates of central black hole mass for the quasars in our sample based on host-galaxy spheroid luminosity agree well with those derived from Hβ emission-line width by McLure & Dunlop (2001). For three objects the latter technique yields a much lower value, but this is as expected for a small subset of objects if the broad-line region has a predominantly disc-like structure.

(ii) Based on the relation $M_{\mathrm{bh}} = 0.0025\, M_{\mathrm{sph}}$, we find that all the quasars in our sample are powered by a black hole of mass $m_{\mathrm{bh}} > 5 \times 10^8\, \mathrm{M}_\odot$, but that the radio-loud objects lie above an even higher mass threshold, with $m_{\mathrm{bh}} > 10^9\, \mathrm{M}_\odot$.

(iii) The most efficient RQQ in our sample appears to be radiating at $\simeq$35 per cent of the Eddington limit, but the vast majority of these low-redshift AGN are emitting at 1–10 per cent of the Eddington limit. Based on these calculations, the most massive objects in this low-redshift sample appear capable (if fuelled at maximum efficiency) of producing quasars with $M_V \simeq -28$, comparable to the most luminous objects known at high redshift.

(iv) The black hole mass difference between RLQs and RQQs reflects the existence of an apparent upper and lower limit to the radio output that can be produced by a black hole of a given mass. Both the upper and lower thresholds on radio luminosity appear to be a strong function of black mass ($\propto m_{\mathrm{bh}}^{2-2.5}$). At least some RQQs in our sample appear to be as radio-weak as 'normal' inactive comparably massive spheroids found in the low-redshift universe, despite the fact that they must be receiving sufficient fuel to power the optical quasar nucleus.

(v) While there is a broad and clear trend for increasing radio luminosity with increasing black hole mass, it is now clear that host morphology, black hole mass and fuel supply can each be excluded as the primary physical explanation of why a subset of quasars are up to four orders of magnitude more radio luminous than their 'radio-quiet' counterparts. Consequently, we argue that black hole spin is the most plausible (perhaps only) remaining feasible explanation for the production of a powerful radio source.

10.5 Cosmological implications

Considering the implications of our results for our understanding of the nature and evolution of AGN populations as a function of redshift, we find the following (as detailed in Section 9).

(i) The relative numbers of radio-loud and radio-quiet quasars can be naturally explained by the above-mentioned mass thresholds, combined with the form of the bright end of the elliptical galaxy luminosity function.

(ii) The activation fraction of massive black holes is $\simeq 0.1$ per cent in the present-day Universe, rising to $\simeq$10 per cent at $z \simeq 2$–3, corresponding to the peak epoch of quasar activity in the Universe.

(iii) The black hole mass threshold for powerful radio activity can explain the trend for a growing gap with increasing redshift between the masses of RLQ hosts and RQQ hosts uncovered by recent *HST*-based studies of high-redshift quasars.

ACKNOWLEDGMENTS

This work was based on observations make with the NASA/ESA *Hubble Space Telescope*, obtained at the Space Telescope Science Institute, which is operated by The Association of Universities for Research in Astronomy, Inc. under NASA contract no NAS526555. JD, RMcL and MK all acknowledge the support of PPARC through the awards of a Senior Fellowship, a Personal Fellowship and a PDRA position, respectively. Marek Kukula also acknowledges support for this work provided by the Space Telescope Science Institute under grant nos 00548 and 00573.

REFERENCES

Abraham R.G., Crawford C.S., McHardy I.M., 1992, ApJ, 401, 474
Bahcall J.N., Kirhakos S., Schneider D.P., 1994, ApJ, 435, L11
Bahcall J.N., Kirhakos S., Saxe D.H., Schneider D.P., 1997, ApJ, 479, 642
Barnes J.E., Hernquist L., 1992, ARA&A, 30, 705
Barthel P.D., 1989, ApJ, 336, 606
Blandford R.D., 2000, PTRSA, in press (astro-ph/0001499)
Boyce P.J. et al., 1998, MNRAS, 298, 121
Boyle B.J., Shanks T., Croom S.M., Smith R.J., Miller L., Loaring N., Heymans C., 2000, MNRAS, 317, 1014
Brinkmann W., Yuan W., Siebert J., 1997, A&A, 319, 413
Canalizo G., Stockton A., 1997, ApJ, 480, L5
Capaccioli M., Caon N., D'Onofrio M., 1992, MNRAS, 259, 323
Crawford C.S., Fabian A.C., 1995, MNRAS, 273, 827
Croft R.A.C., Dalton G.B., Efstathiou G., Sutherland W.J., Maddox S.J., 1997, MNRAS, 291, 305
de Koff S., Baum S.A., Sparks W.B., Biretta J., Golombeck D., Macchetto F., McCarthy P., Miley G.K., 1996, ApJS, 107, 621
de Vries W.H., O'Dea C.P., Barthel P.D., Fanti C., Fanti R., Lehnert M.D., 2000, AJ, 120, 2300
Disney M.J. et al., 1995, Nat, 376, 150
Dunlop J.S., Peacock J.A., 1990, MNRAS, 247, 19
Dunlop J.S., Taylor G.L., Hughes D.H., Robson E.I., 1993, MNRAS, 264, 455
Faber S.M. et al., 1997, AJ, 114, 1771
Fabian A.C., 1999, MNRAS, 308, L39

Franceschini A., Vercellone S., Fabian A.C., 1998, MNRAS, 297, 817
Franceschini A., Hasinger G., Miyaji T., Malquori D., 1999, MNRAS, 310, L5
Fukugita M., Shimasaku K., Ichikawa T., 1995, PASP, 107, 945
Gardner J.P., Sharples R.M., Frenk C.S., Carrasco B.E., 1997, ApJ, 480, L99
Gebhardt K. et al., 2000, ApJ, 539, L13
Genzel R., Tacconi L.J., Rigopoulou D., Lutz D., Tecza M., 2001, ApJ, 563, 527
Goldschmidt P., Kukula M.J., Miller L., Dunlop J.S., 1999, ApJ, 511, 612
Granato G.L., Silva L., Monaco P., Panuzzo P., Salucci P., De Zotti G., Danese L., 2001, MNRAS, 324, 757
Haehnelt M.G., Rees M.J., 1993, MNRAS, 263, 168
Hamabe M., Kormendy J., 1987, IAUS, 127, 379
Hamilton T.S., Casertano S., Turnshek D.A., 2002, ApJ, 576, 61
Hoessel J.G., Schneider D.P., 1985, ApJ, 480, L95
Holtzman J.A., Burrows C.J., Casertano S., Hester J.J., Trauger J.T., Watson A.M., Worthey G., 1995, PASP, 107, 1065
Hooper E.J., Impey C.D., Foltz C.B., Hewett P.C., 1995, ApJ, 445, 62
Hooper E.J., Impey C.D., Foltz C.B., 1997, ApJ, 480, L95
Hughes D.H., Kukula M.J., Dunlop J.S., Boroson T., 2000, MNRAS, 316, 204
Hunt L.K., Malkan M.A., Rush B., Bicay M.D., Nelson B.O., Stanga R.M., Webb W., 1999, ApJS, 125, 349
Hutchings J.B., Neff S.G., 1992, AJ, 104, 1
Hutchings J.B., Neff S.G., 1997, AJ, 113, 550
Jarvis M.J., Rawlings S., Eales S., Blundell K.M., Willott C.J., 2001, in Marquez I. et al., QSO Hosts and their Environments. Kluwer, Dordrecht, p. 333 (astro-ph/0103364)
Jørgensen I., Franx M., Kjaergaard P., 1996, MNRAS, 280, 167
Kauffmann G., Haehnelt M., 2000, MNRAS, 311, 576
Kirhakos S., Bahcall J.N., Schneider D.P., Kristian J., 1999, ApJ, 520, 67
Kochanek C.S. et al., 2001, ApJ, 560, 566
Kormendy J., 1977, ApJ, 217, 406
Kormendy J., Bender R., 1996, ApJ, 464, L119
Kormendy J., Gebhardt K., 2001, in Martel H., Wheeler J.C., eds, AIP, 20th Texas Symp. on Relativistic Astrophysics. AIP, New York, p. 363, (astro-ph/0105230)
Kukula M.J., Dunlop J.S., Hughes D.H., Rawlings S., 1998, MNRAS, 297, 366
Kukula M.J., Dunlop J.S., McLure R.J., Miller L., Percival W.J., Baum S.A., O'Dea C.P., 2001, MNRAS, 326, 1533
Lacy M., Laurent-Muehleisen S.A., Ridgway S.E., Becker R.H., White R.L., 2001, ApJ, 551, L17
Laor A., 2000, ApJ, 543, L111
Laor A., Fiore F., Elvis M., Wilkes B.J., McDowell J.C., 1997, ApJ, 477, 93
Lin H., Kirshner P.P., Schectman S.A., Landy S.D., Oemler A., Tucker D.L., Schechter P.L., 1996, ApJ, 464, 60
Lin H., Yee H.K.C., Carlberg R.G., Morris S.L., Sawicki M., Patton D.R., Wirth G., Shepherd C.W., 1999, ApJ, 518, 533
Londish D., Boyle B.J., Schade D.J., 2000, MNRAS, 318, 411
Magorrian J. et al., 1998, AJ, 115, 2285
McCarthy P.J., Spinrad H., van Breugel W., 1995, ApJS, 99, 27
McLeod K.K., McLeod B.A., 2001, ApJ, 546, 782
McLeod K.K., Rieke G.H., 1994, ApJ, 431, 137
McLeod K.K., Rieke G.H., 1995, ApJ, 441, 96
McLure R.J., Dunlop J.S., 2000, MNRAS, 317, 249
McLure R.J., Dunlop J.S., 2001, MNRAS, 327, 199
McLure R.J., Dunlop J.S., 2002, MNRAS, 331, 795
McLure R.J., Kukula M.J., Dunlop J.S., Baum S.A., O'Dea C.P., Hughes D.H., 1999, MNRAS, 308, 377
McLure R.J., Dunlop J.S., Kukula M.J., 2000, MNRAS, 318, 693
Merritt D., Ferrarese L., 2001, MNRAS, 320, L30
Nolan L.A., Dunlop J.S., Kukula M.J., Hughes D.H., Boroson T., Jimenez R., 2001, MNRAS, 323, 308
Oshlack A.Y.K.N., Wenster R.L., Whiting M.T., 2001, ApJ, 558, 578
Peacock J.A., 1987, in Kundt W., ed., Astrophysics Jets and Their Engines. Reidel, Dordrecht, p. 185
Prestage R.M., Peacock J.A., 1988, MNRAS, 230, 131
Ridgway S., Heckman T., Calzetti D., Lehnert M., 2001, ApJ, 550, 122
Rix H.-W., Falco E., Impey C., Kochanek C., Lehar J., McLeod B., Munoz J., Peng C., 2001, in Brainerd T.G., Kochanek C.S., eds, ASP Conf. Ser. Vol. 237, Gravitational Lensing: Recent Progress and Future Go. Astron. Soc. Pac., San Francisco, p. 169 (astro-ph/9910190)
Ryden S., 1992, ApJ, 396, 445
Sadler E.M. et al., 2002, MNRAS, 329, 227
Sandage A.R., Freeman K.C., Stokes N.R., 1970, ApJ, 268, 831
Sanders D.B., Mirabel I.F., 1996, ARA&A, 34, 749
Schade D., Boyle B.J., Letawsky M., 2000, MNRAS, 315, 498
Scoville N.Z. et al., 2000, ApJ, 119, 991
Silk J., Rees M., 1998, A&A, 331, L1
Simpson C., Ward M., Wall J.V., 2000, MNRAS, 319, 963
Small T.A., Blandford R.D., 1992, MNRAS, 259, 725
Smith E.P., Heckman T.M., 1990, ApJ, 348, 38
Smith E.P., Heckman T.M., Bothun G.D., Romanishin W., Balick B., 1986, ApJ, 306, 64
Stocke J.T., Liebert J., Gioia I.M., Maccacaro T., Griffiths R.E., Danziger I.J., Kunth D., Lub J., 1983, ApJ, 273, 458
Szokoly G.P., Subbarao M.U., Connoly A.J., Mobasher B., 1998, ApJ, 492, 452
Taylor G.L., Dunlop J.S., Hughes D.H., Robson E.I., 1996, MNRAS, 283, 930
Trauger et al., 1994, ApJ, 435, L3
Urry C.M., Padovani P., 1995, PASP, 107, 803
Véron-Cetty M.-P., Woltjer L., 1990, A&A, 236, 69
Warren S.J., Hewett P.C., Osmer P.S., 1995, ApJ, 438, 506
Wilson A.S., Colbert E.J.M., 1995, ApJ, 438, 62
Wisotzki L., Kuhlbrodt B., Jahnke K., 2001, in Marquez I. et al., eds, QSO Hosts and their Environments. Kluwer, Dordrecht, p. 83 (astro-ph/0103112)
Wright G.S., James P.A., Joseph R.D., McLean I.S., 1990, Nat, 344, 417
Yuan W., Brinkmann W., Siebert J., Voges W., 1998, A&A, 330, 108

APPENDIX A: NEW HOST-GALAXY IMAGES AND MODEL FITS

The images, two-dimensional model fits, and model subtracted images for the 14 AGN for which the new *HST* data are reported in this paper are presented in this appendix in Figs A1–A14. A grey-scale/contour image of the final reduced F675W *R*-band image of each AGN is shown in the top left-hand panel (panel A) of each figure, covering a region of 12.5×12.5 arcsec^2 centred on the target source. The surface-brightness level of the lowest contour is indicated in the top right-hand corner of this panel, and the grey-scale has been chosen to highlight structure close to this limit. Higher surface-brightness contours are spaced at intervals of 0.5 mag arcsec^{-2}, and have been superimposed to emphasize brighter structure in the centre of the galaxy/quasar. Panel B in each figure shows the best-fitting two-dimensional model, complete with the unresolved nuclear component (after convolution with the empirical PSF described above), contoured in a manner identical to panel A. Panel C shows the best-fitting host galaxy as it would appear if the nuclear component were absent, while panel D is the residual image that results from subtraction of the full two-dimensional model (in panel B) from the raw *R*-band image (in panel A), in order to highlight the presence of any morphological peculiarities such as tidal tails, interacting companion galaxies, or secondary nuclei. Within each figure, all four panels are displayed using the same grey-scale.

A1 Notes on individual objects

Here we provide a brief discussion of each of the 14 new *HST* images, with reference to other recent *HST* and ground-based data. Comparably detailed descriptions of the other 19 objects in the sample can be found in McLure et al. (1999) and are not repeated here.

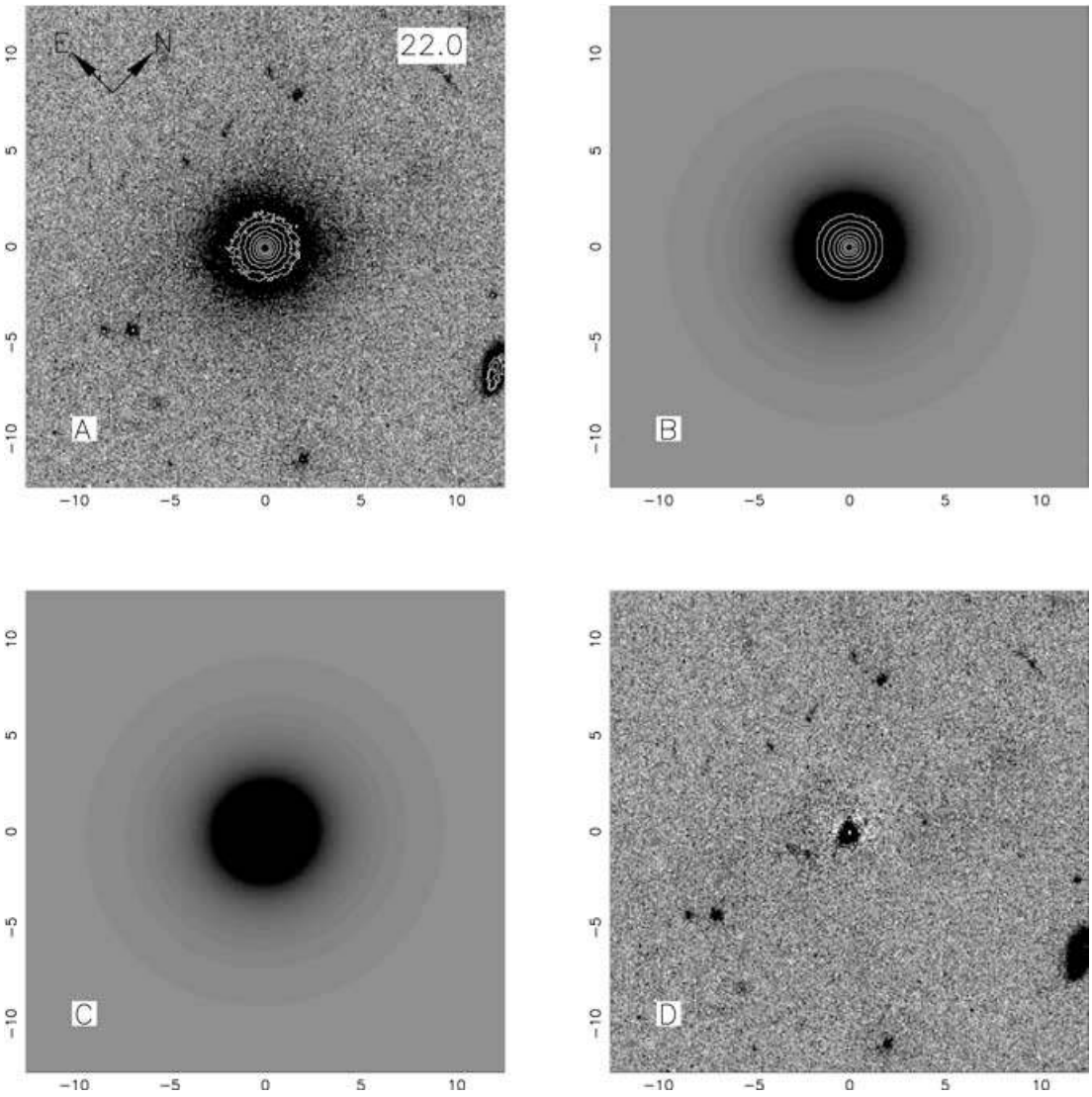

Figure A1. The radio galaxy 0230−027.

Additional details on each object, along with a description of the main features of our *K*-band images, can be found in Dunlop et al. (1993) and Taylor et al. (1996). The results of off-nuclear optical spectroscopy and resulting spectral model-fitting for several of the objects in this sample can be found in Hughes et al. (2000) and Nolan et al. (2001).

A1.1 The radio galaxies

0230−027 (PKS 0230−027, OD −050). The new *R*-band *HST* image shows this galaxy to be uniform and round with no sign of obvious distortion. The detail of the WF2 image shown in Fig. A1 reveals $\simeq$10 apparent companion objects lying in a roughly circular formation around the galaxy, at a radius of $\simeq$30–60 kpc. The brightest of these companions lies at a projected distance of $\simeq$60 kpc to the NW. The full WF2 chip reveals there to be $\simeq$20 faint companion objects within a radius of $\simeq$200 kpc.

0307+169 (3C 079, 4C +16.07). The *R*-band image of this source shown in Fig. A2 reveals it to be a classic brightest-cluster galaxy (BCG). Two bright companion objects can be seen to the north and south with three or four accompanying tidal arm features emanating from the central galaxy. The suggestion that this source is in the process of undergoing merger activity is strengthened by the overlying contours that show three distinct cores. The image of the full WF2 chip reveals several more bright companions within a radius of $\leqslant$100 kpc.

This source has recently been imaged by the *HST* PC during the 3CR snapshot survey (de Koff et al. 1996) through the F702W (wide *R*) filter. The 280-s integration presented by de Koff et al. confirms the complex multiple structure of this object with the authors noting that the optical and radio axes are aligned to within 15°. McCarthy, Spinrad & van Breugel (1995) imaged this source both in the *R* band and through an Hα emission-line filter, detecting a curving filament of extended Hα emission stretching some 12 arcsec to the NW.

1215−033 (PKS 1215−033). The *R*-band image of this source shows it to be a uniform round galaxy with no obvious signs of interaction or disturbance. There are two companion objects lying just on the edge of the detail shown in Fig. A3, to the SW and ESE at projected distances of $\simeq$60 kpc.

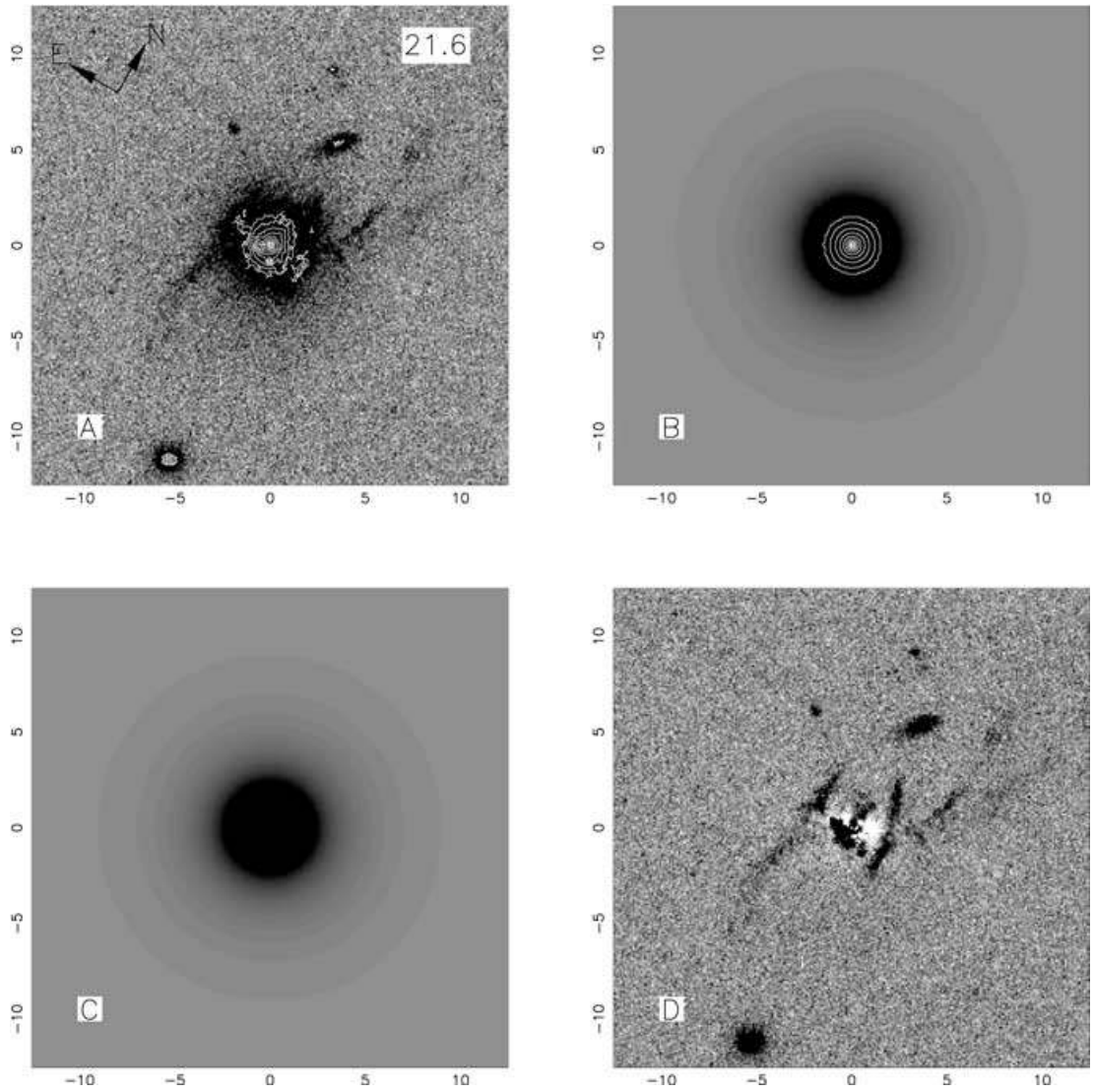

Figure A2. The radio galaxy 0307+169.

1215+013 (PKS 1215+013). The *R*-band image of this source shown in Fig. A4 reveals numerous faint companion objects around the central galaxy, the brightest lying $\simeq$ 30 kpc to the south. The overlying contours for this source suggest some sort of disturbance immediately to the north of the galaxy core.

1330+022 (3C 287.1, 4C+02.36). Numerous companion objects are seen in the new *R*-band image of this source shown in Fig. A5, the brightest of which can be seen some 25 kpc to the NE. There is a linear tidal feature $\simeq$ 35 kpc to the SW. The overlying contours for this source show there to be an apparent second nucleus at less than 1-arcsec separation to the WNW.

This object was in the sample imaged in the *R* band during the 3CR snapshot survey (de Koff et al. 1996). The 280-s image presented by de Koff et al. confirms the presence of the second nucleus. 3C 287.1 has been shown to have a power-law X-ray spectrum by Crawford & Fabian (1995).

1342−016 (PKS 1342 − 016, MRC 1342−016). The new *HST* image shows this galaxy to be large, luminous and uniform. A bright foreground star is present $\simeq$ 13 arcsec to the SWW, on the edge of the frame shown in Fig. A6. No obvious companion objects are present in the detail shown in Fig. A6 although the full WF2 chip image shown in Fig. 12 reveals there to be a large number of companion objects, consistent with a moderately rich cluster.

A1.2 The radio-loud quasars

1020−103 (PKS 1020−103, UT 1020−103). The *R*-band image of this source shown in Fig. A7 reveals it to have a comparatively small and faint host, with an obvious PA of $\simeq$110°. There is a triangle of three faint companions directly to the south. This object was identified as an X-ray source in the *ROSAT* All-Sky Survey (Brinkmann, Yuan & Siebert 1997).

1217+023 (PKS 1217+02, ON 029). The *R*-band image of this relatively nuclear-dominated object shown in Fig. A8 clearly reveals an elliptical-looking host galaxy with an apparent PA of $\approx$100°. There is a group of four faint apparent companion objects running north–south at a projected distance of $\simeq$40 kpc.

2135−147 (PKS 2135−14, PHL 1657). The image of this source shown in Fig. A9 shows a large companion galaxy at a projected

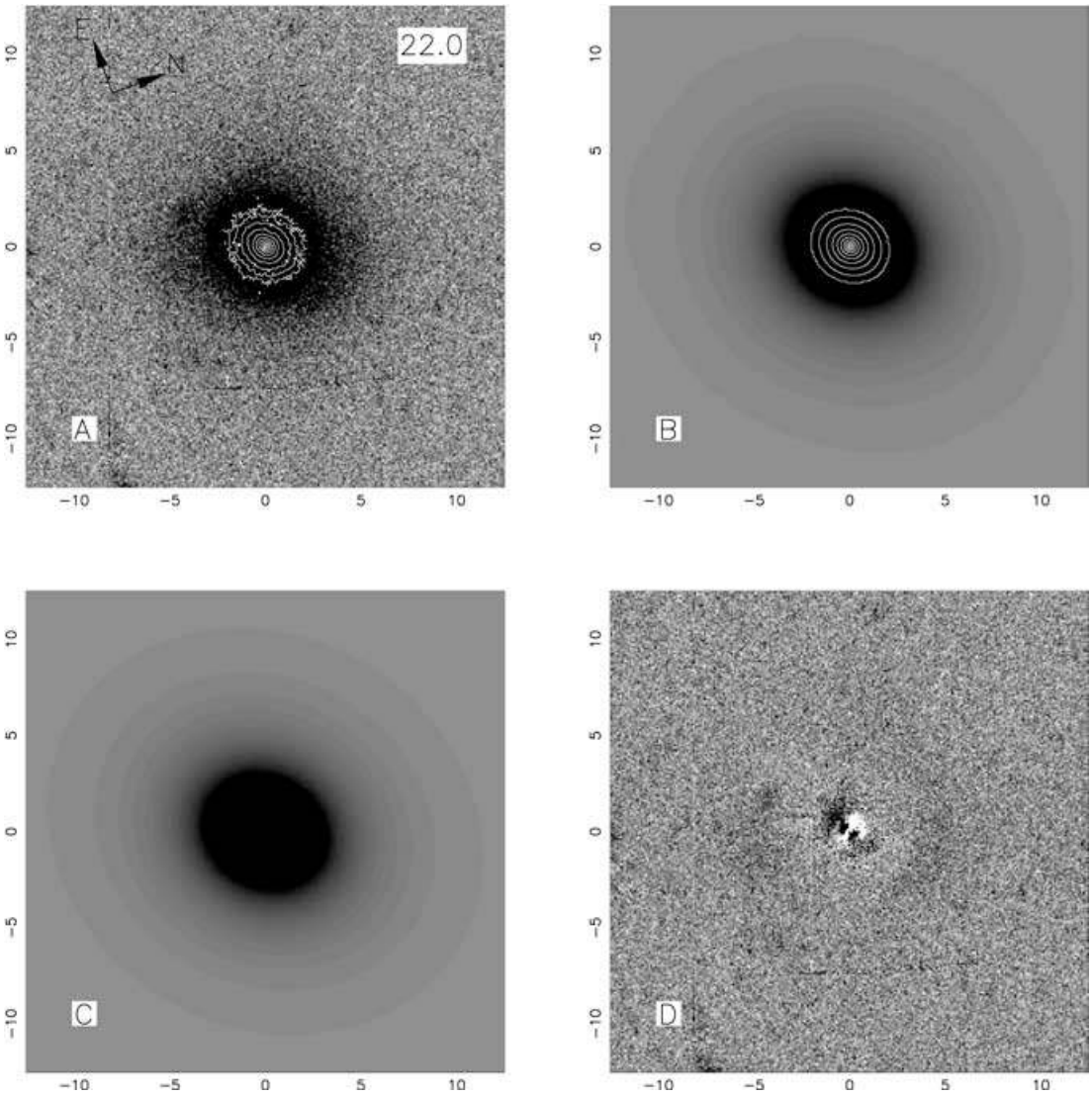

Figure A3. The radio galaxy 1215−033.

distance of ≃30 kpc ESE and an apparent close-in companion, or secondary nucleus, at a distance of ≃10 kpc. A recent analysis of the spectrum of the close-in companion by Canalizo & Stockton (1997) has shown that this object is actually a foreground star. This object has also been imaged in the *V* band with the *HST* by Bahcall, Kirhakos & Schneider (1994). Their analysis also reveals the underlying host to be best matched by an elliptical galaxy model. This quasar was identified as an X-ray source in the *ROSAT* All-Sky Survey (Brinkmann et al. 1997).

2355−082 (PKS 2355−082, PHL 6113). The new *R*-band *HST* image of this source in Fig. A10 reveals the presence of an apparently early-type host with a PA of ≈180°. A group of five small companion objects can be seen to the NE. This object was identified as an X-ray source in the *ROSAT* All-Sky Survey (Brinkmann et al. 1997).

A1.3 The radio-quiet quasars

0052+251 (PG 0052+251). Although not very obvious in the grey-scale representation used in Fig. A11, the host galaxy of this quasar can be seen to have clear spiral structure in the raw *R*-band image. There are two spiral arms present to the east and west of the nucleus with the eastern arm being more extended and apparently terminating in a companion object. The overlying contours for this image reveal it to have a highly luminous nuclear component.

This object has recently been imaged in the *H* band by McLeod & Rieke (1994) and in *J*, *H* and *K* bands by Hutchings & Neff (1997). Hutchings & Neff performed an analysis of the numbers, magnitudes and colours of the companion objects of this source, covering an angular extent comparable to the full WF2 image. They identify some 22 companion objects brighter than $K = 19.6$, the vast majority of which have colours consistent with mature stellar populations. Comparing their near-infrared images with previous optical studies, Hutchings & Neff note that there is no evidence for tidal structure made up of old stars, but conclude that the host is in a phase of secondary star formation possibly induced by interaction with one of the close group of companions. 0052+251 was also included in the *V*-band *HST* imaging programme of Bahcall, Kirhakos & Schneider, who list the host morphology as spiral and identify many of the knots seen in the eastern arm with H II regions. Interestingly, Bahcall, Kirhakos & Schneider comment that the inner regions of the surface-brightness profile of 0052+251 are well matched by

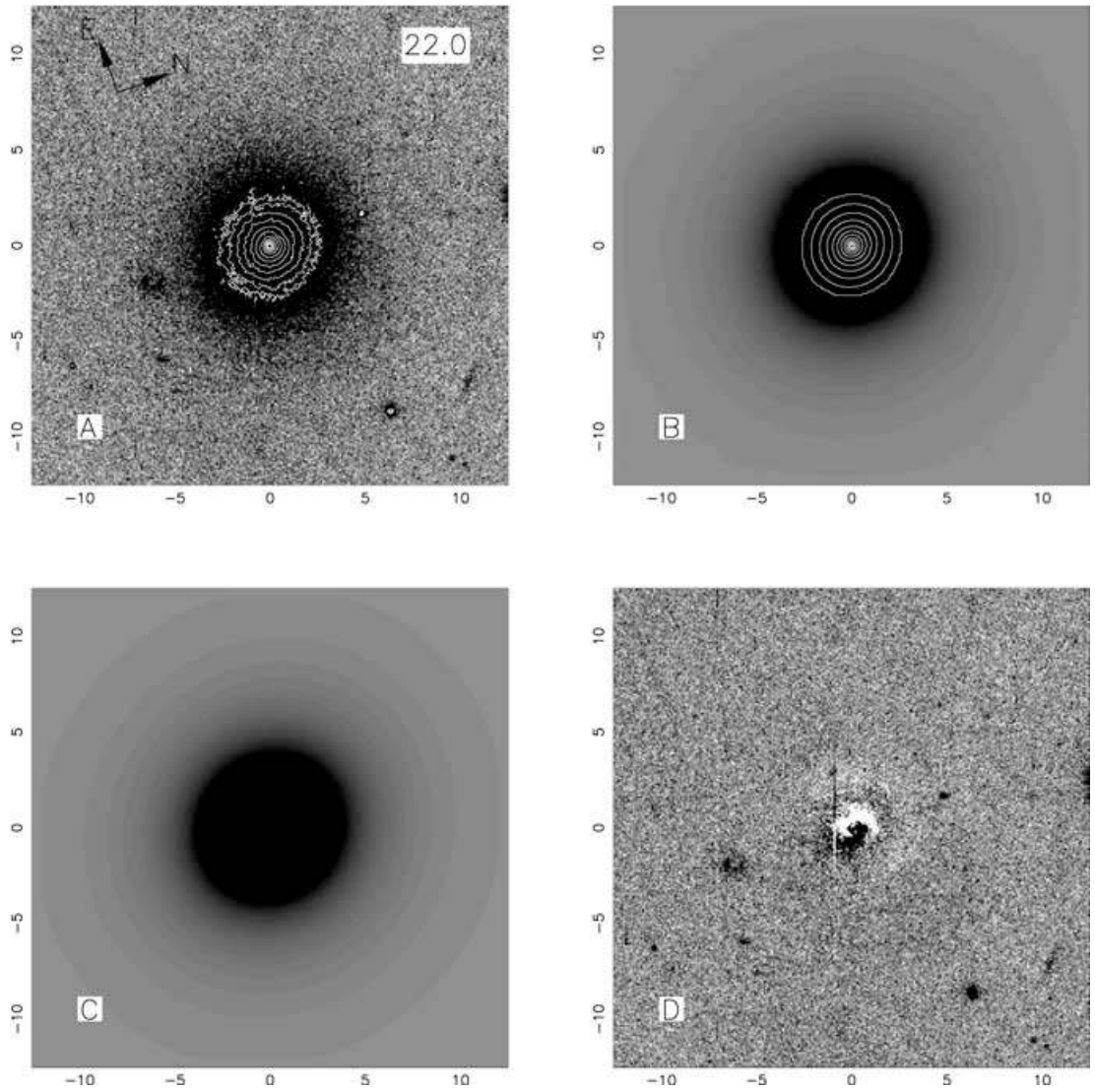

Figure A4. The radio galaxy 1215+013.

an $r^{1/4}$-law, consistent with the best-fitting elliptical host from the *K*-band imaging of Taylor et al. (1996), and suggestive that there may be a strong bulge component to the host galaxy. This is of course precisely what we have found through the construction of a combined disc+bulge model for the galaxy as detailed in Section 5. Despite the fact that the eye is drawn to the high surface-brightness spiral arms in the *HST* image, we find that in fact 70 per cent of its total *R*-band light is contributed by the spheroidal component. Finally, we note that this quasar has also been identified as an X-ray source in the *ROSAT* All-Sky Survey (Yuan et al. 1998).

0204+292. In the new *R*-band image of this quasar the host galaxy appears to be elliptical with a well-defined position angle of $\approx 90^\circ$. There are two companion objects on the subimage shown in Fig. A12, $\simeq$70 kpc to the WSW and $\simeq$45 Kpc to the NW, respectively. This quasar was identified as an X-ray source in the *ROSAT* All-Sky Survey (Yuan et al. 1998).

1549+203 (LB 906, 1E 15498+203). It is immediately obvious from the new *R*-band image of this object that the host galaxy is small, and relatively faint compared with the nuclear component. Using a different grey-scale to that used in Fig. A13, there is a suggestion of spiral-like features to the NW and SE of the nucleus, with the SE arm terminating at the apparent companion object that can be seen $\simeq$20 kpc to the east of the nucleus. A large, luminous elliptical galaxy can just be seen on the edge of the frame to the SW, with numerous fainter companions visible inside a radius of $\simeq$60 kpc. The full WF2 image would appear to show numerous companion objects although, as pointed out by Taylor et al. (1996), the density of the environment of this quasar is uncertain because of the presence of a nearby foreground cluster at $z \simeq 0.14$ (Stocke et al. 1983). The first electronic images of this quasar were presented by Hutchings & Neff (1992). They imaged the object in both the *V* and *I* bands, detecting what looked like a bar structure running north–south through the nucleus, while noting that the surface-brightness profile of 1549+203 was not exponential. This quasar was identified as an X-ray source in the *ROSAT* All-Sky Survey (Yuan et al. 1998).

2215−037 (EX 2215−037). The image of this quasar shown in Fig. A14 reveals the host to be compact and apparently undisturbed. A small apparently unresolved companion is detected only $\simeq$10 kpc to the SW of the quasar nucleus. A large elliptical galaxy can be seen some 65 kpc to the north with a second apparently unresolved

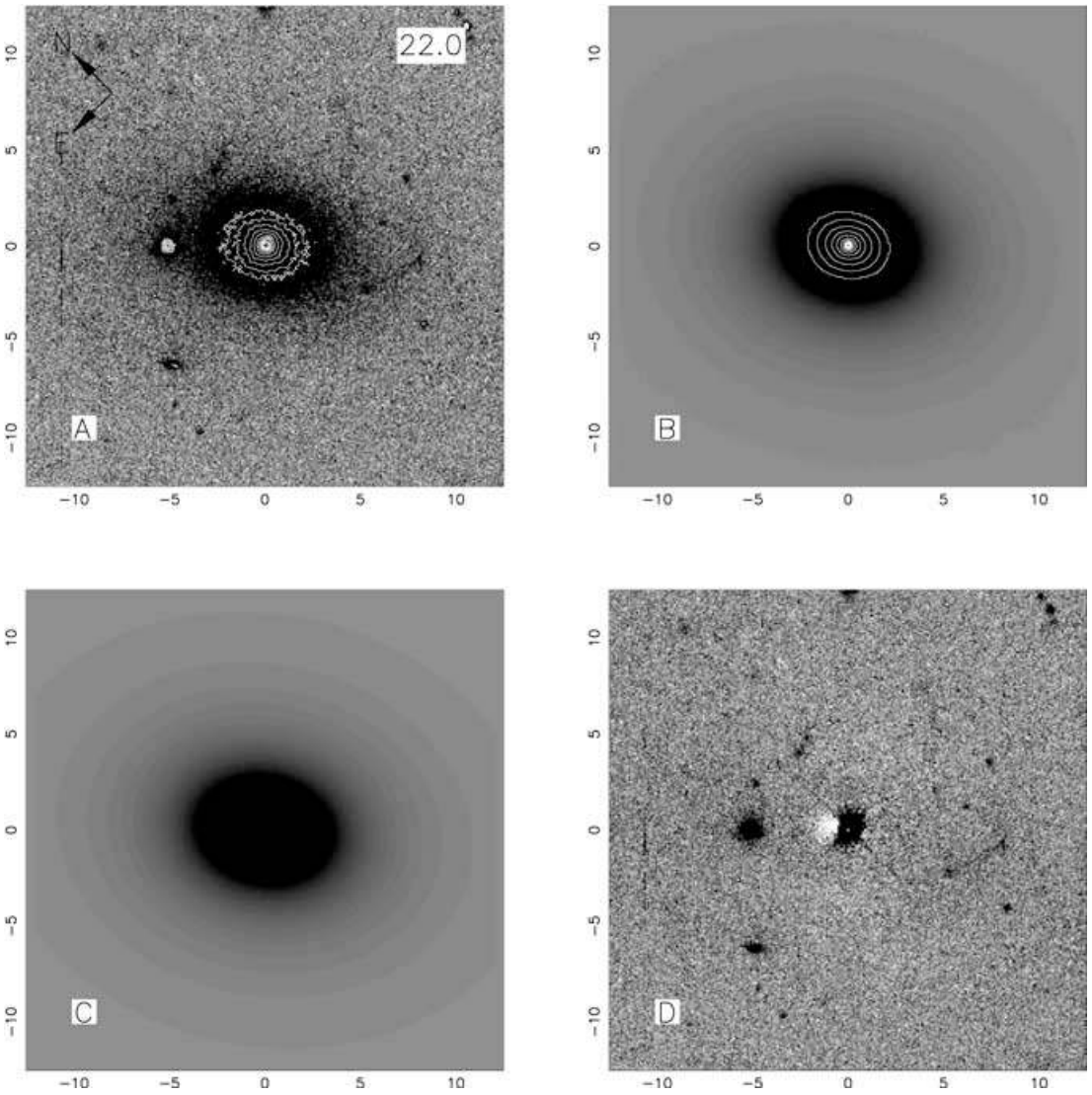

Figure A5. The radio galaxy 1330+022.

companion ≃50 kpc to the east. This object has been previously imaged on the *HST* PC using the F702W (wide *R*) filter by Disney et al. (1995). Using a two-dimensional cross-correlation modelling technique, Disney et al. found the host galaxy to be excellently matched by an elliptical galaxy model. Their wide-*R* image confirms the existence of the unresolved companion at ≃2 arcsec separation from the nucleus and suggests that the environment of 2215−037 resembles a poor cluster. This suggestion is supported by the image of the full WF2 chips, which shows ⩾10 companion objects inside a radius of ≃100 kpc. This quasar was identified as an X-ray source in the *ROSAT* All-Sky Survey (Yuan et al. 1998).

APPENDIX B: LUMINOSITY PROFILES

In this appendix we provide the observed and best-fitting model luminosity profiles for 14 AGN for which the new *HST* data are reported in this paper, see Figs B1–B14. The profiles are followed out to a radius of 10 arcsec, which is representative of the typical outer radius used in the image modelling. In each figure the azimuthally averaged data are indicated by circles, the azimuthal average of the best-fitting two-dimensional model is shown by the solid line, and the dotted line indicates the contribution made to the surface-brightness profile by the point-source component of the model (after convolution with the PSF).

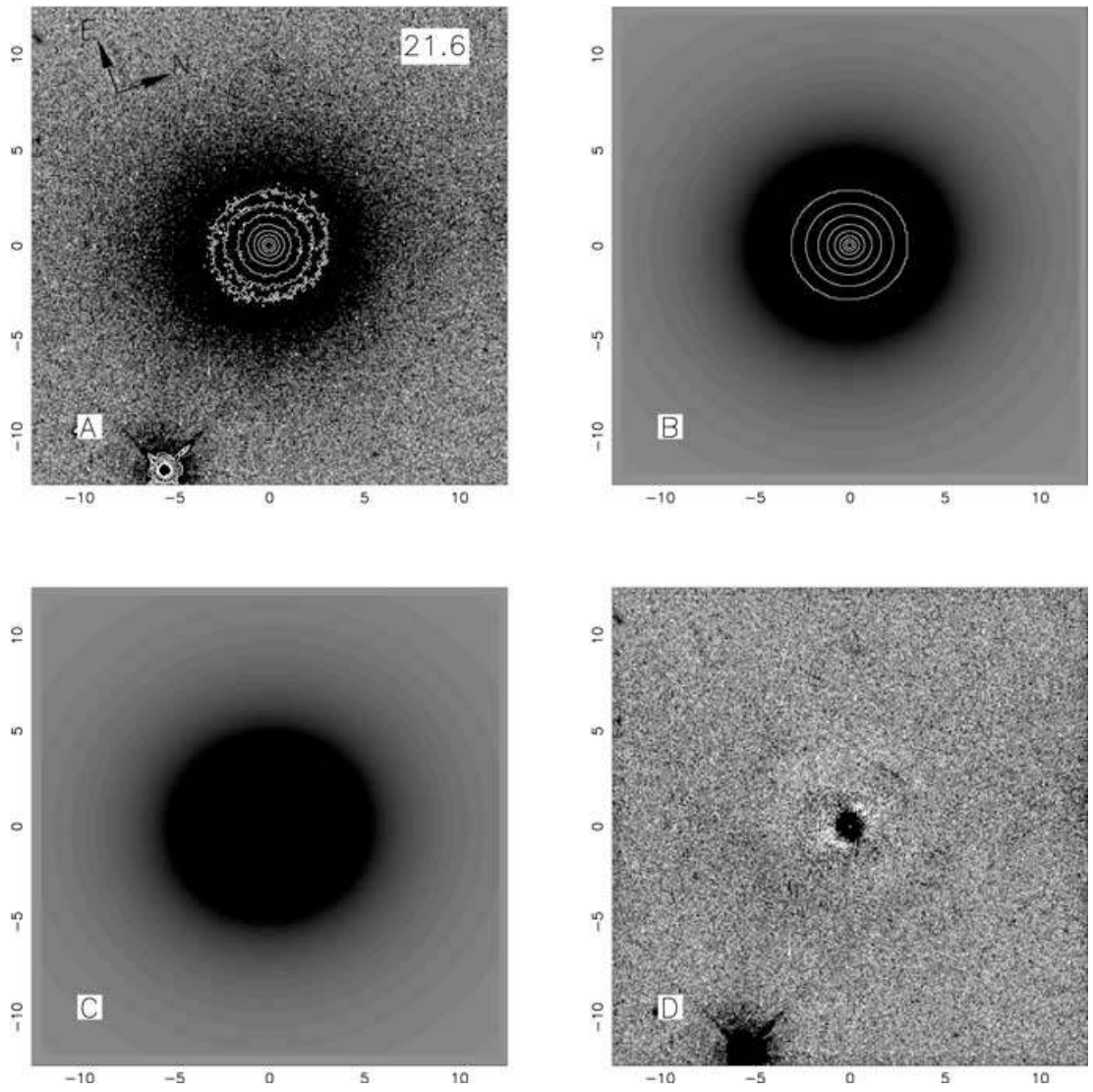

Figure A6. The radio galaxy 1342−016.

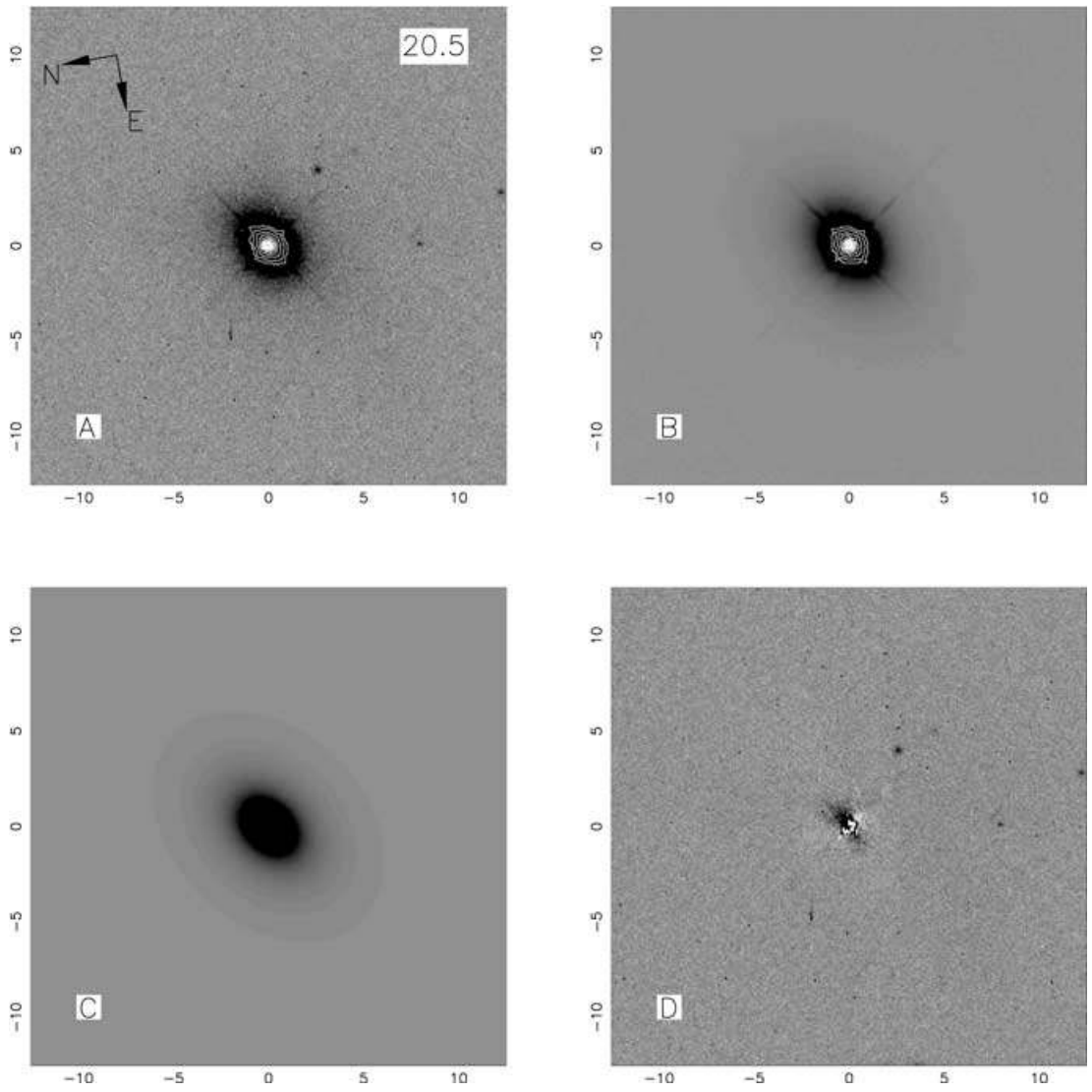

Figure A7. The radio-loud quasar 1020−103.

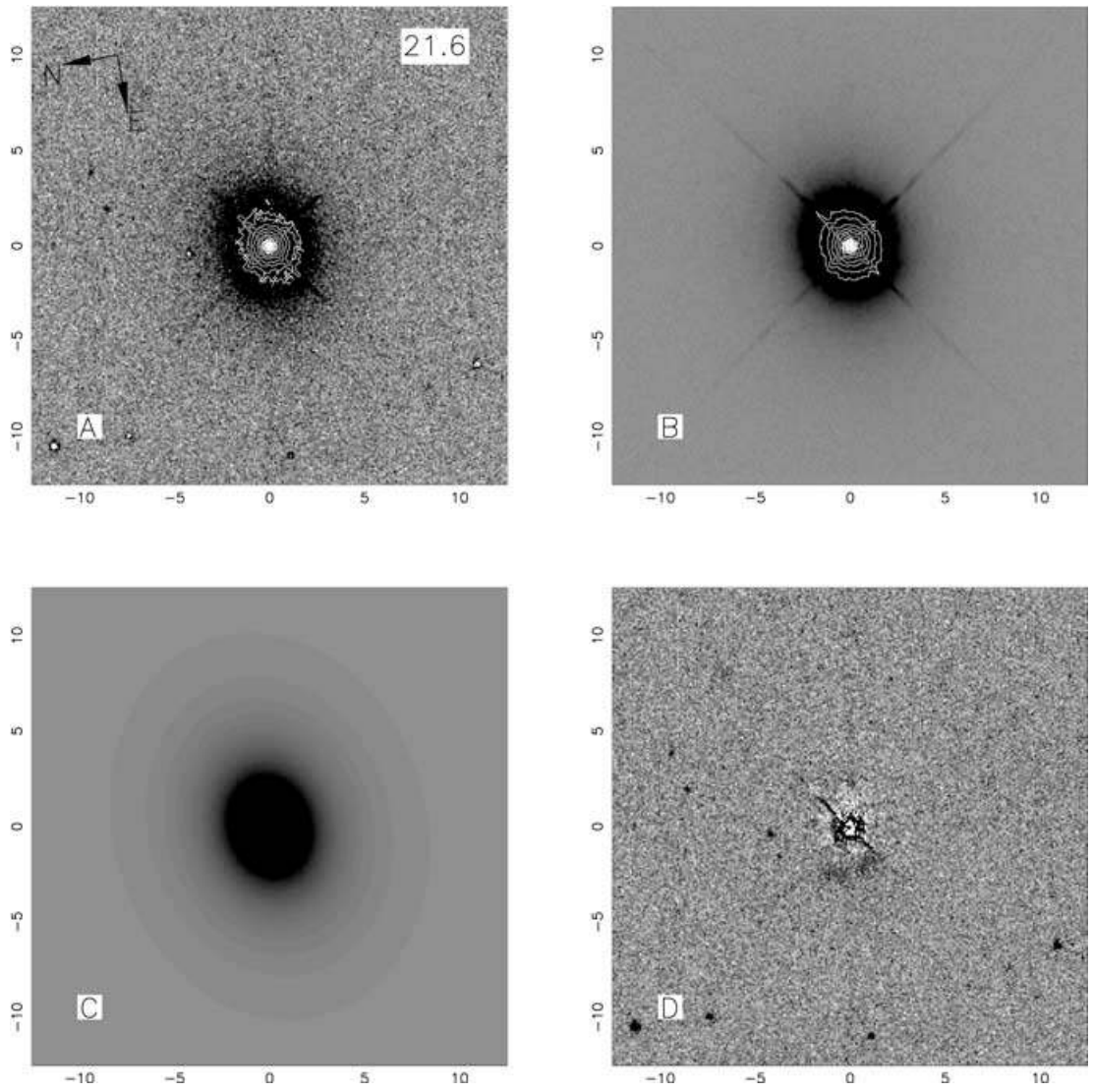

Figure A8. The radio-loud quasar 1217+023.

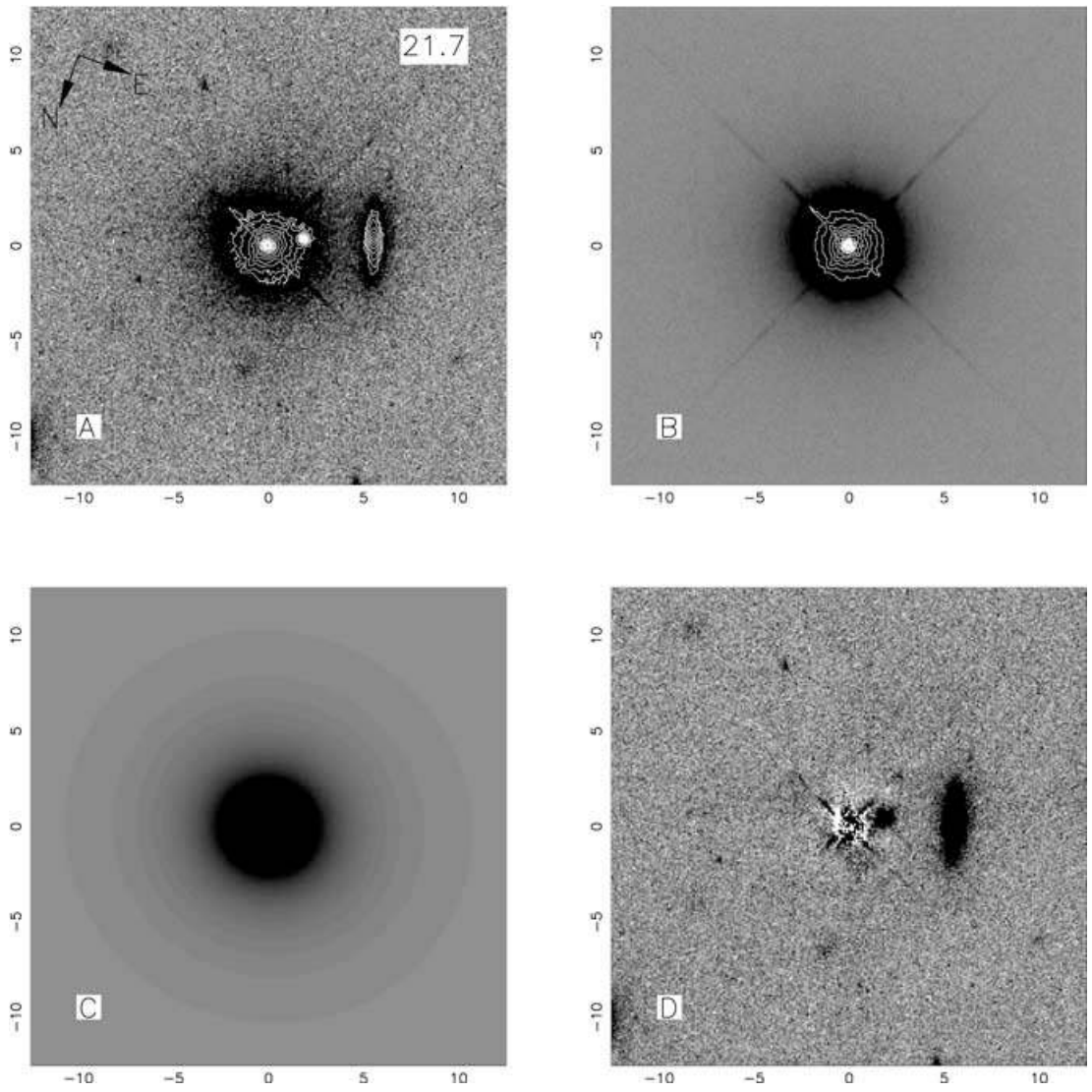

Figure A9. The radio-loud quasar 2135−147.

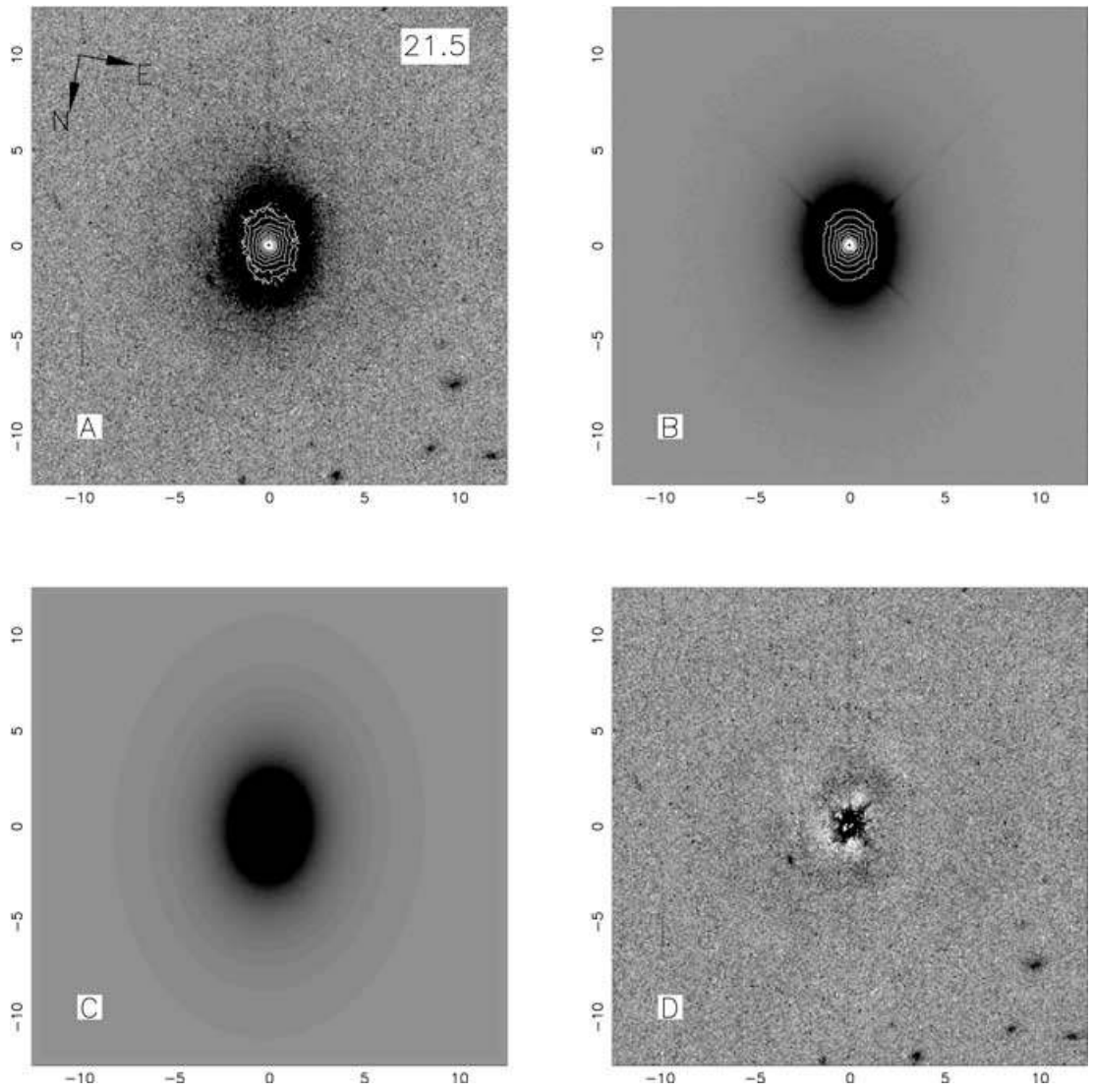

Figure A10. The radio-loud quasar 2355−082.

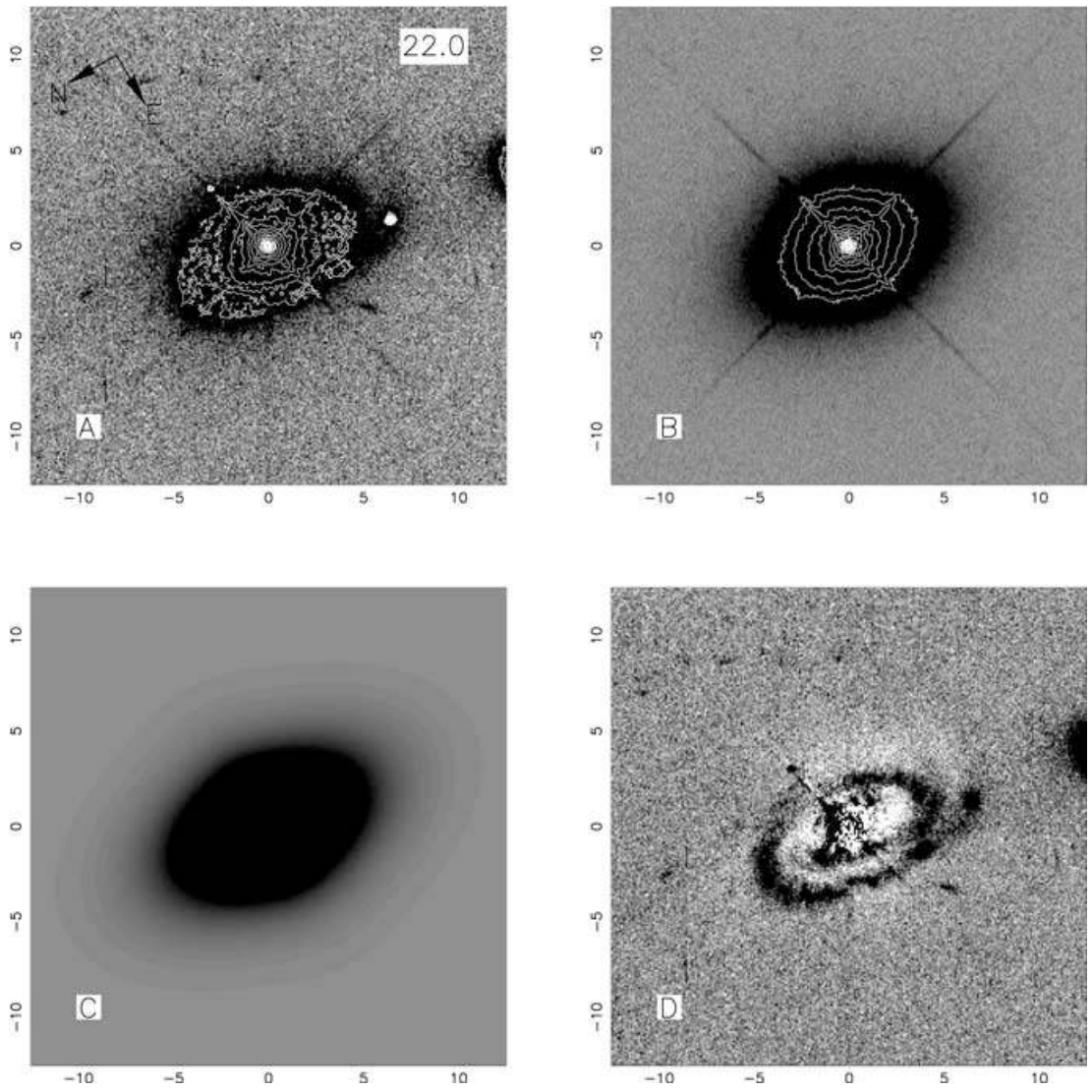

Figure A11. The radio-quiet quasar 0052+251.

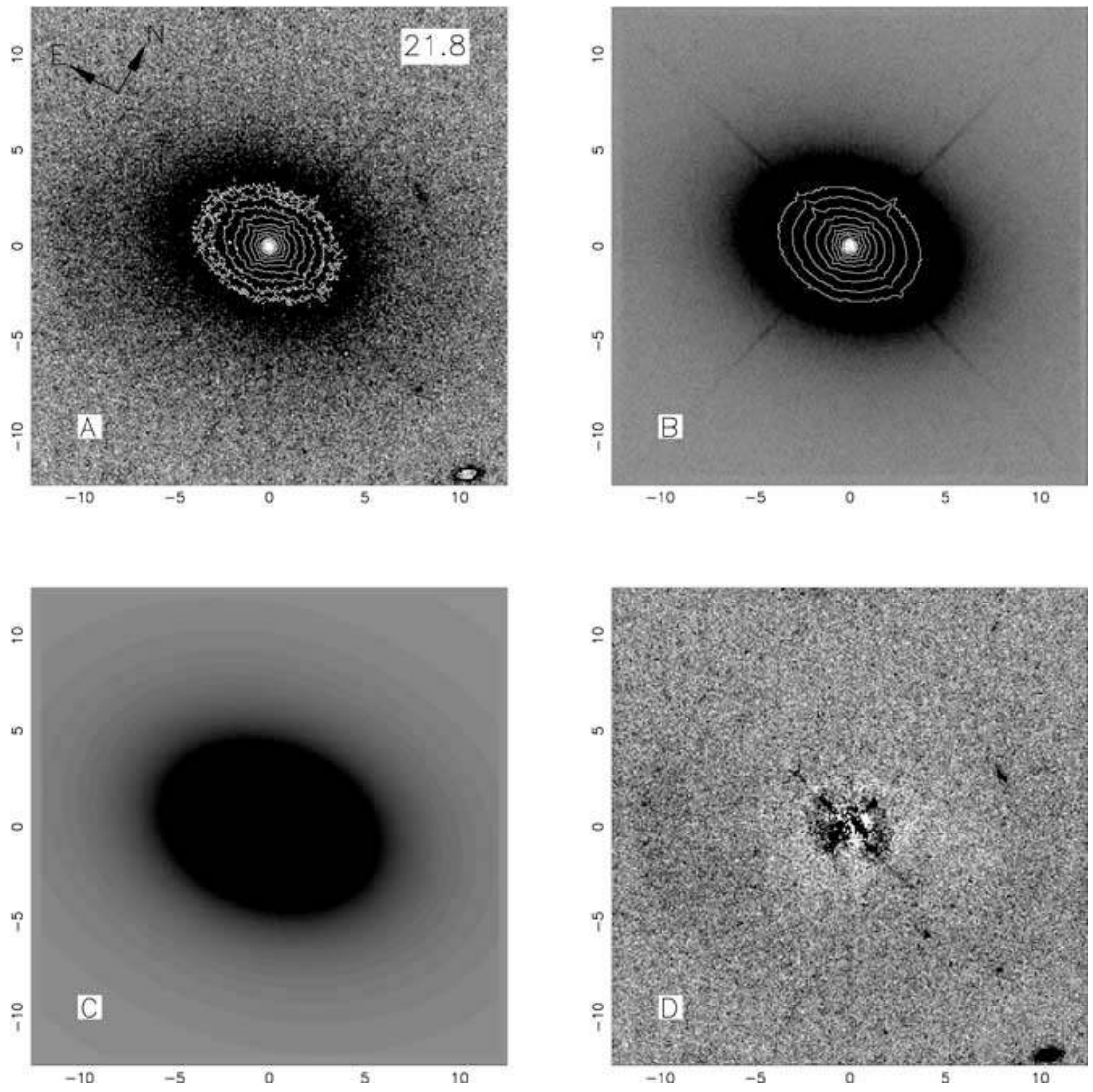

Figure A12. The radio-quiet quasar 0204+292.

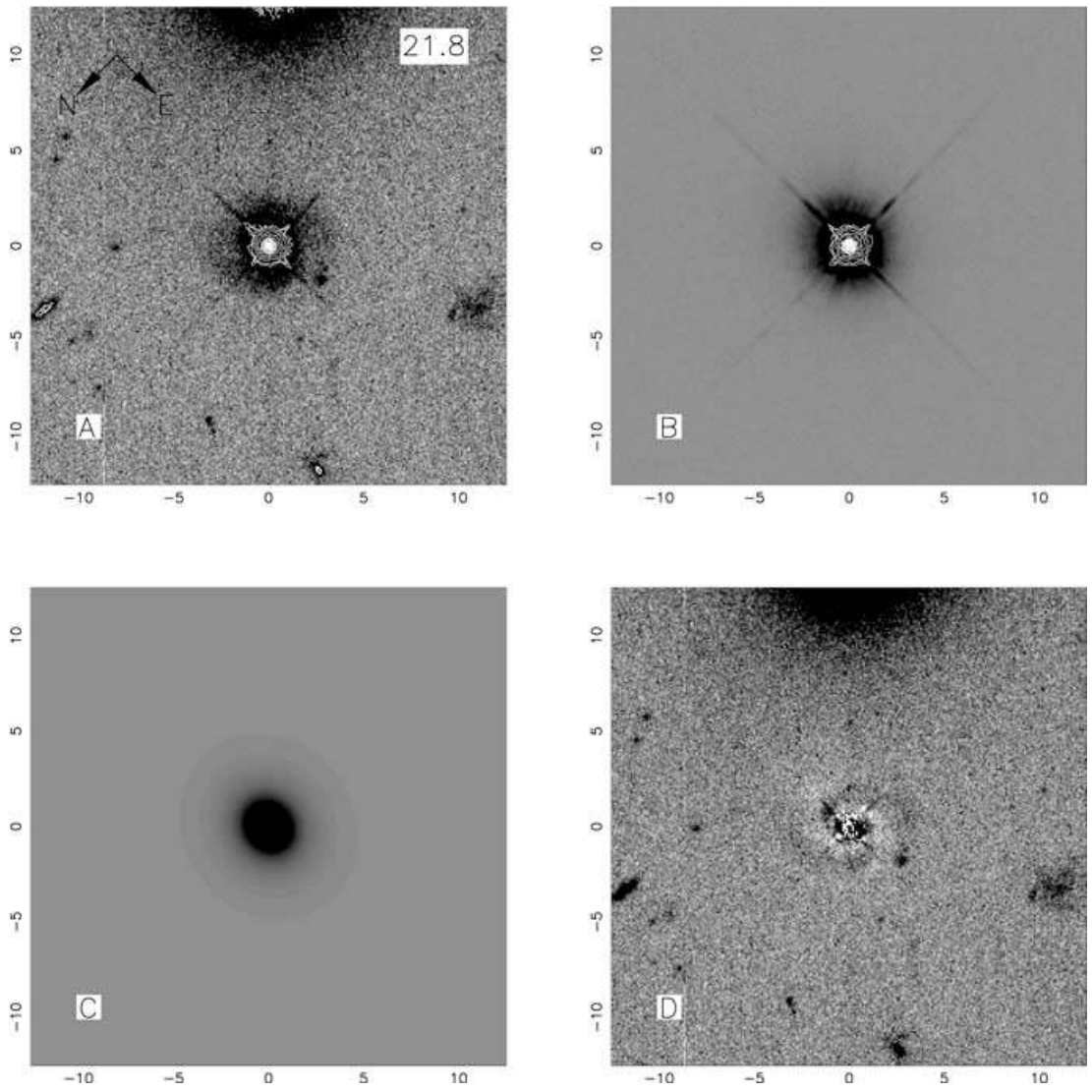

Figure A13. The radio-quiet quasar 1549+203.

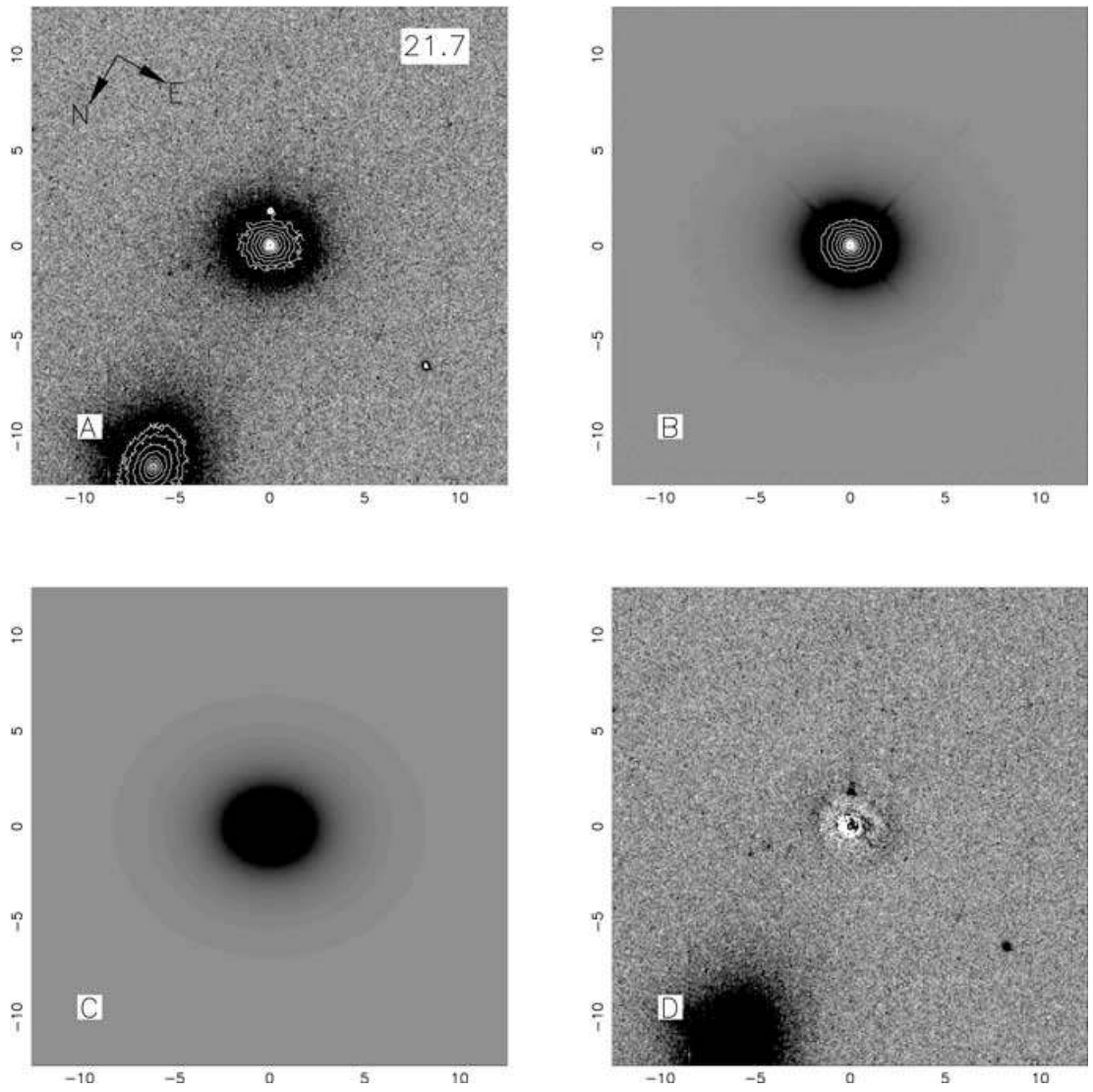

Figure A14. The radio-quiet quasar 2215−037.

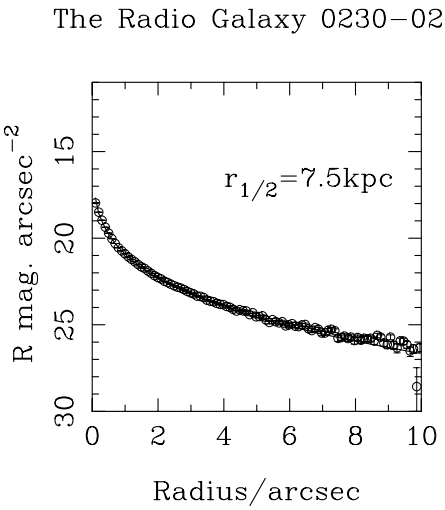

Figure B1. The radio galaxy 0230–027.

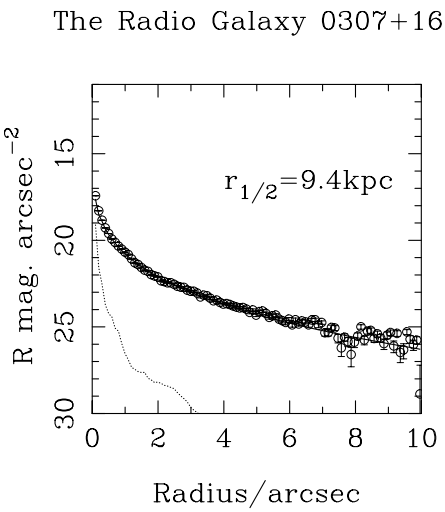

Figure B2. The radio galaxy 0307+169.

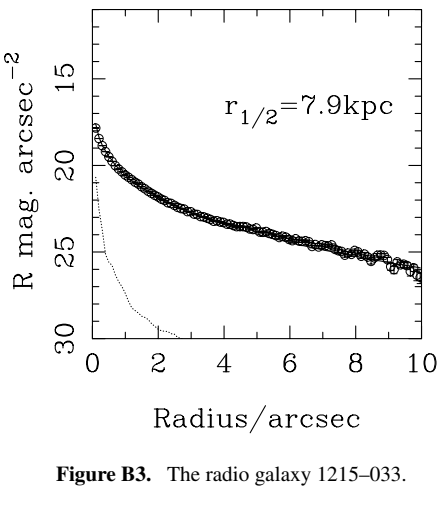

Figure B3. The radio galaxy 1215–033.

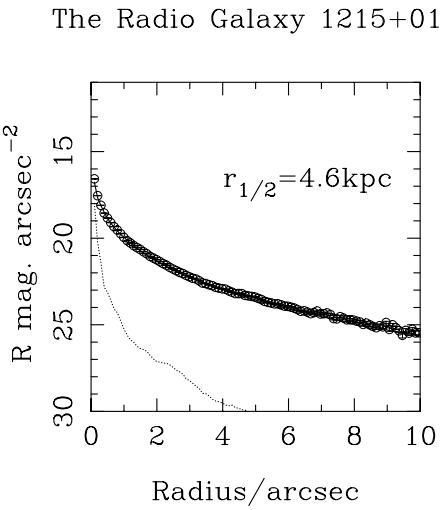

Figure B4. The radio galaxy 1215+013.

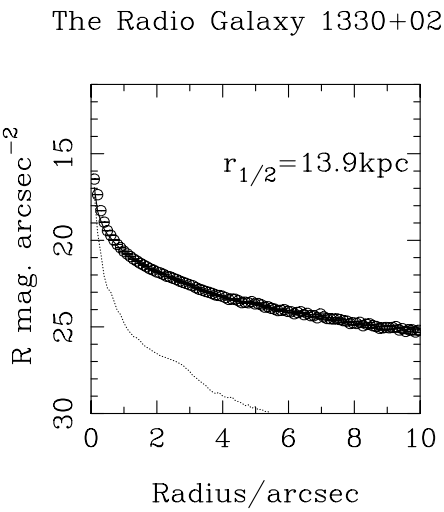

Figure B5. The radio galaxy 1330+022.

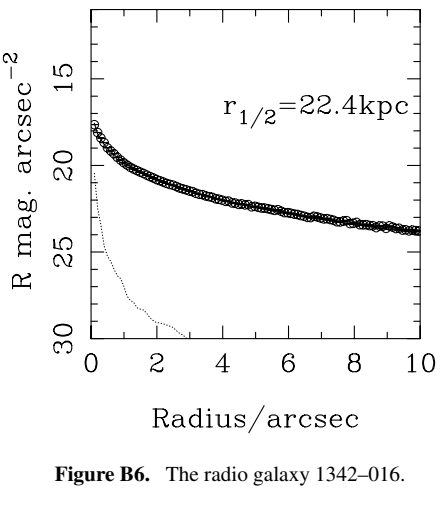

Figure B6. The radio galaxy 1342–016.

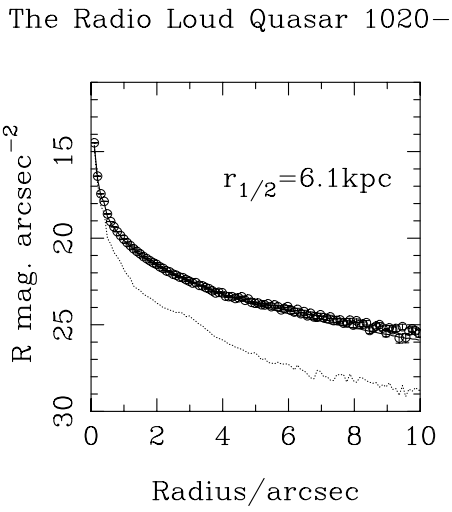

Figure B7. The radio-loud quasar 1020–103.

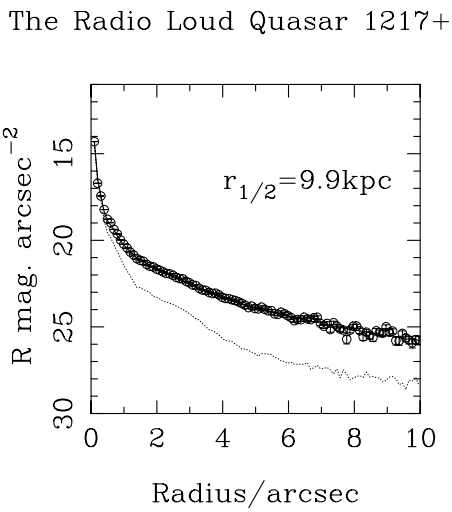

Figure B8. The radio-loud quasar 1217+023.

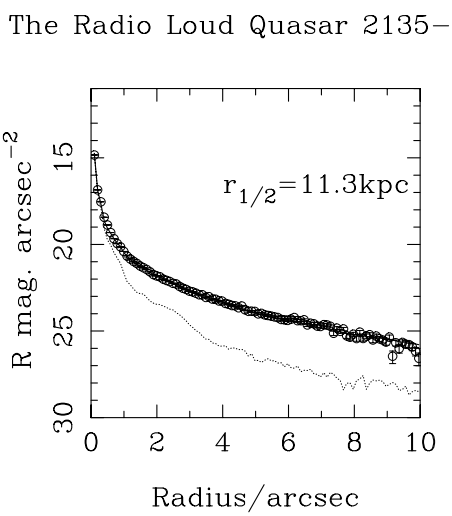

Figure B9. The radio-loud quasar 2135–147.

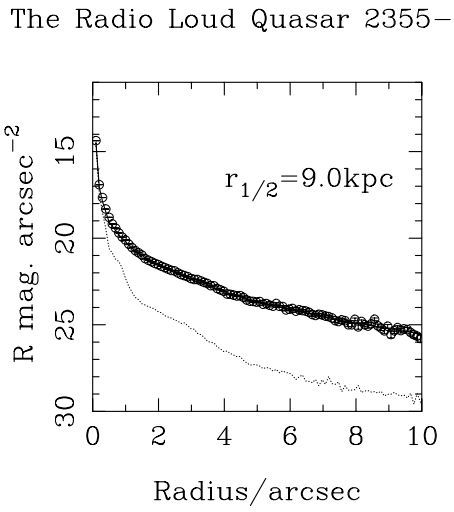

Figure B10. The radio-loud quasar 2355–082.

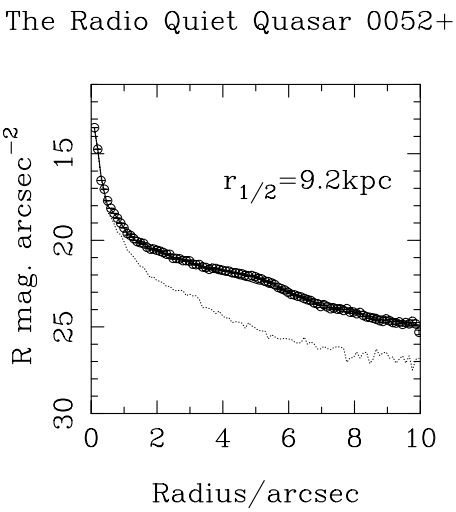

Figure B11. The radio-quiet quasar 0055+251.

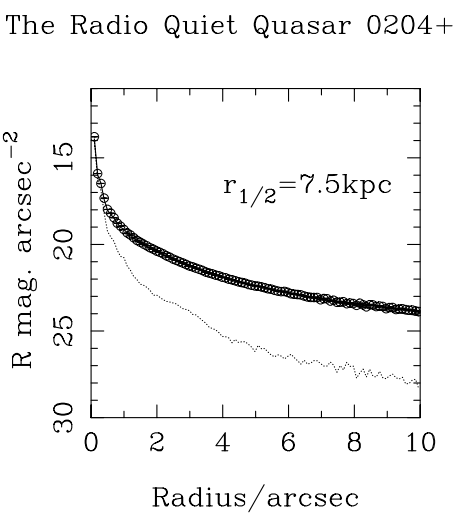

Figure B12. The radio-quiet quasar 0204+292.

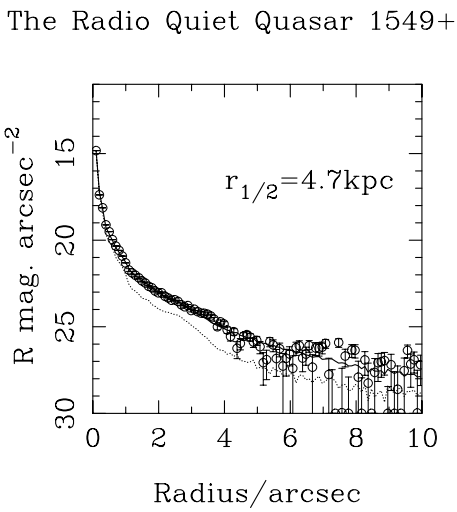

Figure B13. The radio-quiet quasar 1549+203.

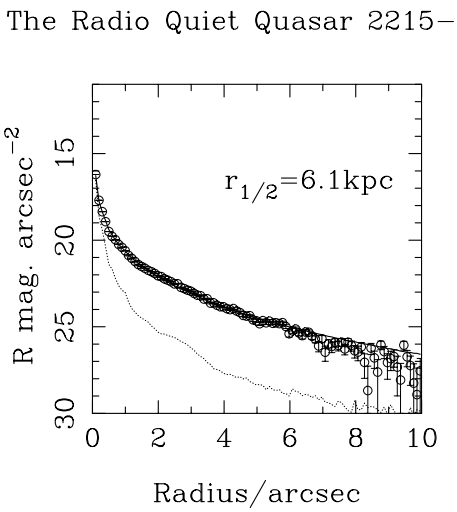

Figure B14. The radio-quiet quasar 2215–037.

This paper has been typeset from a TEX/LATEX file prepared by the author.